Division of Radiotherapy
Ghent University Hospital

Intensity modulated radiation therapy
for ethmoid sinus cancer

Filip G. Claus

promotor : Prof. Dr. W. De Neve

Thesis submitted to fulfill the requirements for achievement
of the degree of Doctor in the Medical Sciences

June 2002

Humanity needs practical men, who get the most out of their work, and, without forgetting the general good, safeguard their own interests. But humanity also needs dreamers, for whom the disinterested development of an enterprise is so captivating that it becomes impossible for them to devote their care to their own material profit. Without doubt, these dreamers do not deserve wealth, because they do not desire it. Even so, a well-organized society should assure to such workers the efficient means of accomplishing their task, in a life freed from material care and freely consecrated to research.

Marie Curie (1867-1934)

promotor

Prof. Dr. W. De Neve, PhD	Division of Radiotherapy
	Ghent University Hospital

examination commission

Prof. Dr. E. Achten, PhD	Department of Radiology
	Ghent University Hospital
Prof. Ir. C. De Wagter, PhD	Division of Radiotherapy
	Ghent University Hospital
Prof. Dr. V. Gregoire, PhD	Department of Radiotherapy
	Brussels UCL University Hospital
Dr. M. Lemmerling, PhD	Department of Radiology
	Ghent Sint-Lucas Academic Hospital
Prof. Dr. M. Mareel, PhD	Division of Radiotherapy
	Ghent University Hospital
Dr. C. Rasch, PhD	Department of Radiotherapy
	Amsterdam National Cancer Institute
Prof. Dr. G. Storme, PhD	Department of Radiotherapy
	Brussels VUB University Hospital
Lic. D. Verellen, PhD	Department of Radiotherapy
	Brussels VUB University Hospital
Prof. Dr. P. Van Cauwenberge, PhD	Department of Otorhinolaryngology
	Ghent University Hospital
Prof. Dr. H. Vermeersch	Department of Head and Neck Surgery
	Ghent University Hospital

dean of the faculty and president of the examination commission

Prof. Dr. P. Van Cauwenberge, PhD

Contents

1 Summary - Samenvatting - Résumé

Summary

Radiotherapy planning technology is rapidly changing the last decade. Intensity modulated radiation therapy (IMRT), a new radiation delivery technique, has increased the therapeutic window by allowing an increased tumor dose while selectively sparing the surrounding normal tissues. For head and neck cancer, IMRT is on the verge of clinical implementation. The first five papers presented in this thesis, subsections 4.1-4.5, report on the treatment planning aspects and early clinical experience of IMRT at Ghent University Hospital (GUH), in particular for head and neck cancer. The main objective was the outlining of clinical implementation protocols and the generation of disease site specific planning solutions for various subsites in the head and neck region. Further automation of this approach has facilitated to maintain the patient flow. IMRT at GUH is now the standard radiation technique for various subsites in the head and neck region.

Ethmoid sinus cancer is a rare head and neck malignancy, the majority of patients presenting in advanced disease stages. Surgery and postoperative radiation is generally recommended as standard treatment. Survival and local control are strongly correlated with the primary tumor extent, and most failures of treatment occur within 3 years. An overview of patients diagnosed with adenocarcinoma of the ethmoid sinuses and treated with surgery and radiotherapy at GUH is presented in subsection 4.9. An IMRT planning strategy for ethmoid sinus cancer is presented in subsections 4.6 and 4.7, as well as the preliminary results and short term toxicity profile (subsection 4.8).

Samenvatting

Radiotherapie planning technologie onderging grote veranderingen de afgelopen 10 jaar. Intensiteitsgemoduleerde radiotherapie (IMRT) is een nieuwe bestralingstechniek die toelaat tumoren meer selectief te bestralen, met name een hogere dosis ter hoogte van het doelvolume te combineren met een lagere belasting van de omliggende gezonde weefsels. Het klinisch gebruik van

IMRT voor hoofd- en halstumoren neemt alsmaar toe. De eerste 5 artikels van de thesis, te vinden in subsecties 4.1 tot 4.5, gaan dieper in op de plantechnische aspecten van IMRT en de klinische ervaring opgedaan met deze nieuwe techniek op de Dienst Radiotherpie van het Universitair Ziekenhuis Gent (R-UZG), meer bepaald voor de behandeling van hoofd- en halstumoren. Het accent van dit onderzoek lag op het uitwerken van klinische implementatieprotocollen en het ontwikkelen van een specifieke planningsstrategie voor verschillende deelgebieden in de hoofd- en halsregio. IMRT is nu de standaard behandelingstechniek in R-UZG voor verschillende hoofd- en halstumorlokalisaties.

Tumoren van de ethmoidale sinussen zijn zeldzaam en de diagnose wordt vaak in een vergevorderd stadium gesteld. Chirurgie en aanvullende radiotherapie wordt algemeen als standaardbehandeling beschouwd. Overleving en lokale tumorcontrole houden sterk verband met de uitgebreidheid van het primaire letsel en ziekteherval wordt voornamelijk gezien binnen de 3 jaar na behandeling. Een overzicht van adenocarcinoma van de ethmoidale sinussen en de behandelingsresultaten met heelkunde en radiotherapie in R-UZG kan men vinden in subsectie 4.9. Een implementatiestrategie voor het behandelen van ethmoidale sinustumoren met IMRT staat beschreven in de subsecties 4.6 en 4.7, evenals een tussentijdse analyse van de behandelingsresultaten en vroegtijdige bijwerkingen (subsectie 4.8).

Résumé

La technologie de planification en radiothérapie a rapidement évolué au cours de la dernière décennie. La radiothérapie avec modulation de l'intensité (IMRT pour Intensity Modulated Radiation Therapy), une nouvelle technique d'irradiation, a augmenté la fenêtre thérapeutique en permettant une majoration de la dose delivrée à la tumeur tout en épargnant sélectivement les tissus sains avoisinants. Dans le cas des cancers de la région de la tête et du cou, l' IMRT est à l'aube de l'utilisation clinique. Les 5 premiers articles présentés dans cette thèse, chapitres 4.1-4.5, décrivent la planification des traitements et l'expérience clinique initiale en IMRT à l'Hôpital Universitaire de Gand (GUH), particulièrement pour les cancers de la région tête et cou. Le principal objectif était de démontrer les protocoles d'implémentation clinique

et la génération de solutions de planification spécifiques adaptées à différent sites et sous-sites de la région tête et cou. Le cancer du sinus ethmoidal est une tumeur maligne rare de cette région. La majorité des patients affectés se présentent à un stade avancé de la maladie. La chirurgie suivie d'une irradiation post-opératoire est généralement recommandée comme traitement standard. La survie et le contrôle local sont fortement correlés à l'extension de la tumeur primitive et la plupart des échecs thérapeutiques surviennent en dedans les trois ans. Une revue des patients atteints d'un adénocarcinome du sinus ethmoidal et traités par chirurgie et radiothérapie à GUH est présentée dans le chapitre 4.9. Une stratégie de planification IMRT pour les cancers du sinus ethmoide est présentée dans les chapitres 4.6 -4.7 , ainsi que les résultats préliminaires et le profil de toxicité à court terme (chapitre 4.8).

2 Introduction

Ethmoid sinus tumors account for less than 20 % of all paranasal sinus cancers and less than 1 % of all head and neck malignancy. Tumors are often diagnosed in locally advanced stages with extensions through the bony walls of the paranasal sinuses, the orbit, the nasopharynx and the anterior skull base. Volumes of the tumor are at close distance to ocular and visual pathway structures. A combined treatment of surgery and radiation therapy is generally recommended [1]. However, despite invasive surgical techniques and high radiation doses, local control rates of less than 50 % are reported for advanced disease stages [2]. The radiotherapy prescription dose often exceeds the tolerance of the surrounding optic structures, resulting in radiation induced damage such as corneal and lacrimal injury, retinopathy and optic neuropathy.

The last decade radiotherapy planning technology is rapidly changing. New developments such as 3D conformal radiotherapy and intensity modulated radiation therapy (IMRT) have increased the therapeutic window by increasing the dose to the tumor while selectively sparing the surrounding normal tissues [3]. At Ghent University Hospital (GUH), ethmoid cancer patients are treated with IMRT since 1998. The hypothesis to implement IMRT is to improve local control while preserving binocular vision.

The aim of the present thesis is to give the reader some insights in the clinical aspects of ethmoid sinus cancer, then to situate the application of IMRT for head and neck cancer in general, and finally to present an implementation strategy of IMRT for ethmoid sinus cancer together with the first clinical results. Section 3, the collating part of the thesis, can be divided in three parts. The first one describes the clinical picture of ethmoid sinus cancer, the second part discusses the principles of IMRT and the last part the implementation of IMRT for ethmoid sinus cancer. The papers of the thesis are grouped in section 4. Papers 1, 2, 3, 4 and 5 discuss the principles of IMRT and its implementation for head and neck cancer at GUH. The papers 6, 7 and 8 discuss the use of IMRT for ethmoid sinus cancer. Paper 9 reports on the results of postoperative radiotherapy for adenocarcinoma of the ethmoid sinuses for patients treated between 1985 and 2001 at GUH.

References

1. Physician Data Query (PDQ) of the National Cancer Institute : Treatment options for health professionals. Paranasal Sinus and Nasal Cavity Cancer. CancerNet http://cancernet.nci.nih.gov.

2. Schantz S, Harrison L, Forastiere A. Tumors of the nasal cavity and paranasal sinuses, nasopharynx, oral cavity and oropharynx. In: Cancer: Principles and Practice of Oncology. 5th ed. Lippincott Raven 1997;741-801.

3. Intensity Modulated Radiation Therapy Collaborative Working Group. Intensity-modulated radiotherapy: current status and issues of interest. Int J Radiat Oncol Biol Phys 2001;51:880-914.

3 IMRT for ethmoid sinus cancer

3.1 Ethmoid sinus cancer

3.1.1 Anatomy

The paranasal sinuses consist of the maxillary, ethmoidal, frontal and sphenoidal sinuses. A clear understanding of the relationship between the nasal cavity and paranasal sinuses is important to have a good insight in the spread of sinonasal disease [1]. The ethmoid sinuses are a labyrinth of thin-walled air cells, originating from the ethmoid bone, and lying between the medial walls of the orbits and the lateral wall of the nasal cavity [2]. The ethmoid bone consists of a horizontal perforated lamina above, called the cribriform plate, a median perpendicular plate and two lateral labyrinths. The labyrinths consist of three groups of ethmoidal air cells - anterior, middle and posterior - ranging from 3 to 18 cells. The anterior and middle air cells drainage into the middle meatus of the nasal cavity, the posterior cells empty into the superior nasal meatus. Special ethmoid sinus cells include the Agger nasi air cells, defined as the anterior-inferior extramural air cells, and the infraorbital Haller's cells, extending along the medial floor of the orbit. The ethmoid bulla is the convex, inferomedial bony wall overlying the middle ethmoid air cells [1]. The thin, lateral wall separating the ethmoidal air cells from the orbit is called the lamina papyracea.

The vascular supply of the ethmoid sinus is through the anterior and posterior ethmoid arteries, branches of the ophthalmic artery and the innervation is through the ophthalmic nerve, the first division of the fifth cranial nerve. The intimate relationships of the ethmoid sinus include the maxillary sinus inferiorly, the cranial fossa superiorly, the nasal fossa medially, the orbit laterally and the sphenoid sinus posteriorly.

3.1.2 Epidemiology and etiology

Tumors of the paranasal sinuses are rare. The incidence of sinonasal carcinoma is about one case per 100.000 people per year. Ethmoid sinus tumors account for less than 20 % of all paranasal sinus cancers, of which the most common

---
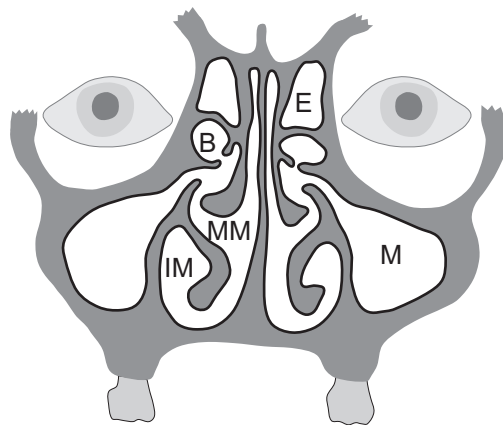
Figure 1: *Schematic drawing of the nasal cavity and paranasal sinuses in a coronal plane at the level of the middle ethmoidal air cells (B:bulla ethmoidalis, E:middle ethmoid air cells, IM:inferior nasal meatus, M:maxillary sinus, MM:middle nasal meatus)*
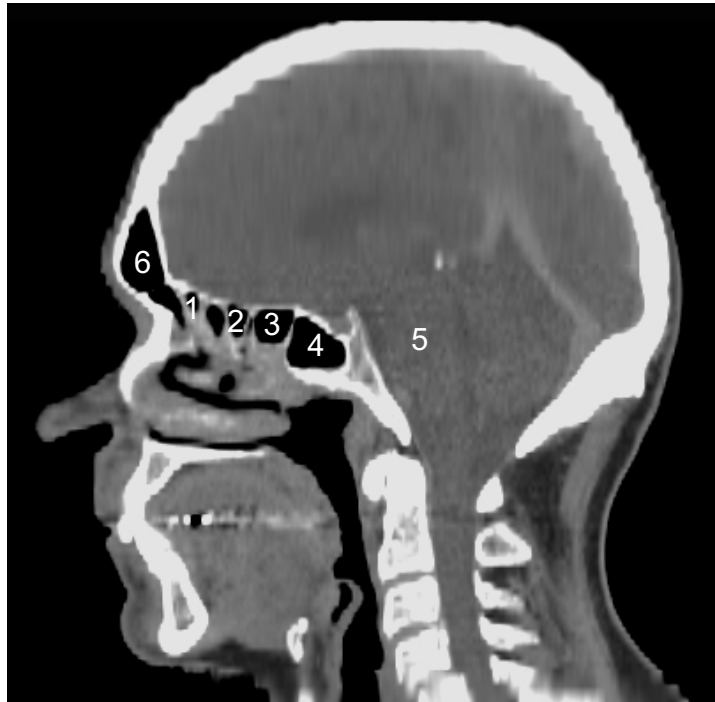
Figure 2: *Sagittally reconstructed CT slice (1:anterior ethmoidal cells, 2:middle ethmoidal cells, 3:posterior ethmoidal cells, 4:sphenoid sinus, 5:brainstem, 6:frontal sinus)*

Figure 3: *Transverse MRI slice (1:anterior ethmoidal cells, 2:middle ethmoidal cells, 3:posterior ethmoidal cells, 4:right retina, 5:left retina, 6:left optic nerve, 7:right optic nerve, 8:optic chiasm)*

type are maxillary sinus tumors (80-90%). The frontal and sphenoid sinuses are rarely involved. Table 1 lists the incidence in Belgium of nasal cavity, paranasal sinus and middle ear tumors, classified as ICD-160 (ICD : International Classification of Disease) or ICD-O C30-31 (ICD-O : International Classification of Disease for Oncology), for the years 1984-1995 (source : Belgian National Cancer Registry). The data presented are most probably an underestimate of the real incidence. After 1995, only incidences for oral cavity and pharyngeal cancer were registered for the head and neck region, as for most of the international cancer registry reports. In Japan, the age adjusted death rate per 100.000 people for paranasal sinus tumors (ICD-O C31) was in 1995 0.2 for males and 0.1 for females [3]. Paranasal sinus tumors were responsible for approximately 0.2 % of the total number of deaths caused by malignant neoplasms. The Eindhoven Cancer Registry [4] reported on the incidence of tumors in the middle ear, nasal cavity and paranasal sinuses (ICD-160) for the period 1973-1992. The incidence per 10^5 person-years for paranasal sinus tumors between 1973-1982 and 1983-1992 was respectively 0.16 and 0.08 for females, and 0.39 and 0.44 for males. The estimated number of new patients

nasal cavity, paranasal sinuses, middle ear				
incidence (absolute number)				
year(s)	men	women	$\rightarrow$	total
1984	47	23	$\rightarrow$	70
1985	58	18	$\rightarrow$	76
1986	59	26	$\rightarrow$	85
1987-89	192	66	$\rightarrow$	258
1993	61	30	$\rightarrow$	91
1994	66	17	$\rightarrow$	83
1995	54	13	$\rightarrow$	67

Table 1: *ICD 160 / ICD-O C30-31 : 1984-95 (Belgium)*

with a sinonasal or middle ear tumor per physician was 1 in 50 years for a general practitioner, 1 per year for an ear-nose-throat surgeon and between 10 and 15 new patients for a center for head and neck oncology.

Various etiologic factors have been linked to malignant tumors of the sinonasal tract, most of them occupational exposures including nickel, chromium, isopropyl oils, volatile hydrocarbons and organic fibers that are found in wood, shoe and textile industry. Cohort and case control studies of cancer of the nasal cavity and paranasal sinuses have shown increased risks associated with exposure to wood dust [5][6][7]. These findings are supported by numerous case studies [8][9]. Hardwood (angiosperm) dust is proven to be carcinogenic to humans and possesses genotoxic properties. The carcinogens consist of insoluble high-molecular components, such as cellulose and lignin, and insoluble low-molecular components, such as terpenes. The carcinogenicity of softwood (gymnosperm) dust is insufficiently investigated and is therefore categorized as a suspected human carcinogen. Adenocarcinoma of the ethmoid sinuses is clearly associated with exposure to hardwood dust, as illustrated by the high incidence among people working in the wood furniture industry.

Figure 4: *Transverse MRI slice of a patient presenting with epistaxis, obstructive sinusitis and impaired vision at the left side (biopsy revealed an adenocarcinoma, gross tumor volume in white dots)*

3.1.3 Clinical presentation and staging

The majority of ethmoid sinus tumors present with advanced disease. Less advanced tumors grow within the bony confines of the sinuses and may remain asymptomatic until they invade adjacent structures. This makes early detection of malignancy difficult. Early symptoms and signs may mimic those of inflammatory disease, or usually result from secondary obstructive sinusitis. Nasal complaints, such as polyposis, intermittent epistaxis, anosmia, watery or bloody discharge and pain are common presenting symptoms. Ocular symptoms, such as diplopia, acuity changes and exophthalmos, due to direct tumoral invasion of the orbit, and neurologic symptoms, due to cranial invasion, indicate advanced disease (Figure 4). Delay in diagnosis is often caused by the low incidence of these tumors (low index of suspicion) and the very similar symptoms as observed in benign sinonasal diseases.

Nodal involvement is infrequent, less than 10 % at the time of diagnosis [10]. The mucosa of the ethmoid sinuses has sparse capillary lymphatics and therefore metastases are uncommon, even in advanced stages. The lymphatics drain to the submandibular, parotid and jugulodigastric nodes and posteriorly towards the nasopharynx, i.e to the retropharyngeal nodes and deep superior jugular nodes.

The most common cell types are squamous cell carcinoma and adenocarcinoma. Other cell types include adenoid cystic carcinoma, melanoma, lymphomas, soft tissue sarcomas and osteo- or chondrosarcomas.

The TNM staging (Table 2) system is a clinical estimate of the extent of disease [11]. The T-stage describes the extension of the primary tumor, the N-stage the extent of involvement of lymph nodes and the M-stage the presence of distant metastasis.

3.1.4   Management and results of treatment

The first opportunity to treat patients with ethmoid sinus cancer is the most effective and multidisciplinary planning of the treatment should be a standard [12][13]. The generally accepted method of treatment is a combination of radical surgery, to remove the bulk of the tumor, followed by high dose radiation therapy within 6 weeks after surgery [14]. Even for small lesions (T1) resected with clear surgical margins, postoperative radiation therapy should be a standard. Removal of the eye is performed if the orbit is extensively invaded by cancer. Radical neck dissection or neck nodal irradiation is recommended only for patients presenting with positive nodes.

The treatment results for patients presenting with paranasal sinus cancer is generally poor, with most centers reporting 5-year survival rates in the range of 30-40 %. Survival and local control are strongly correlated with the primary tumor extent [15]. Since most failures of treatment occur within 2 years, the follow-up of patients must be frequent and meticulous during this period. Although distant metastases are found in 20 to 40 % of patients who fail treatment, locoregional recurrence is the rule and accounts for the majority of cancer deaths.

Related papers of the thesis : Paper 9 of Section 4 "Papers in the field of the thesis" discusses the treatment results for 47 patients diagnosed with adenocarcinoma of the ethmoid sinuses and treated with surgery and radiotherapy at GUH between 1985 and 2001.

Primary tumor (T)	
Tx :	primary tumor cannot be assessed
T0 :	no evidence of primary tumor
Tis :	carcinoma in situ
T1 :	tumor confined to the ethmoid with or without bone erosion
T2 :	tumor extends into the nasal cavity
T3 :	tumor extends to the anterior orbit and/or maxillary sinus
T4 :	tumor with intracranial extension, orbital extension including apex, involving sphenoid and/or frontal sinus and/or skin of external nose

Regional lymph nodes (N)		
Nx :	regional lymph nodes cannot be assessed	
N0 :	no regional lymph node metastasis	
N1 :	metastasis in a single ipsilateral lymph node, 3 cm or less in greatest dimension	
N2 :	metastasis in a single ipsilateral lymph node, more than 3 cm but not more than 6 cm in greatest dimension, or in bilateral or contralateral lymph nodes, none more than 6 cm in greatest dimension	
	N2a :	metastasis in a single ipsilateral lymph node more than 3 cm but not more than 6 cm in greatest dimension
	N2b :	metastasis in multiple ipsilateral lymph nodes, none more than 6 cm in greatest dimension
	N2c :	metastasis in bilateral or contralateral lymph nodes, none more than 6 cm in greatest dimension
N3 :	metastasis in a lymph node more than 6 cm in greatest dimension	

Distant metastasis (M)	
Mx :	distant metastasis cannot be assessed
M0 :	no distant metastasis
M1 :	distant metastasis

Table 2: *TNM classification for ethmoid sinus cancer*

3.1.5   Sequelae of radiation treatment

High dose radiation therapy for ethmoid sinus cancer may be complicated by the proximity of a number of critical structures surrounding the clinical target volume (CTV). These organs at risk (OARs) include the brainstem, the spinal cord, the brain tissue, the pituitary gland and the various components of the optic apparatus (the lacrimal glands, the cornea, the lens, the retina, the optic nerve and the optic chiasm).

Lens

Ionizing radiation is known to be cataractogenic [16]. This loss of normal transparency of the lens is dose rate and fractionation dependent and may vary from a small stationary cataract to a more progressive cataract, resulting in loss of vision. The time of onset of cataract ranges from 6 months to several years and is inversely related to the total dose delivered to the lens. Lowering the fraction size of the radiation treatment reduces the risk and delays the onset of cataract formation. Additional risk factors include the patient age, diabetes, genetic predisposition and previous radiation. Doses between 5 and 10 Gy may cause lens opacity, usually without visual impairment. Doses between 12 and 16 Gy (2 Gy daily fractions) may induce cataract in 20 % of the individuals over a period of 5 years. Doses above 18 Gy may result in cataract formation in 50 % of the individuals (cumulative incidence of 5 years). Since nowadays cataract surgery is considered as a minor operation with a high success rate and almost no risk for complications, the lens is no longer considered as an organ at risk for radiotherapy planning of these tumors.

Lacrimal apparatus

The lacrimal apparatus consists of the major lacrimal gland and the accessory glands. The function of the former gland is believed to be responsible for reflex secretion, while the latter supporting glands are believed to maintain the basal secretion of tears. The main functions of the lacrimal apparatus are to prevent the conjunctiva and cornea from drying up, to form a natural barrier against particles, noxious fumes and micro-organisms, to increase the smoothness of

the cornea in order to improve the visus, and to facilitate the movements of the eyelids. Damage to this lacrimal apparatus may thus debilitate the natural host defense and increase the susceptibility of the conjunctiva and cornea to radiation damage. Symptoms related to a break-up of the tear film, known as a dry eye, include a red, painful and itchy eye, photophobia, foreign body sensation and sensitivity to wind. Secondary symptoms include corneal epithelial breakdown, ulceration, infection or perforation of the eye. Damage to the innervated corneal epithelium may give rise to severe pain. The probability of complications appears to increase steeply at doses above 30 Gy. The dose threshold for dry eye syndrome is 40 Gy (2 Gy daily fractions) and symptoms present within one month after completion of the radiation treatment [17]. Atrophy of the lacrimal gland may occur with doses of 50-60 Gy. The treatment of dry eye syndrome is symptomatic (artificial tears, antibiotics, analgesic), however in many instances of severe dry eye syndrome enucleation of the eye is necessary.

Cornea

Early and late effects due to radiation of the cornea include keratitis, corneal ulcers and severe dry eye syndrome. Punctate keratitis is observed after radiation with doses of 30-50 Gy (2 Gy daily fractions) [18], and is characterized by small defects in the corneal epithelium. Symptoms such as irritation and tearing of the eye are treated with artificial tears and local antibiotics (in case of infection), and heal within a few months after radiation therapy. Superficial keratitis may be followed by corneal ulceration giving rise to corneal scarring or severe dry eye syndrome. The incidence of corneal injuries is less than 20 % over 5 years if the dose does not exceed 55 Gy [19].

Retina

Radiation retinopathy is characterized by vascular changes such as microvascular occlusion and leakage. Microvascular occlusion leads to retinal ischemia, which in turn causes retinal hypoxia. The subsequent formation of collateral channels and neovascularization may cause retinal and vitreous hemorrhages,

neovascular glaucoma and tractional retinal detachments. Microvascular leakage may cause micro-aneurysmata, retinal edema and deposition of exsudates. The latency period ranges between 6 to 36 months and clinical symptoms may range from minimal to complete loss of vision depending on the site and size of the lesion. Diabetic and hypertensive retinopathy may potentiate the effect of radiation. The radiation fraction size is one of the most important factors in producing retinal damage, and daily fractions should not exceed 2 Gy. Doses between 45 and 55 Gy result in retinopathy in 50 % of the individuals, doses exceeding 65 Gy in 100 % of the patients [19]. No effective treatment for severe retinal damage exists and spontaneous regression is very rare.

Optic nerve and optic chiasm

Radiation optic neuropathy may cause unilateral or bilateral loss of vision [20]. Two types of optic neuropathy have been described, both believed to be mainly due to vascular injury : (1) anterior ischemic optic neuropathy and (2) retrobulbar optic neuropathy. The first type affects the nerve head, giving rise to funduscopic changes, while the latter type affects the more proximal part of the nerve. Both types may cause visual field defects, such as nerve fiber bundle defects, central scotomas, altitudinal defects and generalized constriction. Damage of the endothelial cell lining of small vessels is assumed to be the causal factor. The resulting histopathologic changes include vessel wall thickening, thrombosis and luminal occlusions. This gives rise to ischemia, edema and cell death in the surrounding nervous tissue. A direct demyelination of the nerve due to the radiation has also been described. Loss of myelin results in dysfunction, visual impairment and optic atrophy. In summary, the vasa nervorum and the oligodendroglia are the targets of optic radiation injury. The occurrence frequency of optic neuropathy is dependent on the total dose and the daily fraction size, with a latency period between 12 and 48 months. The daily radiotherapy fraction size influences more the dose-response curves than the total dose, age or previous administration of chemotherapy. The product of the total dose and the dose per fraction is considered to be a good predictive parameter. The incidence of neuropathy for doses between 50 and 60 Gy (2 Gy daily fractions) is lower than 10 %. Therefore, a dose limit of 60 Gy is

often reported. Treatment of radiation-induced neuropathy includes the administration of corticosteroids, anticoagulative medication, anti-oxidants and hyperbaric oxygen [21]. Optic nerve sheath fenestration has also been described [22]. However, the succes rates of these treatments are very low.

Other organs

Other organs that may be affected by radiation treatment for ethmoid sinus tumors include the oro- and nasopharyngeal mucosa (mucositis), the pituitary gland (hypothyroidism), the inner ear (otitis), the skin (erythema) and the central nervous system (cognitive disorders). For more details, we refer the reader to textbooks of radiotherapy.

3.1.6 References

1. Harsberger H. Handbook of Head and Neck Imaging. 2nd ed. Mosby 1995;339-95.

2. Gray H. Gray's Anatomy. 38th ed. Churchill Livingstone 1995;595-7.

3. Tominaga S, Oshima A. Cancer mortality and morbidity statistics. Japan and the world-1999. Monograph on cancer research no.47, Japan Societies Press, 1999, Tokyo, Japan.

4. Coebergh JWW, van der Heijden LH, Janssen-Heijnen MLG. Cancer incidence and survival in the Southeast of the Netherlands 1955-1994. A report from the Eindhoven Cancer Registry. IKZ Comprehensive Cancer Centre South. 1995, Eindhoven, The Netherlands.

5. Health Council of the Netherlands: Dutch Expert Committee on Occupational Standards (DECOS) Wood dust. Rijswijk: Health Council of the Netherlands. 1998, publication no. 1998/13WGD.

6. Health Council of the Netherlands: Hardwood and softwood dust; evaluation of the carcinogenicity and genotoxicity. The Hague: Health Council of the Netherlands. 2000, publication no. 2000/08OSH.

7. International Agency for Research on Cancer (IARC). Wood dust and formaldehyde. Lyon IARC, 1995:32-215 (IARC Monographs on the evaluation of carcinogenic risks to humans; vol.62).

8. Hadfield EH, Macbeth RG. Adenocarcinoma of ethmoids in furniture workers. Ann Otol Rhinol Laryngol 1971;80:699-703.

9. Klintenberg C, Olofsson J, Hellquist H, et al. Adenocarcinoma of the ethmoid sinuses. A review of 28 cases with special reference to wood dust exposure. Cancer 1984;54:482-8.

10. Robin PE, Powell DJ. Regional node involvement and distant metastases in carcinoma of the nasal cavity and paranasal sinuses. J Laryngol Otol 1980;94:301-9.

11. Ethmoid sinus. In: American Joint Committee on Cancer: AJCC Cancer Staging Manual. Philadelphia, Pa: Lippincot-Raven Publishers, 5th ed., 1997;47-52.

12. Giri SP, Reddy EK, Gemer LS, et al. Management of advanced squamous cell carcinomas of the maxillary sinus. Cancer 1992;69:657-61.

13. Le QT, Fu KK, Kaplan M, et al. Treatment of maxillary sinus carcinoma: a comparison of the 1997 and 1977 American Joint Committee on cancer staging systems. Cancer 1999;86:1700-11.

14. Fowler JF, Lindstrom MJ. Loss of local control with prolongation in radiotherapy. Int J Radiat Oncol Biol Phys 1992;23:457-67.

15. Alvarez I, Suarez C, Rodrigo JP, et al. Prognostic factors in paranasal sinus cancer. Am J Otolaryngol 1995;16:109-14.

16. Belkacemi Y, Touboul E, Meric JB, et al. Cataracte radio-induite : aspects physiopathologiques, radiobiologiques et cliniques. Cancer Radiother 2001;5:397-412.

17. Parsons J, Bova F, Fitzgerald C, et al. Severe dry-eye syndrome following external beam irradiation. Int J Radiat Oncol Biol Phys 1994;30:775-80.

18. Alberti W. Effects of radiation on the eye and ocular adnexa. In: Radiopathology. Berlin-Heidelber(Germany), Springer-Verlag, 1991;269-82.

19. Jiang G, Tucker S, Guttenberger R, et al. Radiation-induced injury to the visual pathway. Radiother Oncol 1994;30:17-25.

20. Parsons J, Bova F, Fitzgerald C, et al. Radiation optic neuropathy after megavoltage external-beam irradiation: analysis of time-dose factors. Int J Radiat Oncol Biol Phys 1994;30:755-63.

21. Glantz MJ, Burger PC, Friedman AH, et al. Treatment of radiation-induced nervous system injury with heparin and warfarin. Neurology. 1994;44:2020-27.

22. Mohamed IG, Roa W, Fulton D, et al. Optic nerve sheath fenestration for a reversible optic neuropathy in radiation oncology. Am J Clin Oncol. 2000;23:401-5.

3.2 Intensity modulated radiation therapy (IMRT)

3.2.1 IMRT : background and principles

The continuing advances in computer technology have led to major progresses in radiotherapy treatment planning systems. This translational research is mainly performed by teams of physicists, engineers and physicians. Conventional 2D techniques are now being replaced by 3D planning techniques. Three-dimensional conformal radiation therapy (3D-CRT) conforms the spatial distribution of the dose distribution of the prescribed dose to the planning target volume (PTV), i.e. an irradiation of the PTV with a minimal dose to surrounding tissues. IMRT is a form of 3D-CRT in which the radiation beams are characterized by a non-uniform intensity across the field (intensity modulated beams), enabling a higher degree of target conformity and normal tissue sparing. Several methods to deliver IMRT are investigated. Most of the clinical implementations are reported with the following three methods : (1) tomotherapy IMRT, (2) multileaf collimator (MLC) IMRT and (3) scanned beam IMRT. At the present state, IMRT for head and neck cancer is an intense topic of research and routinely implemented in very few centers, most of them academic ones. The clinical studies reported consist of very small numbers of patients, or studies where IMRT was limited to boost the primary tumor site. No results of prospective randomized trials are reported yet.

For an overview of the history of IMRT, its principles and the early clinical implementations, we refer to the textbook written by S. Webb [1] and a manuscript published by the 'Intensity Modulated Radiation Therapy Collaborative Working Group' [2].

3.2.2 IMRT at the Ghent University Hospital

Since 1996 patients are treated at GUH with IMRT by the use of an MLC. The delivery method is referred to as SMLC-IMRT (Segmental Multileaf Collimator IMRT). Other terms for this method are 'step-and-shoot IMRT' or 'multiple-static-field IMRT by MLC'. Between June 1st 1996 and December 31th 2001, 250 patients were treated with IMRT at GUH. Almost half of the patients (47 %) were treated for head and neck cancer, 44 % was treated for urologic
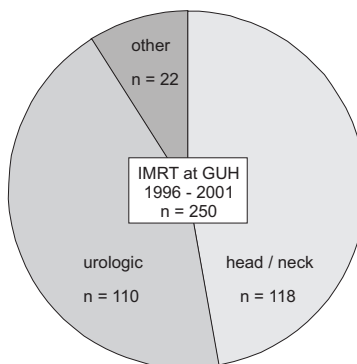
Figure 5: *Patients treated with IMRT at GUH (1996 - 2001).*

malignancies, the majority prostate cancer, and for the remaining 9 % IMRT was used to treat thoracic, abdominal and pelvic tumors.

At GUH research is focused to generate IMRT solutions for specific tumor sites [3], since many tumor sites share common challenges in terms of tumor geometry and spread, as well as for the anatomical location of the organs at risk (OARs). In such a planning approach, optimal beam incidences and planning related parameters are very similar for different patients. Machine parameters (the number of beams, the isocenter location, the gantry, couch and collimator rotations), the choice of the segmentation algorithm [4] (i.e. how segments must be shaped for each beam incidence), the objective function for plan optimization and its minimization algorithm [5][6][7] are defined up-front. This limits the domain of search for plan optimization algorithms. Such site-specific databases, further called class solutions have now been realized for various sites, including lung cancer [8][9], prostate cancer [10], pharyngeal cancer [11], oral cavity cancer [12], paranasal sinus cancer [13][14] and breast cancer [15]. A specific class solution for head and neck re-irradiations was also developed [16]. The Intensity Modulated Radiation Therapy Collaborative Working Group describes a class solution as follows [2] : "This term refers to the historical experience in designing RT plans for a particular site. Examples include breast tangents, 3-field head-and-neck plans, 4-field pelvic plans, and

so forth. Class solutions are often the starting point for optimized forward treatment planning. An IMRT class solution for a given treatment site and stage of disease consists of the criteria for optimization (the form of the objective function and values of its parameters) and the specification of the beam techniques used, typically including beam directions and number. Once developed, a class solution may be applied repeatedly to generate IMRT plans for patients with the same stage of disease at the same site and for similar clinical considerations.".

Related papers of the thesis : The IMRT planning strategy at GUH is described in the papers 1-4 of section 4 "Papers in the field of the thesis". An example of an IMRT class solution generated at GUH for oral cavity and oropharyngeal cancer is discussed in paper 5 of that section.

3.2.3   References

1. Webb S. Intensity-Modulated Radiation Therapy. Bristol (UK), Institute of Physics Publishing, 2001.

2. Intensity Modulated Radiation Therapy Collaborative Working Group. Intensity-modulated radiotherapy: current status and issues of interest. Int J Radiat Oncol Biol Phys 2001;51:880-914.

3. W. De Neve, F. Claus, P. Van Houtte, et al. Intensity modulated radiotherapy with dynamic multileaf collimators. Technology and clinical experience. Cancer Radiother. 1999;3:378-92.

4. W. De Gersem, F. Claus, C. De Wagter, et al. An anatomy based segmentation tool for intensity modulated radiotherapy of head and neck cancer. Int J Radiat Oncol Biol Phys 2001;51:849-59.

5. De Gersem W, Derycke S, Colle C, et al. Inhomogeneous target-dose distributions: a dimension more for optimization? Int J Radiat Oncol Biol Phys 1999;44:461-8.

6. De Gersem W, Claus F, De Wagter C, et al. Leaf position optimization for step and shoot IMRT. Int J Radiat Oncol Biol Phys 2001;51:1371-88.

7. Claus F, De Gersem W, Vanhoutte I, et al. Evaluation of a leaf position optimization tool for IMRT of head and neck cancer. Radiother Oncol 2001;61:281-6.

8. Derycke S, De Gersem W, Van Duyse B, et al. Conformal radiotherapy of stage III non-small cell lung cancer: a class solution involving non-coplanar intensity modulated beams. Int J Radiat Oncol Biol Phys 1998;41:771-7.

9. Derycke S, Van Duyse B, De Wagter C, et al. Non-coplanar beam intensity modulation allows large dose-escalation in stage III lung cancer. Radiother Oncol 1999;45:53-261.

10. De Meerleer GO, Vakaet LA, De Gersem WR, et al. Radiotherapy of prostate cancer with or without intensity modulated beams: a planning comparison. Int J Radiat Oncol Biol Phys 2000;47:639-48.

11. De Neve W, De Wagter C, De Jaeger K, et al. Planning and delivering high doses to targets surrounding the spinal cord at the lower neck and upper mediastinal levels: static beam-segmentation technique executed by a multileaf collimator. Radiother Oncol 1996;40:271-9.

12. F. Claus, W. Duthoy, T. Boterberg, et al. Intensity modulated radiation therapy for oropharyngeal and oral cavity tumors : clinical use and experience. Oral Oncol (in press).

13. F. Claus, L. Vakaet, W. De Gersem, et al. Postoperative radiotherapy for paranasal sinus tumours : a challenge for intensity modulated radiotherapy. Acta Oto-Rhino-Laryngol Belg 1999;53:263-9.

14. F. Claus, W. De Gersem, C. De Wagter, et al. An implementation strategy for IMRT of ethmoid sinus cancer with bilateral sparing of the optic pathways. Int J Radiat Oncol Biol Phys 2001;51:318-31.

15. V. Remouchamps, F. Claus, S. Vermael, et al. Intensity modulated radiation therapy for large breast: physical wedges versus segmented tissue compensation. Radiother Oncol 1996;56(Suppl 1):S107.

16. De Neve W, De Gersem W, Derycke S, et al. Clinical delivery of intensity modulated conformal radiotherapy for relapsed or second-primary head and neck cancer using a multileaf collimator with dynamic control. Radiother Oncol 1999;50:301-14.

3.3 IMRT for ethmoid sinus cancer

Conventional radiotherapy for ethmoid sinus cancer, either as primary treatment or in a postoperative setting, is unable to produce local control rates above 50% for T3-4 tumors [1]. Radiation doses $\geq$ 65 Gy have shown to improve survival for paranasal sinus cancer [2][3]. However, the dose the surrounding organs at risk can safely tolerate is much lower [4]. The risk of radiation induced optic neuropathy increases rapidly with doses above 60 Gy [5] and for retinopathy and lacrimal gland injury dose thresholds of respectively 45 and 40 Gy are reported [6][7]. Due to the rarity of paranasal sinus cancer and the complexity to safely irradiate these tumors to high doses, very few data are reported with respect to radiotherapy planning and delivery of these type of tumors with 3D-CRT [8][9][10] or IMRT [11][12]. We hypothesized that IMRT would allow us to customize the dose distribution to spare the optic pathways and lacrimal apparatus, and in this way increase the likelihood of uncomplicated local control [13]. Therefore, shortcomings with regard to imaging, definition of target volumes, definition of organs at risk and planning techniques had to be identified and eliminated. A protocol was designed, setting the tumor prescription dose to 70 Gy in 2-Gy fractions, while simultaneously limiting the maximal dose to the optic chiasm, optic nerves and retinae to 60 Gy. After the protocol was accepted, a strategy for planning and delivering IMRT that would meet the protocol prescriptions was investigated. The result was an IMRT class solution for ethmoid sinus cancer [14]. Between February 1999 and February 2002, 27 ethmoid sinus cancer patients were treated with IMRT at GUH.

Related papers of the thesis : The IMRT implementation strategy for ethmoid sinus cancer at GUH is described in the papers 6-7 of section 4 "Papers in the field of the thesis". Paper 8 of section 4 reports on the preliminary results

and short term toxicity profile of IMRT for 32 sinonasal cancer patients.

References

1. Gospodarowicz M, Henson D, Hutter R, et al. (eds): Prognostic factors in cancer, 2nd ed. New York, Wiley-Liss, 2001.

2. Kondo M, Ogawa K, Inuyama Y, et al. Prognostic factors influencing relapse of squamous cell carcinoma of the maxillary sinus. Cancer 1985;55:190-6.

3. Giri S, Reddy E, Gemer L, et al. Management of advanced squamous cell carcinomas of the maxillary sinus. Cancer 1992;69:657-61.

4. Jiang G, Tucker S, Guttenberger R, et al. Radiation-induced injury to the visual pathway. Radiother Oncol 1994;30:17-25.

5. Parsons J, Bova F, Fitzgerald C, et al. Radiation optic neuropathy after megavoltage external-beam irradiation: analysis of time-dose factors. Int J Radiat Oncol Biol Phys 1994;30:755-63.

6. Parsons J, Bova F, Fitzgerald C, et al. Radiation retinopathy after external-beam irradiation: analysis of time-dose factors. Int J Radiat Oncol Biol Phys. 1994;30:765-73.

7. Parsons J, Bova F, Fitzgerald C, et al. Severe dry-eye syndrome following external beam irradiation. Int J Radiat Oncol Biol Phys 1994;30:775-80.

8. Brizel DM, Light K, Zhou SM, et al. Conformal radiation therapy treatment planning reduces the dose to the optic structures for patients with tumors of paranasal sinuses. Radiother Oncol 1999;51:215-8.

9. Lohr F, Pirzkall A, Debus J, et al. Conformal three-dimensional photon radiotherapy for paranasal sinus tumors. Radiother Oncol 2000;56:227-31.

10. Tsien C, Eisbruch A, Cornblath W, et al. Results of 3 Dimensional Conformal Radiotherapy (3D XRT) for Paranasal Sinus and Nasal Cavity Tumors. (abstract annual ASCO-meeting 2001).

11. Krasin MJ, King S, Digan N, et al. Significant reduction in critical structure doses in paranasal sinus and nasopharynx patients planned with intensity modulated radiotherapy compared with 3-D conformal radiotherapy. (abstract annual ASTRO-meeting 1999).

12. Tsien C, Eisbruch A, McShan D, et al. Intensity modulated radiotherapy (IMRT) for locally advanced paranasal sinus cancer: application of clinical decisions in the planning process. (abstract annual ASTRO-meeting 2001).

13. Claus F, Vakaet L, De Gersem W, et al. Postoperative radiotherapy for paranasal sinus tumours : a challenge for intensity modulated radiotherapy. Acta Oto-Rhino-Laryngol Belg 1999;53:263-9.

14. Claus F, De Gersem W, De Wagter C, et al. An implementation strategy for IMRT of ethmoid sinus cancer with bilateral sparing of the optic pathways. Int J Radiat Oncol Biol Phys 2001;51:318-31.

4 Papers in the field of the thesis

1. W. De Neve, **F. Claus**, P. Van Houtte, S. Derycke and C. De Wagter. Intensity modulated radiotherapy with dynamic multileaf collimators. Technology and clinical experience. Cancer Radiother 1999;3:378-92.

2. W. De Gersem, **F. Claus**, C. De Wagter and W. De Neve. An anatomy based segmentation tool for intensity modulated radiotherapy of head and neck cancer. Int J Radiat Oncol Biol Phys 2001;51:849-59.

3. W. De Neve, **F. Claus**, W. Duthoy, G. De Meerleer and C. De Wagter. Intensity modulation techniques for improvement of normal tissue tolerance. Front Radiat Ther Oncol Basel Karger 2001;37:163-73.

4. **F. Claus**, W. De Gersem, I. Vanhoutte, W. Duthoy, V. Remouchamps, C. De Wagter and W. De Neve. Evaluation of a leaf position optimization tool for IMRT of head and neck cancer. Radiother Oncol 2001;61:281-6.

5. **F. Claus**, W. Duthoy, T. Boterberg, W. De Gersem, J. Huys, H. Vermeersch and W. De Neve. Intensity modulated radiation therapy for oropharyngeal and oral cavity tumors : clinical use and experience. Oral Oncol 2002;in press.

6. **F. Claus**, L. Vakaet, W. De Gersem, M. Lemmerling, I. Vanhoutte, S. Vermael, R. Van Severen, B. Van Duyse, H. Vermeersch, M. Moerman and W. De Neve. Postoperative radiotherapy for paranasal sinus tumours : a challenge for intensity modulated radiotherapy. Acta Oto-Rhino-Laryngol Belg 1999;53:263-9.

7. **F. Claus**, W. De Gersem, C. De Wagter, R. Van Severen, I. Vanhoutte, W. Duthoy, V. Remouchamps, B. Van Duyse, L. Vakaet, M. Lemmerling, H. Vermeersch and W. De Neve. An implementation strategy for IMRT of ethmoid sinus cancer with bilateral sparing of the optic pathways. Int J Radiat Oncol Biol Phys 2001;51:318-31.

8. **F. Claus**, T. Boterberg, P. Ost and W. De Neve. IMRT for sinonasal cancer: short term toxicity profile for 32 patients. (submitted).

9. **F. Claus**, T. Boterberg, P. Ost, J. Huys, H. Vermeersch, S. Braems, K. Bonte, M. Moerman, C. Verhoye and W. De Neve. Postoperative radiotherapy for adenocarcinoma of the ethmoid sinuses: treatment results for 47 patients. (submitted).

4.1 Intensity modulated radiotherapy with dynamic multileaf collimators. Technology and clinical experience. W. De Neve, F. Claus, et al. Cancer Radiother 1999;3:378-92.

topics discussed :	→ the history of IMRT
	→ the principles of IMRT
	→ the initial clinical experience
key question : What is IMRT ?	

paper 4.1

Intensity modulated radiotherapy with dynamic multileaf collimators.
Technology and clinical experience

Wilfried De Neve[1], Filip Claus[1], Paul Van Houtte[2], Sylvie Derycke[1] and
Carlos De Wagter[1]

[1]Division of Radiotherapy
Ghent University Hospital

[2]Department of Radiotherapy
Institute Jules Bordet, Brussels

Abstract

Since early 1997, dynamic multileaf collimators (DMLCs) are used in our division, for intensity modulated radiotherapy (IMRT). We have used IMRT to i) irradiate concave targets (head and neck, paraspinal tumors); ii) combine beams with shallow hinge angles (mediastinum, lung tumors); and iii) deliver intentionally inhomogeneous dose distributions (prostate, paranasal sinuses, brain tumors). IMRT is now our standard treatment for locoregional relapse (after high-dose radiotherapy) of head and neck cancer and for radical treatment of localized prostate cancer. For a variety of other tumors, conventional 3D-plans are compared with IMRT-plans, the latter being clinically implemented if superior.

We developed a geometry based IMRT planning strategy to create assemblies of static intensity modulated (IM)-beams which consist of uniform (unmodulated) segments. By a translator program, segments are combined in a single prescription which allows delivery under computer control. Cost-containment is further improved by automation of the planning. After manual or semi-automated contouring of PTV and the organs at risk, prostate IMRT plans, based on a class solution, are generated and optimized by a computer. IMRT for pharyngeal relapses and most other tumor sites is planned semi-automatically.

IMRT replaces gradually conventional treatments in our division. Interesting dose distributions generated by IMRT allow better sparing of normal tissues with decreased acute and late toxicity and offer a window for further dose escalation.

keywords : intensity modulation, multileaf collimator

1 Introduction

Within a year of discovery, more than a century ago, x-rays were used therapeutically. Over time, many technological developments took place that aimed to improve the delivery of radiation to the tissues where it is wanted and that reduced the radiation to normal tissues. This aim, for which the modern implementations are called conformal radiotherapy, is

obviously as old as radiotherapy itself. For many decades, improvements in conformal radiotherapy were hampered by our inability to determine accurately the geometrical location of tumors. Bony landmarks, air-soft tissue edges, skin-topography or contrast (liquid, surgical clips) related to the location of the tumor were used to define roughly shaped fields. With the development of medical CT-scanners, progress in conformal radiotherapy was boosted. The 3-dimensional information given by CT was further finetuned by magnetic resonance and functional imaging. Roughly shaped fields did not fit the modern criteria of conformal radiotherapy anymore. Gantry-based linear accelerators and isocentric pedestal treatment couches offered a large window of possible beam orientations in space. Conformal radiotherapy became the issue of tightening the dose distribution to the target shape in 3D.

For long times, treatment machines were designed to deliver flat (unmodulated: the radiation fluence is practically the same over the whole cross-sectional area of the beam) and later also wedged beams. Spatial combinations of flat and wedged beams collimated to the projection of the target create a convex high-dose volume (i.e. it cannot create high-dose volumes with concave surfaces). The treatment of tumor volumes with concave surfaces by these beams would over-dose sensitive tissues in the concavities. In the 80s, Brahme demonstrated the unique potential intensity modulated (IM) beams to create homogeneous concave dose distributions [1]. Inside IM-beams, the radiation fluence (intensity) was not equal at all sites inside the field (i.e. the beam was not flat (unmodulated)) but had a value that was function of its location inside the field [16]. The concept of inverse optimization was proposed by Brahme as a possible strategy to make the design of IM-beams feasible [2]. From the work and mathematical formalisms of Brahme and others, clinicians appreciated IMRT as too complicated, unfeasible, rarely indicated, ..; low priority. IMRT remained a research topic in physics laboratories until, in 1993, Carol proposed a novel planning and delivery system (NOMOS MiMiC) capable of clinical IMRT tomotherapy [4]. Carol, being a clinician (neurosurgeon) himself, gained clinical attention with his comprehensive system and made IMRT a marketed and sales argument. This fact activated the major vendors of radiotherapy equipment who abandoned their philosophy of inertia i.e. developing and implementing new radiation technology as slow as they possibly (competitively) could. Since 1993, much happened. The 3 (remaining) major vendors developed multileaf collimator (MLC) technology capable of delivering IMRT. Smaller companies developed micro-MLCs, for which they claim IMRT capability. Now, anno 1999, delivery systems outperform the planning systems on the market i.e. MLC equipped linear accelerators are capable of delivering much more sophisticated treatments than can be efficiently designed by today's commercial general planning systems. IMRT planning research is intense. Against this background this paper aims to provide an update on the potential clinical merit of IMRT and on its applicability with MLC technology.

2 IMRT: a physicist's toy or a clinician's tool?

When we compared, for various tumor sites, IMRT plans with 3D-plans (non-modulated beams) designed by experienced planners, large advantages in favor of IMRT-plans were

---

found in the following situations: i) when the PTV featured invaginated or concave surfaces (head and neck, paraspinal tumors); ii) with restricted spatial range of "good (favorable and feasible)" beam directions (mediastinum, lung tumors); and iii) for the delivery of intentionally inhomogeneous dose distributions (prostate, paranasal sinuses, brain tumors). Each situation is discussed further.

2.1 Concave PTV surfaces

Beautiful examples of concave PTVs are found in each of the 3 subsites (figure 1) of pharyngeal cancer.

Figure 1 : Anatomical subsites of the pharynx.

Pharynx
Section Sagittale
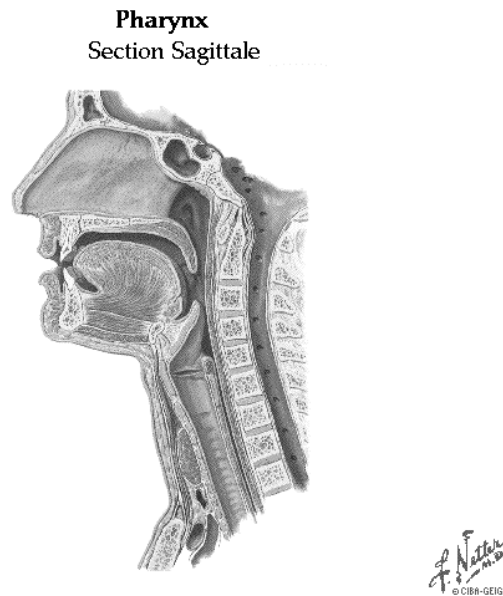
The pharynx is located anteriorly and antero-laterally from the brain stem and spinal cord. The pharynx is spaced (distance 1-2.5 cm) from these nervous structures by little more than the sphenoidal body (corpus ossis sphenoidalis) and the cervical vertebrae. As a result, brain stem and/or spinal cord are the posteriorly located organs at risk (OARs) in the irradiation of pharyngeal cancers. Superiorly (cranially), various other central nervous system (CNS) form a corona of OARs (brain, pituitary, chiasma opticum, optic nerves) that give rise to planning problems especially for nasopharyngeal tumors. Antero-superiorly, the eyes

restrict access to incoming or outgoing beam trajectories. Left and right lateral OARs are mandibular bone and parotid glands for nasopharynx and oropharynx subsites. Pharyngeal cancers show a high incidence of subclinical or clinical node metastases to many areas of the cervical lymphatic drainage system (figure 2).

Figure 2 : Regions of lymphatic drainage of the neck.
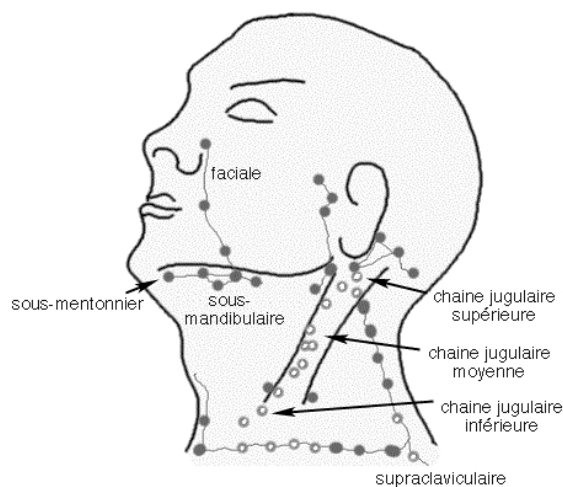
Of special concern to the radiotherapy planner are the deep jugulary chain, the retropharyngeal and posterior cervical (nasopharynx) nodes, the lateral pharyngeal recesses and the parapharyngeal space, sites being frequently invaded macroscopically. The matchline between electron and photon beams typically projects through these structures when conventional irradiation techniques are used (i. e. latero-lateral photon beams including the spinal cord, followed by shrinked photon beams (to exclude the spinal cord) complemented by postero-lateral electron beams). Because of a rapidly widening of the electron beam penumbra with depth, the conventional technique carries substantial risk for underdosage of the anatomical structures located at the deep portion of the matchline at the electron beam side. By direct or lymphatic extension, pharyngeal cancers tend to create a planning target volume that sweeps backwards, lateral to the spinal cord. The conformal irradiation of this target volume remains a technical problem that can be solved by IMRT-techniques. IMRT-techniques avoid underdosage at the deep jugulary chain, the lateral pharyngeal recesses

and the parapharyngeal space. IMRT exhibits significant potential to spare the brainstem or spinal cord. In cancers of the naso- or oropharyngeal subsites, a tumor-free distance of 1-1.5 cm is sufficient to spare the mandibular bone and one or both parotid glands. This is illustrated in figure 3.

IMRT was initially proposed as a method to create concave dose distributions and substantial literature exists. Despite years of study and the clinical need for concave dose distributions, few institutes are able to solve this challenge by IMRT. There is a need for translational research to take the physics and engineering developments into everyday practical use. A focused approach (i.e. disease-site focused translational research) is more efficient than attempts for general IMRT implementation. In this context is translational research focused on pharyngeal cancer, of high priority.

2.2 Restricted spatial range of good beam directions

This situation is encountered in mediastinal and centrally located lung tumors. Non-coplanar IMRT has been studied by our group at the R-UZG. From a pilot study [8] on 3D-planning in stage III nsclc, the basic requirements regarding favorable beam incidences were inferred :

1. Beam incidences were favorable if the angle of the beam axis with the sagittal plane of the patient was shallow. When larger angles with the sagittal plane were used, the length of the trajectory through the lungs and thus the irradiated lung volume increased rapidly.

2. From an assembly of such incidences, beams with axes in the transverse plane or entering from the cranio-lateral direction were technically executable (no linac-patient or linac-couch collisions).

When a plan is constructed by combining beams that fit the abovementioned criteria, the high-dose region shows an elongated shape in the antero-posterior direction, encompassing the spinal cord. Beam intensity modulation is efficient to push a concavity in the high-dose region at the location of the spinal cord (figure 4). When compared to non-IMRT 3D-plans, assemblies of para-sagittal IM-beams allowed 20-30% dose escalation at equitoxic levels for lung and spinal cord [9][10]. The study of the 3D dose distributions, generated by non-coplanar IMRT with para-sagittal beams reveals typically a high dose gradient (up to 50% dose increase over a distance of 1 cm) that is located at the edge of the spinal cord. Set-up errors may bring this dose gradient inside the spinal cord.

Figure 3
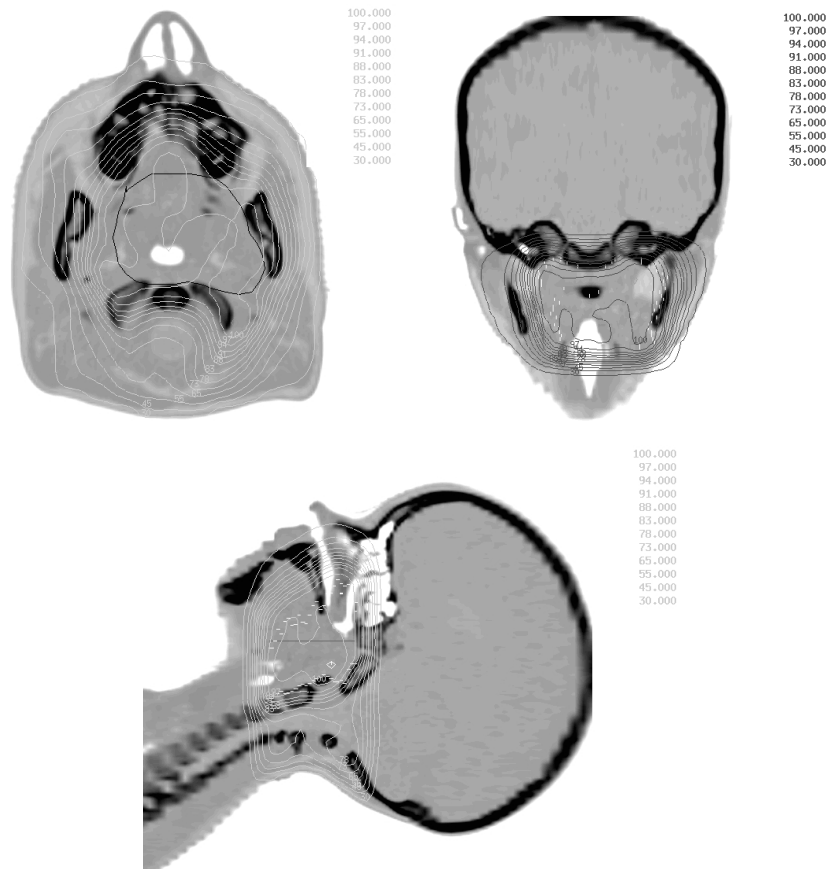
Legend : Rhabdomyosarcoma in a 7 year-old child. IMRT plan using 6 beam incidences (gantry at 45°, 75°, 165°, 195°, 285° and 315°). Relative dose distribution (isocenter dose = 100%) in a transverse (panel a: CTV contour in black), sagittal (panel b: CTV in white ticks) and coronal plane (panel c: CTV in white ticks). IMRT delivery in 13 minutes.

Figure 4


```
100.000
 97.000
 94.000
 91.000
 88.000
 83.000
 78.000
 73.000
 65.000
 55.000
 45.000
 30.000
```
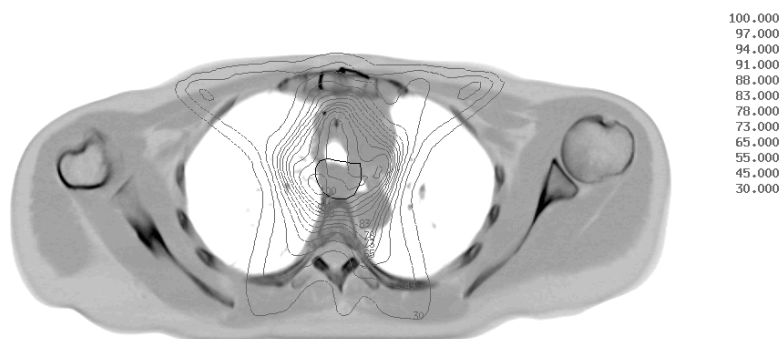
Legend : Aggressive mediastinal fibromatosis in a 50 year-old woman. Beam setup using 6 beams in a transverse plane (30°, 45°, 165°, 195°, 315°, 330°). All beams featuring (unsigned) angles with the sagittal plane ≤45°. Relative dose distribution (isocenter dose = 100%) in a transverse plane showing sparing of spinal cord (CTV contour in black line). IMRT delivery in 16 minutes.

2.3 Intentionally inhomogeneous dose distributions

The prime example of successful application of intentionally inhomogeneous dose distributions is prostate [17]. The rectal wall, in close vicinity of the posterior portion of the prostate and seminal vesicles, is dose limiting. When accounting for motion, the resulting PTV generally intersects the anterior rectal wall. The maximal homogeneous dose, that can be given to the PTV, is then directly determined by the intersected portion of the rectal wall. Escalating the dose above the rectal tolerance level can only be attempted safely to the non-intersecting PTV-part. Although this strategy has not yet been shown conclusively to produce higher cure rates, it looks promising and does seem to limit side effects [13]. Rather than attempting to repeat the published data in prostate cancer, we will focus on a planning problem with similar flavor. In ethmoid cancer, tumor edges adjacent to one or more of the numerous OARs (eyes, optic nerves and chiasm, brain stem, frontal lobes) are common. IMRT allows to irradiate with an inhomogeneous dose distribution so that at each fraction the PTV portion that intersects with or is close to the OAR(s) is slightly underdosed. If the tumor has a larger α / β than the OAR(s) (often the case if the OAR is nerve tissue), a radiobiological advantage can be exploited by the smaller fraction size at the OAR. As a result of the smaller fraction size to OARs, the tolerance dose is increased. In figure 5, panels b and c the dose gradient between optic nerves, chiasm and tumor runs through a small portion of the tumor. This example highlights a window of opportunities for therapeutic gain by altered fractionation schedules.

Figure 5
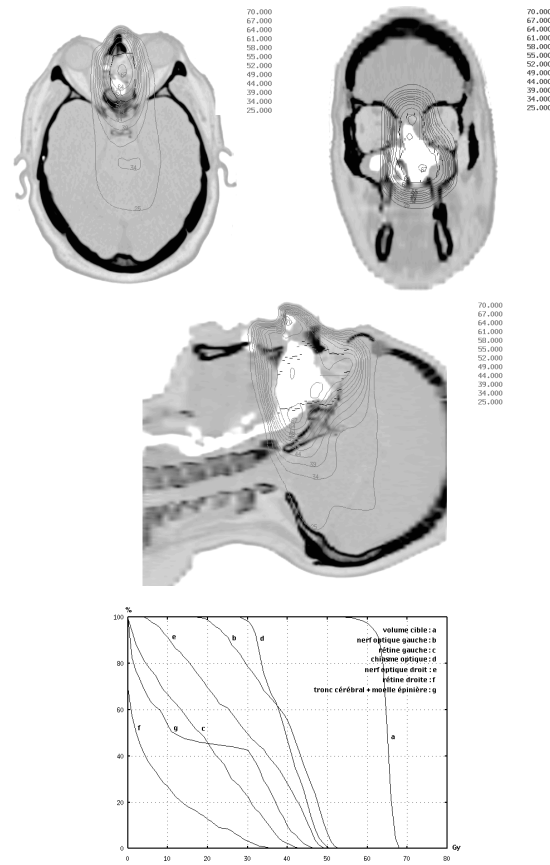
Legend : Ethmoid adenocarcinoma in a 57 year-old man. IMRT post-surgery. Five beams incidences in a sagittal plane. Absolute dose (66 Gy in 33 sessions at isocenter) distribution in a transverse (panel a), sagittal (panel b) and coronal plane (panel c). CTV contour in black. Dose-volume histograms in panel d. IMRT delivery in 12 minutes. Large air cavity is of concern as secondary electron transport was not modeled in the beam computation algorithm. Pre-clinical and in-vivo dosimetrical (subject of a follow-up paper) verification is a necessity. Adaptive measures may be needed.

## 3 Is IMRT planning synonymous to inverse planning?

It is often stated that IMRT requires inverse planning. In pure terms, inverse planning is supposed to start from the desired clinical objective of the treatment and a planning computer must calculate the requested machine parameters in order to secure the closest possible match between the desired objective and the actual treatment plan. The inverse planning systems in academic institutions, on the market or coming to the market do not have inverse planning ability in its true sense. They do little more than so called in-field optimization of fluence. They still require substantial human input in initial beam configuration (number of beams, orientation, field size, ..), which demands expert planning knowledge. The user faces a steep learning curve to be able to define a suitable objective function i.e. the mathematical form of the clinical treatment objective. To perform acceptable in-field optimization, the systems need physical surrogates (dose-volume histograms, dose ranges, hard and soft constraints on doses) or biological indices which must be properly adapted to the clinical objective. The idea promoted at commercial exhibitions, that it is sufficient to push the button of a newly available (often expensive) module to obtain a clinically useful IMRT plan, is grossly naive.

If we leave the magic kingdom of exhibitions to focus on clinical reality, we encounter two classes of methods for in-field optimization, namely bixel based (MSKCC, New York; DKFZ, Heidelberg) and geometry based (UoM, Ann Arbor; R-UZG, Gent) optimization methods.

Bixel based methods (figure 6) divide the beams in beam elements of unity size (often squares of 1.0 cm cross-sectional sides at isocenter). These cross-sectional areas form a matrix of elements called bixels (in analogy to pixels). By minimizing an objective function, a weight (intensity) is accorded to each bixel and a modulation matrix is obtained for each beam. Plans developed by bixel based planning strategies are not delivered bixel after bixel because delivery in this way would be very inefficient and dosimetrically inaccurate. An interpreter step is needed, first, to group neighboring bixels for simultaneous delivery and, second, to assign the proper weights to the bixel groups (static interpreters). If weights are assigned to transition states between consecutive bixel groups a dynamic interpreters would result. Note that, in reality, dynamic interpreters are not built in this way and the interested reader is referred to Papatheodorou [19].

Geometry based strategies define shaped in-field areas (segments) upfront (figure 7). Various segmentation methods are described [12][7][10]. Whenever possible, segment geometries are determined in a way that avoids segment patching and IM-beams typically consist of smaller segments superposed on larger segments. A weight (intensity) is accorded by minimizing an objective function [7][5]. For static delivery, geometry based strategies do not require an interpreter step as segments are delivered with the planned geometry and weight. For dynamic delivery, an interpreter must create transition sequences.

Figure 6

modulation matrix   **dynamic MLC sequence**
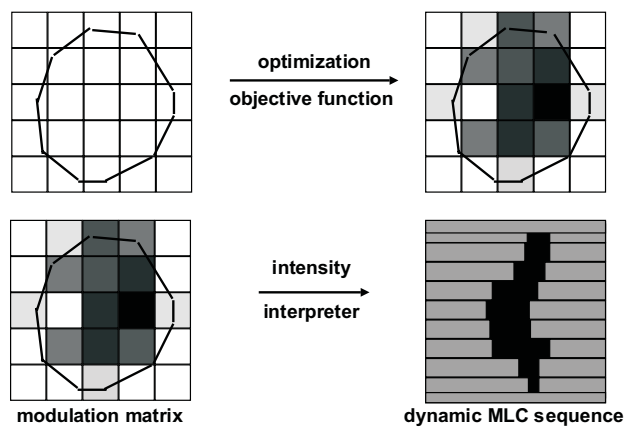
Legend : bixel-based planning. Left upper: chessboard of beam elements of unity size (bixels) projected on BEV of target (black contour). Right upper: after optimization a weight is assigned to each bixel (darkness of grey proportional to the bixel weight) to obtain a modulation matrix. Lower drawings: a (fluence) interpreter converts the modulation matrix to a sequence of MLC geometries. Each MLC geometry makes part of a machine state. In dynamic delivery, the beam is on during transitions between machine states. In step&shoot delivery, the beam is on while the system resides at a given machine state and the beam is off during transitions between machine states.

Figure 7

planification basée sur la géométrie

faisseau de MIRT : 3

segment préalablement
défini

fonction objective

optimalisation de poids
relatif du segment
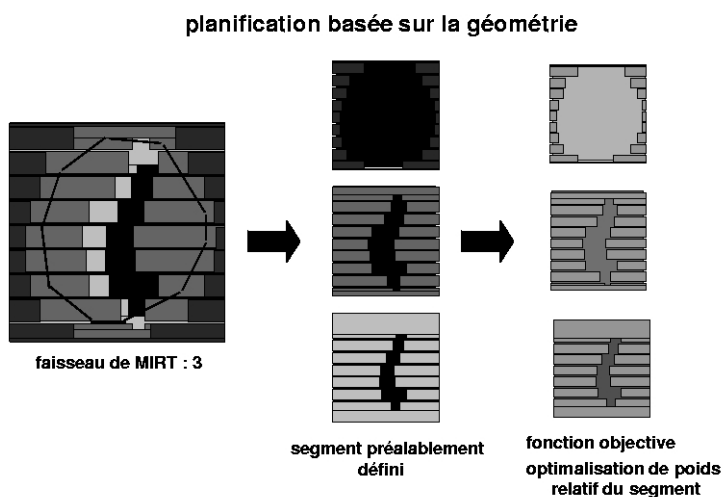
Legend : geometry-based planning. Left part: In this example, three superposed segments are defined upfront. The largest segment encompasses the BEV projection of target (black contour). Smaller segments allow to pile up intensity centrally. Middle part: geometry of each of the 3 segment. Right part: optimization assigns a weight to each segment (darkness of grey inside the MLC aperture is proportional to the segment weight). In dynamic delivery, the beam is on during transitions between segments. In step&shoot delivery, the beam is on while the system resides at a given segment and the beam is off during transitions between segments.

3.1 Bixel- and segment-weight optimization

In theory, weight optimization can be done by human trial and error, a common procedure in conventional planning [6]. If we consider the large number of weights to be assigned in IMRT planning, human trial and error methods would not be efficient. Analytical or combinatorial methods are more appropriate. For examples of analytical methods, the reader is referred to the De Neve [6] or De Wagter [11]. However, combinatorial methods are of more general interest as they can be applied to a large variety of objective functions. The problem of weight assignment (and many other optimization problems in radiotherapy) is related to a class of combinatorial optimization problems from which the "traveling salesman" dilemma is the prototype. Given a list of N cities and a means of calculating the cost of traveling between any 2 cities, one must plan the salesman's route, which will pass trough each city once and return finally to the starting point, minimizing the total cost. All exact methods known for determining an optimal route require a computing effort that increases exponentially with N, so that in practice, exact solutions can only be attempted on problems involving a few hundred cities or less. Problems where a combination with a minimal total "cost" must be found, exist in many areas as the optimal wiring of a computer chip, the optimal arrangement of rooms in a building, the best synchronization of traffic lights, the streamlining of tasks in a radiotherapy department or -our interest- finding the optimal combination of bixel- or segment-weights. A combinatorial optimization algorithm must be efficient in finding minimum (or maximum) value(s) of a function of very many independent variables [14]. This function, called the cost function or objective function, represents a quantitative measure of the "goodness" of some complex system. In our application the cost function could be a minimal dose variation in the target, a minimal absolute dose at normal tissues, a combination of dose variables or -more interesting- biological endpoints as discussed further. Our "complex system" consists of a large number of patient (anatomy, tissue electron density, ..) and machine (number of beams and for each beam, positions of gantry, collimator, leafs (84 in our multileaf collimator), wedges, beam energy, couch x, y, z and isocenter) related variables. Each of the machine variables can assume a number of values (e.g. 359 for gantry rotation, 3250 for each leaf etc.). Each possible combination of all these variables is called a discrete state. It is easy to understand that the number of possible discrete states is extremely large for any radiotherapy plan. Mathematical estimates show that finding the true minimum of the objective function will, with the present computing power, take truly astronomical times. As a matter of fact, the true minimum of the mathematical objective function may not be feasible physically (e.g. optimization must respect the physical feasibility e.g. weights must be ≥ 0; no collision of machine components).

To obtain realistic minimization times two measures are taken: 1) a large number of machine variables are fixed upfront to reduce the number of possible discrete states and 2) approximative optimization is allowed i.e. other solutions than the discrete state that represents the true minimum of the objective function may be accepted. Minimization methods themselves are not the topic of this paper and the interested reader is referred to the marvelous book "The Physics of Conformal Radiotherapy IOP, Bristol and Philadelphia" of Webb.

3.2 The choice of the objective function.

Physicians as well as physicist must understand objective functions in order to use optimization tools efficiently. The choice of the objective function depends from i) the goals of optimization; ii) the type and number of parameters to be optimized; iii) the number of PTV(s) and OAR(s); iv) the complexity of the initial setup; v) other factors e.g. computing power, minimization algorithm. Defining objective functions is as much a learning process as the upfront definition of machine parameters mentioned earlier. Optimization problems that involve only a single PTV and OAR, can be efficiently solved by minimizing simple physical objective functions [11] as:

$$F = A. \sum_{i=1}^{i=n} \left(D_{PTV,i} - D_{PTV} \right)^2 + \sum_{i=1}^{i=m} D_{OAR,i}$$

where $D_{PTV,i}$ is the dose at voxel i of the PTV, D_{PTV} the wanted dose at (all n voxels) of PTV and $D_{OAR,i}$ the dose at voxel i of the OAR. A is a ponderation coefficient that allows to scale the relative importance of deviations from D_{PTV} versus deviations from zero dose at the OAR. The minimal value of F is zero and this occurs if 2 criteria are met: first, for all voxels inside PTV, the dose must be equal to the wanted dose D_{PTV} and second, for all voxels inside the OAR, the dose must be zero. In reality, this ideal can never be reached but it is the task of the minimization algorithm to adjust weights of bixels or segments so that the value of F becomes the minimal, physically possible value. With multiple PTVs and OARs, this type of objective functions becomes rapidly unpracticable. First, the determination of the optimal ponderation coefficients for each PTV and OAR becomes an optimization problem in itself. Second, to obtain an acceptable dose distribution, the radiotherapist must often allow that the dose to one or more OAR(s) reach the level of tolerance. Simple physical terms, as in the above formula, are not appropriate for setting limits to dose levels that are allowed in each OAR. Terms which provide a biologically relevant estimation of OAR toxicity are more appropriate. Similarly, the planner must sometimes exploit inhomogeneous dose distributions. Biological models have been developed that score the advantage or disadvantage of given inhomogeneous PTV and OAR dose distributions.

We tend to use biological terms like Tumor Control Probability (TCP) [20] and Normal Tissue Complication Probability (NTCP) [18][15][3] in most objective functions, typically with a form like:

$$B = \prod (TCP_{PTV})^{a_{PTV}} . \prod (1 - NTCP_{OAR})^{b_{OAR}}$$

Ponderation is done by an exponent a_{PTV} for each PTV and an exponent b_{OAR} for each OAR. Biological indices as TCP and $1 - NTCP$ are treshold-sigmoid with dose. This shape of the dose-effect curve contributes to the robustness of optimization i.e. optimization is not much influenced by small variations of the ponderation exponents. In our experience, robustness was also observed with regard to inter-patient anatomical variations. Once a planner has found a fine set of ponderation exponents for a given tumor site, the set was useful for other patients in a class solution. Optimization with a biological objective function often leads to inhomogeneous target-dose distributions. Most radiotherapists and radiation physicists have been trained with the dogma of homogeneous doses (i.e. target-dose homogeneity

---

Filip Claus

was an obligatory goal of plan optimization) and try to avoid inhomogeneous target-doses. A large burden of the clinical experience has been gained with the use of homogeneous target-doses. Therefore, we like to limit target-dose inhomogeneity by incorporating a physical term in the objective function. The resulting biophysical objective function is the product of a biological factor B and a physical factor F. A typical F is given by

$$F = \left(\frac{d_{min}}{d_{max}}\right)^a \cdot \left(\frac{d_{mean}}{SD}\right)^b$$

where d_{min}, d_{max}, d_{mean} and SD were the minimum, maximum, mean and standard deviation of the doses at PTV. The first term of F affects primarily the dose difference between hot and cold spots in PTV. The second term allows to manipulate the dose inhomogeneity more globally by involving SD as a measure of dispersion of the dose around the mean. The exponent-values a and b are determined during development of the class solution.

For efficient optimization the objective function must be adapted to the nature of the problem. Therefore, the optimization software must provide sufficient freedom regarding the choice of the objective function. Sufficient freedom was not guaranteed in the systems that I have seen in commercial exhibitions.

3.3 Interpreters, translators and sequencers.

As described earlier, bixel-based planning strategies result in a modulation matrix for each beam. An interpreter is needed to create machine-instruction files, which drive the linac-MLC to deliver IM-beams with the planned modulation matrix. Since the physical properties of groups of bixels are different from those of individual bixels and since the grouping pattern is unknown during optimization and has to provide machine-executable geometries, accurate interpreting is a difficult (physically impossible?) task. In practice, interpreting is approximative. Therefore, the machine-instruction file(s) are transferred to a performant 3D-planning system to recalculate the plan (i.e. to verify i) if, for each beam, the delivery sequence results in a modulation matrix that is close enough to the planned one and ii) if, for the whole treatment, the delivery sequence results in a dose distribution that is compatible with the planned one). Re-optimization or other adaptive measures must be possible if necessary.

Geometry-based planning strategies create a number of segments for each beam incidence. A translator groups segments by beam incidence, puts them in an order that secures the fastest possible delivery (sequencing) and creates the machine-instruction files to drive the linac-MLC. In general, a translator is far more easy to program than an interpreter.

Interpreters and translators are the subject of intense research. They are the achilles heel of commercial IMRT planning systems and modules. Upon negotiation with planning vendors who demonstrate to you a beautiful dose distribution, the 5 Euro question (European equivalent of the "5-dollar question") is: Can you write the instruction files for my linac, transfer and execute them? Only if the vendor demonstrates you that the answer is yes, you have to solve the problem of verifying the delivered dose distribution. Upon asking the 5 Euro question, I have been left in solitude, have received looks of disguise or -rarely- was invited to the bar for a drink.

section 4

The machine-instruction file determines the mode of delivery i.e. dynamic or step&shoot (if the linac-MLC supports both modes of delivery). Therefore we distinguish between step&shoot and dynamic interpreters. Similarly, one can distinguish between step&shoot [7] and dynamic translators. A dynamic translator is a close relative to an interpreter, the difference being the use of a geometry-based modulation map (instead of a bixel-based modulation map).

4 Dynamic or step and shoot modes of MLCs

The 3 large linac vendors modified the steering software of their MLCs to support IMRT. To provide insight, the steering mechanism of one of the systems (Elekta DMLC, figure 8a) is described.

A prescription (machine-instruction file) of an IM-beam consists of a series of control points and the total number of monitor units (MUs) for the IM-beam. Each control point defines a machine state (gantry angle, collimator angle, MLC leaf positions, diaphragm positions, etc) of the linac and the fraction of the total (IM-beam) MUs that must have been delivered when the machine terminates the transition from the previous to the actual control point. In the example of figure 8, control points k and k+1 differ with regard to their MLC leaf positions. In dynamic mode, the leaf positions defined by control point k move to the positions defined by control point k+1 while a fraction n-m of the total IM-beam MUs is delivered. This transition is slaved by the MU counter except when the build-in pause mechanism, that stops irradiation, is enabled. This happens if the control software detects that the required MU fraction (n in the example) has been delivered before one or more machine component(s) have reached the positions prescribed by the control point k+1. While the beam pauses, all machine components are allowed to reach the positions prescribed by the control point. If the prescribed positions are reached within a preset time (15 seconds on the R-UZG linacs), counted from the onset of the pause, the beam restarts automatically. The pause mechanism allows the user to force the system into an "autonomous step-and-shoot" mode as illustrated in figure 8b. First each machine state is duplicated to create an IM-beam that contains of a series of twins of (identical) machine states. Control points are created by assigning a fraction of MUs to each machine state. The first member of each twin is assigned a fraction of MUs that is identical to that of the previous control point (that has a different machine state). The second member of each twin is assigned an incremented fraction of MUs, the increment being defined by planning. Such series of control points will force the system in an "autonomous step-and-shoot" mode as the system will perform transitions between consecutive non-identical machine states while delivering zero additional dose.

5 Cost-containment and class solutions

Computer controlled linacs with dynamic or step&shoot MLCs allow us to deliver IM-beams

in little more time than required for unmodulated beams. Typical treatment slots (patient positioning + treatment delivery) at the R-UZG linacs vary from 10 minutes for prostate (3 beam incidences; 10-15 segments) to 20 minutes for large head and neck relapses (6 beam incidences; 30-40 segments). We expect that, by the end of 1999, the delivery part of the treatment time will have been halved. In general we can point out that dynamic delivery is more time-efficient than step&shoot, the difference being most important for highly modulated beams. The user has to consider increased efficiency of dynamic operation against the lower complexity and cost of quality assurance for step&shoot operation. Hybrids, taking the form of "interrupted dynamic sequences (unpublished)" seem an attractive compromise. Planning remains a major cost issue. Accurate contouring of PTV(s) and AOR(s) in thin adjacent slices is required. For organs with parallel functional units, the whole organ must be contoured if biological or dose-volume related indices of organ toxicity are used in optimization. At R-UZG, contouring for IMRT planning varies between 1 hour (for prostate) to a whole day in some head and neck cancers (paranasal sinuses, pharyngeal with nodes). For the latter cases, help from diagnostic radiology or magnetic resonance experts is often asked. There seems little hope on the horizon that robust algorithms will soon allow full automatic contouring. Defining suitable beam incidences for IMRT is a new problem. In our experience, the search for good beam incidences, one by one by means of the BEV-tool available in most 3D-planning systems is not very helpful. This can be understood as follows: An IM-beam features a pattern of peaks and valleys (respectively high and low) of intensity. Peak intensities irradiate primarily the PTV while the OARs are spared by intensity valleys. When using IM-beams from different directions, dose integration from peaks and valleys assures selective build-up of dose in the PTV. Various types of dose integration occur over the PTV (i.e. integration regions consisting of a few peaks; of less peaks complemented by some valleys or of very many valleys). The different beam orientations must allow such integration pattern to occur. Beam orientations are highly interdependent and a good IMRT beam incidence is as much a function of the incidences of other beams than of the projection of PTV and OARs in its BEV.

Figure 8
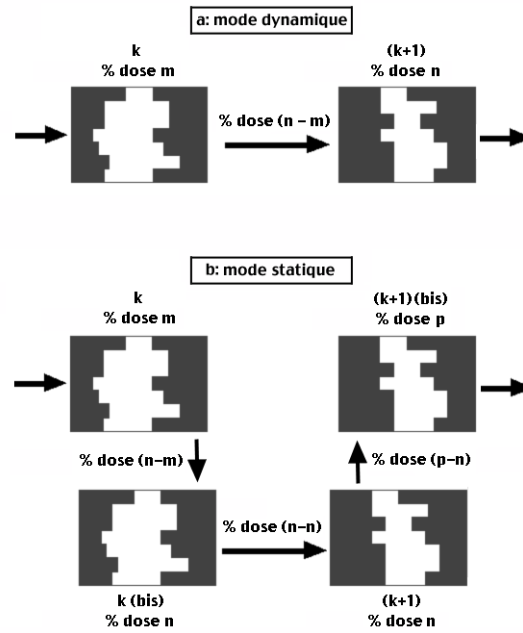
Legend

a : Elekta DMLC: prescription for dynamic delivery. Sequence of control points from which k and k+1 are two members. To control points k and k+1, m% and n% of the total dose for the sequence is assigned. During transition from k to k+1, a dose equal to (n-m)% of the total dose for the sequence is delivered.

b : Elekta DMLC: prescription for step&shoot delivery. The control points k and k+1 are duplicated. The duplicates are k(bis) and (k+1)bis. The fraction of the total (sequence) dose assigned to k(bis) (n%dose) is larger than m%dose assigned to k. So, that dose (n-m)%dose is delivered during the transition from k to k(bis). This also happens for k+1 and (k+1)bis. The consecutive, non-identical control points k(bis) and k+1 are assigned identical fractions of the total dose, in this example n%dose. As a result ((n-n)%dose), that is no dose, is delivered during the transition. The beam-pauze mechanism is enabled to allow the transition without dose delivery.

At R-UZG, planning studies involving 10-30 (virtual) patients, are performed to search for optimal beam sets. This search is tumor site specific because many tumor sites share common challenges in terms of tumor geometry and anatomical location of organs at risk. Geometrical features of planning (like the optimal beam incidences) are often very similar for different patients. In this is the case, the upfront definition in planning protocols of various machine parameters is attractive because the number of discrete states and thus the domain of search for plan optimization algorithms decreases. Our approach is to develop, tumor site specific databases that contain the best set of IMRT planning parameters that we could find. These include machine parameters (number of beams and for each beam the isocenter location, the gantry, couch and collimator rotations); the choice of the segmentation algorithm (i.e. how segments must be shaped for each beam incidence); the objective function for plan optimization and its minimization algorithm. Such data bases, further called class solution databases have been realized for prostate cancer and pharyngeal tumor relapses. The information and instructions in the database, and the anatomical information of the patient are of such nature that they can be used by a class solution planning engine (claplan) to create, under computer control, the IMRT plan by a 3-step procedure. By the first step claplan uses the beam's eye view (BEV) of target(s) and organ(s) at risk to make an assembly of beam segments for each beam incidence. By the second step points are randomly seeded throughout all PTVs and OARs (normally 1,000 points per contoured structure). Using unity weight as a start value, the dose contributed by each segment is calculated for each point. By the third step, each segment-weight is iteratively adjusted to minimize the objective function. The IMRT-plan is then evaluated using isodose displays and dose-volume histograms. If the plan is accepted, a translator writes the machine-instruction files for the linac-MLC. If the plan does not pass the evaluation, adaptive measures are taken. Such adaptive measures are still largely interactive and involve, amongst other, tools to display inappropriately dosed regions in target(s) or OAR(s). Based on the BEV of such regions, existing segments are re-shaped or new segments are created. The second and third step of claplan are executed again. Starting from PTV and OAR contours, prostate plans are generated in about 2 minutes of human time (i.e. time that the planner must do something) and less than 1 hour of CPU time (DEC alpha 3000).

6 Conclusions

In a number of clinical situations, IMRT adds substantially to spare normal tissues. IMRT provides a window for dose escalation and, hopefully, improved local control. Dynamic and step&shoot MLCs on the market are performant tools for IMRT. This is not the case for planning where substantial research is needed. Clinicians and physicians face an intense learning process. Planning and treatment cost will not remain an obstacle for clinical IMRT because cost can be highly reduced by automation.

Acknowledgements

References

1. Brahme A, Roos JE, Lax I. Solution of an integral equitation encountered in rotation therapy. Phys Med Biol 1982;27:1221-9.

2. Brahme A. The inverse problem approach to treatment plan optimization. Proceedings of the 3-D Radiation Treatment Planning and Conformal Therapy Symposium. Session 1. Saint Louis: Washington University; 1993.

3. Burman C, Kutcher G, Emami B, et al. Fitting of normal tissue tolerance data to an analytic function. Int J Radiat Oncol Biol Phys 1991;21:123-35.

4. Carol MP. Integrated 3-D conformal planning/mutivane intensity modulating delivery system for radiotherapy. Proceedings of the 3-D Radiation Treatment Planning and Conformal Therapy Symposium. Session 6. Saint Louis: Washington University; 1993.

5. De Gersem W, Derycke S, Colle C, et al. Inhomogeneous target-dose distributions: a dimension more for optimization? Int J Radiat Oncol Biol Phys 1999;44:461-8.

6. De Neve W, De Wagter C, De Jaeger K, et al. Planning and delivering high doses to targets surrounding the spinal cord at the lower neck and upper mediastinal levels: static beam-segmentation technique executed by a multileaf collimator. Radiother Oncol 1996;40:271-9.

7. De Neve W, De Gersem W, Derycke S, et al. Clinical delivery of intensity modulated conformal radiotherapy for relapsed or second-primary head and neck cancer using a multileaf collimator with dynamic control. Radiother Oncol 1999;50:301-14.

8. Derycke S, Van Duyse B, Schelfhout J, et al. Limits of dose escalation in lung cancer: a dose-volume histogram analysis comparing coplanar and non-coplanar techniques. In: Conformal Radiotherapy: Physics, Treatment Planning and Verification. Belgian Hospital Physicist Association Gent; 1995:209-16.

9. Derycke S, Van Duyse B, De Wagter C, et al. Non-coplanar beam intensity modulation allows large dose-escalation in stage III lung cancer. Radiother Oncol 1999;45:253-61.

10. Derycke S, De Gersem W, Van Duyse B, et al. Conformal radiotherapy of stage III non-small cell lung cancer: a class solution involving non-coplanar intensity modulated beams. Int J Radiat Oncol Biol Phys 1998;41:771-7.

11. De Wagter C, Colle C, Fortan L, et al. 3D-conformal intensity modulated radiotherapy planning: interactive optimization by constrained matrix inversion. Radiother Oncol 1998;47:69-76.

12. Eisbruch A, Marsch LH, Martel MK, et al. Comprehensive irradiation of head and neck cancer using conformal multisegmental fields: assessment of target coverage and noninvolved tissue sparing. Int J Radiat Oncol Biol Phys 1998;41:559-68.

13. Garnick MB, Fair WR. Combatting prostate cancer. Sci Am 1998;279:74-83.

14. Kirckpatrick S, Gelatt CD, Vecchi MP. Optimization by simulated annealing. Science 1983;220:671-80.

15. Kutcher G, Burman C. Calculation of complication probability factors for non-uniform normal tissue irradiation: the effective volume method. Int J Radiat Oncol Biol Phys 1989;16:1623-30.

16. Lax I, Brahme A. Rotation therapy using a novel high-gradient filter. Radiology 1982;145:473-8.

17. Ling CC, Burman C, Chui C, et al. Conformal radiation treatment of prostate cancer using inversely-planned intensity-modulated photon beams produced with dynamic multileaf collimation. Int J Radiat Oncol Biol Phys 1996;35:721-30.

18. Lyman J. Complication probabilities as assessed from dose-volume histograms. Radiat Res 1985;104(Suppl.):513-9.

19. Papatheodorou S, Rosenwald JC, Castellanos ME, et al. The use of multileaf collimator for the generation of intensity-modulated beams. Cancer Radiother 1998;2:392-403.

20. Webb S, Nahum AE. A model for calculating tumour control probability in radiotherapy including the effects of inhomogeneous distributions of dose and clonogenic cell density. Phys Med Biol 1993;38:653-66.

4.2 An anatomy based segmentation tool for intensity modulated radiotherapy of head and neck cancer. W. De Gersem, F. Claus, et al. Int J Radiat Oncol Biol Phys 2001;51:849-59.

topics discussed :	→ an IMRT planning platform
	→ an IMRT segment generation tool
	→ an IMRT head and neck example case
key question : How to generate intensity modulated beams ?	

paper 4.2

An anatomy based beam segmentation tool for intensity modulated radiation therapy and its application to head and neck cancer

Werner De Gersem, Filip Claus, Carlos De Wagter and Wilfried De Neve

Division of Radiotherapy
Ghent University Hospital

Abstract

Purpose: In segmental intensity modulated radiation therapy (IMRT), the beam fluences result from superposition of unmodulated beamlets (segments). In the inverse planning approach, segments are a result of "clipping" intensity maps. At Ghent University Hospital, segments are created by an "anatomy based segmentation tool (ABST)". The objective of this paper is to describe ABST.

Methods and Materials: For each beam direction, ABST generates segments by a multi-step procedure. During the initial steps, beam's eye view (BEV) projections of the planning target volumes (PTVs) and organs at risk (OARs) are generated. These projections are used to make a segmentation grid with negative values across the expanded OAR projections and positive values elsewhere inside the expanded PTV projections. Outside these regions, grid values are set to zero. Subsequent steps transform the positive values of the segmentation grid to increase with decreasing distance to the OAR projections and to increase with longer pathlengths measured along rays from their entrance point through the skin contours to their respective grid point. The final steps involve selection of iso-value lines of the segmentation grid as segment outlines which are transformed to leaf and jaw positions of a multileaf collimator (MLC). Segment shape approximations, if imposed by MLC constraints, are done in a way that minimizes overlap between the expanded OAR projections and the segment aperture.

Results: The ABST procedure takes about 3 seconds/segment on a Compaq Alpha XP900 workstation. In IMRT planning problems with little complexity as laryngeal (example shown) or thyroid cancer, plans that are in accordance with the clinical protocol can be generated by weighting the segments generated by ABST without further optimization of their shapes. For complex IMRT plans like paranasal sinus cancer (not shown), ABST generates a start assembly of segments from which the shapes and weights are further optimized.

Conclusions: ABST is a fast procedure to generate a set of segments for IMRT planning. The plan is finalized by assigning weights to the segments or by direct optimization of segment shapes and weights. ABST allows us to avoid the step of translating optimized intensity maps to sequences of segments.

Keywords: IMRT, anatomy based beam segmentation

1. Introduction

In segmental intensity modulated radiation therapy (IMRT), the beams are composed of

multiple static fields (segments). Segmental IMRT is routinely used at Ghent University Hospital (GUH) to treat head and neck cancer. At GUH, segments shapes are obtained by an "anatomy based segmentation tool (ABST)". ABST derives the shape of segments directly, i.e. without dose computation, from the beam's eye view (BEV) projections of the planning target volumes (PTVs) and organs at risk (OARs). ABST is programmed as a UNIX command, routinely used during the IMRT planning process as shown in figure 1.

Figure 1
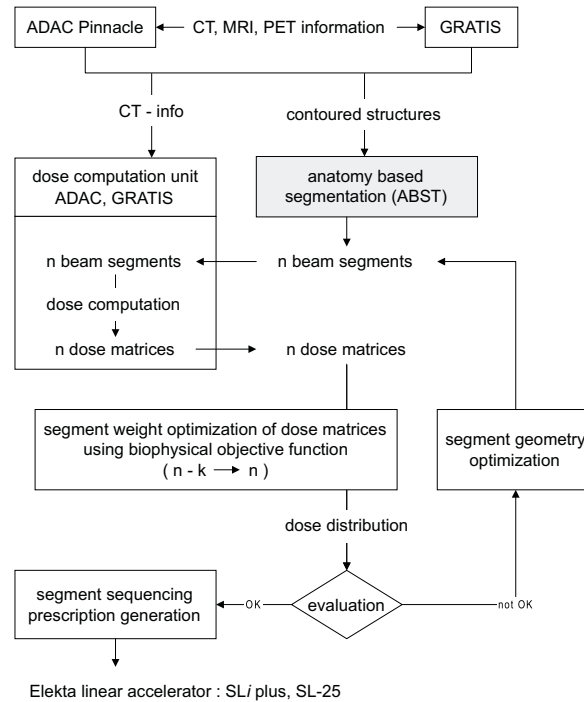
Legend : Chart describing the planning platform used at Ghent University Hospital for IMRT planning. The top of the chart shows that medical images from various sources (PET, MRI, CT) are used to obtain contoured structures related to CT-scan slices taken in treatment position. Two 3D-planning systems - ADAC Pinnacle and George's RAdioTherapy desIgn System (GRATIS) - can be used to provide planning CT-information, contoured

structures and a shoebox, defining the size and resolution of a voxel matrix for dose computation, to the IMRT planning platform. For each segment generated by the Anatomy Based Segmentation Tool (ABST), a unity weighted dose voxel matrix is computed. All matrices are made available to the IMRT planning platform for segment weight optimization. Weight optimization tends to decrease the number of segments by assignment of a zero weight to some segments (figure 1: n-k -> n where n is the number of segments of the plan which are decreased by k if, during weight optimization, k segments receive zero weights). The resulting dose distribution is evaluated and if it meets the clinical objectives, the segment sequence with minimal delivery time is generated and transferred to a linear accelerator. If the dose distribution fails to meet the objectives, an iteration that involves segment geometry optimization [20] is started.

The algorithm behind ABST aims at generating IMRT plans with as little as possible planner-driven trial and error, and compliance with the Elekta MLC constraints. Most segmentation methods are based on optimized intensity maps obtained by inverse treatment planning algorithms. For a review, the reader is referred to Webb [1]. Avoidance of the translation process of complex intensity maps to segment sequences is also part of the rationale behind our approach.

The anatomy based segmentation tool generates superposed segments, which after weight optimization result in intensity modulated beams. The number of superposed segments increases with decreasing distance to the OARs and with increasing pathlengths of rays measured from the skin to the isocentric plane, defined through the isocenter and perpendicular to the central axis. A user-defined avoidance margin can be specified for each OAR to account for internal motion and for patient setup inaccuracy. The method is essentially an extension of a principle described by Brahme [2] who derived that for a homogeneous irradiation of a target surrounding a critical organ, a rotational technique can be used with an increasing intensity towards the critical organ. Lax [3] and De Neve [4] have further elaborated on this principle. For a setup with fixed beam incidences and multiple PTVs and OARs, one can equally apply this principle. If critical organs are close to the PTVs and a number of beams is used to irradiate the PTVs with a flat profile, but with the overlap of critical organs and PTVs blocked, then an underdosage can be expected in the regions of the PTVs that are close to the OARs. When these underdosed regions are boosted from the incidences where this is possible without direct irradiation of OARs, the underdosage is reduced or totally removed. ABST respects this principle by creating segments close to and conformally avoiding the OARs.

The description of the algorithm behind ABST is the subject of this manuscript. To illustrate, step by step, how the algorithm defines segment outlines, the application to a clinical case of a T1N0M0 supraglottic laryngeal cancer is described in detail.

2. Methods and Materials

Anatomy based segment generation

ABST uses as input one or more PTVs, one or more OARs, the skin contours and a template beam that defines the beam incidence and isocenter, the linear accelerator, the radiation modality and energy. The tool is used for each template beam separately. A nine-step algorithm shapes the segments as follows:

1. The PTVs and OARs are projected on the isocentric plane along raylines emanating from the source. This central projection of each structure results in an area on the isocentric plane, further called a PTV- or OAR-projection. To define the outline of the largest possible segment aperture, each PTV-projection is 2D-expanded on the isocentric plane by a user-defined margin to an "expanded PTV-projection" (PTV-EP). The expansion margin accounts for penumbra. The projections of the critical structures are 2D-expanded to "expanded OAR-projections" (OAR-EPs) with user-defined exclusion margins in order to achieve a good sparing by the final dose distribution. The exclusion margins define the minimal distances in BEV between the segments and the respective OARs.

2. A rectangular segmentation grid, encompassing all PTV-EPs by a sufficiently broad margin, is formed in the isocentric plane. The pixel size of the grid is 1x1 mm^2. All pixel values are initialized to zero.

3. For each PTV, all PTV-EP pixel values are incremented by one.

4. For each OAR, all OAR-EP pixel values are decremented by five .
   A 3D-visualization of a segmentation grid, that results from steps 1-4, resembles a landscape where the BEV of an OAR-EP delineates a flat floor canyon while the BEV of a PTV-EP delineates a flat roof mesa (figure 2a).

5. All positive pixel values inside the segmentation grid are divided by $(1 + D)$, where D is the distance in centimeter of the pixel to the nearest contour point of a OAR-EP. This procedure is repeated for each OAR-EP. As a result of step 5, the roof of the mesa is remodeled. A slope is formed by the increasing grid values close to the edge of the canyon.

6. Rays are traced from the virtual source point to each pixel. Along each ray, the distance d (cm) from its entry point through the patient's surface to the isocentric plane is determined. The value of d is set to zero whenever a ray reaches the isocentric plane before entering of the patient's surface. The value of each positive pixel inside the segmentation grid is divided by its respective $(d + 1)$ value. This will result in a small segment shape dependency on the amount of forelaying tissue.

Steps 1 to 6 result in a grid from which all pixels show low values in areas of OAR-EPs and zero values outside areas of OAR-EPs and PTV-EPs. In areas inside the PTV-EPs but outside OAR-EPs, the pixel values show a profile with increasing height towards OAR-EPs (figure 2b). Figure 2c illustrates the influence of the amount of forelaying tissue.

7. The segment contours are determined from iso-value lines of the segmentation grid (figure 2c). A first set of iso-value lines encompass grid points with strictly positive values, and form the "exclusion contours". These contours encompass the parts of the PTVs that are in BEV excluding the OARs with the previously assigned exclusion margins. In figure 2c, one exclusion contour is located left from the spinal cord, the second exclusion contour is right to this critical structure. These exclusion contours contain the whole gray shaded area in figure 2c. By the subsequent steps 8 and 9, these exclusion contours will be converted to exclusion segments.

Further iso-value lines, inside the exclusion contours, are selected for the creation of smaller segments. These iso-value lines are chosen to result in segments with increasing area. The area of the smallest segments is specified by the user. Further segment areas are determined by multiplication of the area of the previous smaller segment with a factor specified by the user. For the example in figures 2c-e, a minimal area of 15 cm^2, and a multiplication factor of 1.5 was specified, resulting in segments with areas of approximately 15, 22.5, 33.8, 50.6, ... cm^2.

8. Leaves and jaws are placed by closing-in on the segment contours determined by steps 1-7. Close-in is halted whenever the contour is reached by the middle point of a leaf tip, or by a corner of a leaf tip for the uppermost and lowermost leaves, or when the leaf reaches the maximum overtravel distance. For the jaws orthogonal to the leaves, close-in is halted when any point of the jaw edge projection reaches the segment contour or when the jaw reaches the zero-position – Elekta's X-jaws are not allowed to overtravel. The backup jaws follow the widest leaf position for each leaf bank. During this step, the minimal distance-constraints of the MLC – for Elekta's MLC : 1 cm between opposed and diagonally opposed leaves – are disregarded as shown in figure 2d at the lower half of the segment. Leaf and jaw positions are rounded to a 1 mm discretization.

Steps 7 and 8 perform a tentative setting of the MLC positions. If this setting violates the MLC-constraints, leaf and jaw positions are adapted in step 9.

9. A 2D MLC-adapting grid that resembles the segmentation grid is formed. All pixel values are initialized to zero. For each PTV, all pixels inside its PTV-EP are incremented by one and for each OAR, the values of all pixels inside its OAR-EP are decremented by fifty. The integral of the MLC-adapting grid over the segment area is used as objective value during the following leaf repositioning procedure. The ex-

position, by a leaf position adaptation, of a part of a OAR-EP to primary irradiation will thereby negatively contribute to the objective value, while the extra exposition of a part of a PTV-EP will contribute positively. As a consequence leaf position adaptations away from critical organs will be favored. This is done as a single-pass two-step procedure:

(a) Field expansion to meet the constraints of minimal distances between opposed and diagonally opposed leaves:

- for all leaf pairs with interleaf distance d < 10 mm:
  - open the right leaf by (10 - d) mm and determine the objective value
  - shift the leaf pair in steps of 1 mm to the left, and determine the objective value for each possibility, the leaf pair position with the highest objective value is retained
- for all diagonally opposed leaves with interleaf distance d < 10 mm: adapt leaf positions in the same way as for opposed leaves: all possibilities with minimal total leaf repositioning distance are compared, and the highest objective value determines the set-up which is selected.

After the repositioning procedure, all MLC constraints are met. Due to the sequential repositioning method, it is not guaranteed that the adaptation is done with minimal total repositioning distance. Therefore, a field shrinking which tends to reposition leaves back towards the tentative settings of step 8 follows.

(b) Field shrinking towards the tentative settings, but without violation of the MLC constraints:

for all leaf pairs of which at least one leaf was repositioned during field expansion:

- reposition both leaves as far as possible towards position before field expansion without taking the minimal opposite leaf distance into account, but without violating the minimal diagonally - opposite leaf distance
- if the distance between the opposite leaves is less than 10 mm, then reposition these leaves again using the field expansion method for opposite leaves, as described above.

Also after field shrinking, it is not guaranteed that the leaf position adaptation is done with minimal total repositioning distance. However the method used is robust, avoids excessive distortion of the tentative leaf positions, implements MLC constraints by field expansion away from OARs, and only takes a limited amount of computation time. The result for the example case is shown in figures 2d for one segment and figure 2e for all segments of one incidence. Further fine-tuning of leaf positions can be done using leaf position optimization based on delivered dose (manuscript submitted to the Int J Radiat Oncol Biol Phys).

Figure 2
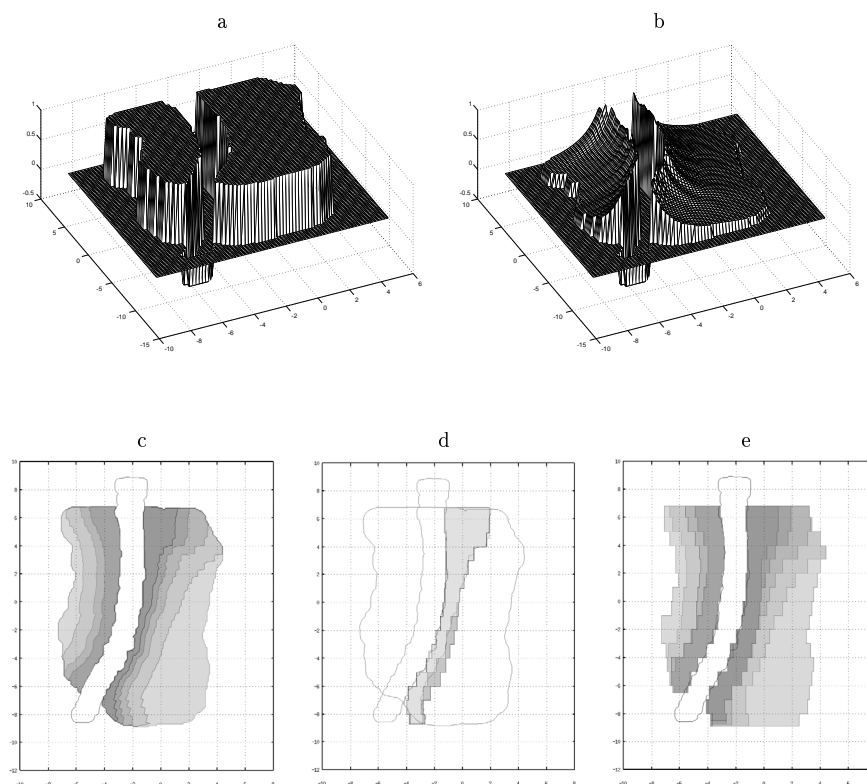
Legend : ABST: Anatomy Based Segmentation Tool. For a detailed description see materials and methods.

a. Steps 1-4 of the ABST algorithm result in a segmentation grid with the grid-values of the spinal cord-EP set to -5 and the PTV1-EP part that does not overlap the spinal cord-EP set to +1. For clarity, the grid is plotted per 2 mm and negative grid values are divided by ten in this graphical representation.

b. result obtained after execution of steps 1-6 of the ABST algorithm. For regions inside PTV1-EP but outside the spinal cord-EP, grid values increase for grid points closer to spinal cord-EP and for longer pathlengths of rays to the grid point. For clarity, the grid is plotted per 2 mm and negative grid values are divided by ten in this graphical representation.

c. after selection of iso-intensity lines as segment outlines (step 7), four segments are shaped at the left side of the spinal cord EP and five segments at the right side. Segments at the left side of the spinal cord EP have their right edge flanking the spinal cord EP. Segments at the right side of the spinal cord EP have their left edge flanking the spinal cord EP.

d. placement of leaves and jaws to collimate the smallest segment at the right side of the spinal cord EP. As a result of step 8, leaf pairs located below the zero position (horizontal midline) violate the MLC constraints (apertures between opposite and/or diagonally opposite leaves are too narrow). By step 9, all the right-bank leaves located below the zero position are moved outwards to meet the MLC constraints. Note that the lowest left-bank leaf is also moved outwards.

e. final leaf and jaw settings for all segments.

Optimization

A dose-grid file is computed for each segment with a weight of one. Dose computation is performed using the 3D-differential scatter air ratio algorithm [5] distributed with the GRATIS 3D treatment planning system [6], without corrections for tissue-density heterogeneity. The first optimization pass of the segment weights is done using constrained matrix inversion (CMI) [7], using a physical objective function. When requested by the user, a second pass of optimization of segment weights is done using a more sophisticated biophysical objective function. This objective function includes biological indices computed according to the tumor control probability (TCP) model of Webb and Nahum [8] for PTVs, according to the normal tissue complication probability (NTCP) model of Lyman, Kutcher and Burman [9][10][11] for OARs. The physical part of the biophysical objective function imposes the prescribed dose and a maximum heterogeneity to the PTVs. The function is minimized by a gradient method [12] modified to allow escape from local minima [13].

3. Results

Patient

To illustrate the function of ABST we used a case, distributed as a planning exercise by Levendag, Nowak and Wijers from the Academic Hospital Rotterdam, The Netherlands. The study case was a female patient with a T1N0M0 supraglottic laryngeal cancer. A clinical description and radiographic documents including copies of the planning CT-scan on CD-ROM were sent to a number of centers including ours. By the investigators from Rotterdam, the CTV related to the macroscopic tumor, the CTV for the elective nodal irradiation (lymph node areas II, III and IV, bilateral), both parotid glands, both submandibular glands and the spinal cord were drawn on the CT-slices. Dose prescription of 70 Gy to the primary tumor

and 46 Gy to the elective nodal regions were planning goals. Fractionation was prescribed at 2 Gy/fraction, 5 fractions/week.

Using the CTV contours, we assembled a CTV1, which included CTVs of both macroscopic tumor and elective nodal sites, and renamed the CTV of the macroscopic tumor to CTV2. CTV1 was 3D-isotropically expanded by 3 mm to form PTV1. CTV2 was 3D-isotropically expanded by 3 mm to form PTV2. The 3D-isotropical expansions were done by in-house software. For optimization and for analyzing the results, two additional PTVs were created by displacing the most superficial edges of PTV1 and PTV2 to a depth of at least 0.5 cm below the skin contours in 3D. These structures obtained from PTV1 and PTV2 are respectively called PTV1wb and PTV2wb. Dose points for optimization are seeded in these eroded volumes, in order to avoid large effects of the buildup region of the 6 MV photon segments on the value of the segment weights.

Planning software

The plan was designed for biphasic delivery. The first phase consisted of 23 x 2 Gy, planned to the PTV1. The second phase consisted of 12 x 2 Gy planned to the PTV2.

The structure of our planning platform is shown in figure 1. A class solution provided the isocenter location (XYZ-midpoint of PTV2 for both phases) and the gantry-collimator-table isocentric rotation angles for 6 beam incidences used for phase 1 and for 4 beam incidences used for phase 2. The beam incidences are drawn in figure 3. For four beams, the beam axes were located in the transverse plane. The gantry-table-collimator (GTC) angles, expressed in degrees, were G45T0C0, G75T0C0, G285T0C0 and G315T0C0 (beams 1-4 in figure 3). Two beam incidences were non-coplanar to avoid beam entry through the mentum (G30T300C55 and G330T60C300: beams 5 and 6 in figure 3). The choice of the beam incidences was the result of a search for a left-right symmetric beam setup with approximately (due to rounding of the gantry and table angles) 30° spacing of the projected beam-axes in the transverse plane (transverse plane-projected angle). Actually the transverse plane-projected angular spread of the non-coplanar beam axes is 32° with respect to each other and 29° with the respective G45T0C0 and G315T0C0 beams. The transverse plane-projected angle of beams G30T300C55 and G330T60C300 was calculated as [14]

$$\arctan\left(\frac{\cos\left(T\right).\sin\left(G\right)}{\cos\left(G\right)}\right)$$

For the second phase of treatment, which involved a 24 Gy boost to PTV2, the 4 coplanar beam incidences (G45T0C0, G75T0C0, G285T0C0 and G315T0C0 : beams 1-4 in figure 3) were used.

Figure 3
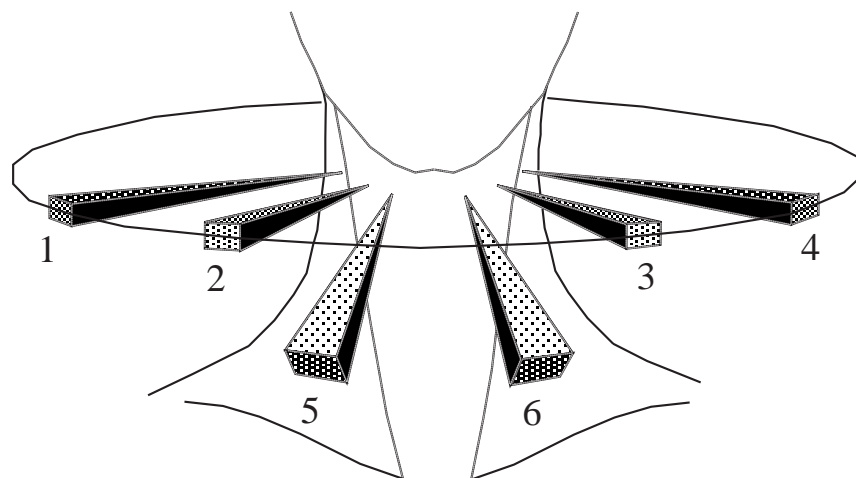
Legend : Drawing of the beam incidences. Gantry-table-collimator (GTC) angles, expressed in degrees: 1: G45T0C0; 2: G75T0C0; 3: G285T0C0; 4: G315T0C0; 5: G30T300C55; 6: G330T60C300. The central beam axes of beams 1-4 are located in a transverse plane. Beam 5 is anterior-inferior-left. Beam 6 is anterior-inferior-right.

First phase of treatment

A total number of 50 segments was created by the ABST procedure. Segment weight optimization was done using the biophysical objective function $f = B.P$ with

$$B \quad = \quad -TCP_{PTV1wb}^{2.5} \cdot \left(1 - NTCP_{spinal\ cord}\right) \cdot \left(1 - NTCP_{left\ parotid}\right)$$
$$\cdot \left(1 - NTCP_{right\ parotid}\right)$$

$$P \quad = \quad \sum_{i=1}^{n} \frac{\left| D_{PTV1wb,i} - 80 \right|^5}{n}$$

The physical term P consists of a parameter that specifies the prescribed dose of 80 Gy to PTV1wb, and 5 as its relative importance. $D_{PTV1wb,i}$ was the computed dose at voxel i of PTV1. In the biological term B, the TCP was computed with a clonogenic cell density of 10^7 cm^{-3}, a mean radiosensitivity $\alpha_0 = 0.28$ Gy^{-1} and a radiosensitivity standard deviation $\sigma_\alpha = 0.05$ Gy^{-1}. The exponent 2.5 was set empirically. After segment weight optimization, 44 segments remained with a non-zero weight. Figure 4a shows a graphical printout of the segment sequence for phase 1 and the resulting intensity map for each beam. The largest segment of each beam incidence encompassed PTV by a margin of 0.7 cm and contributed primary radiation to the spinal cord. The other segments avoid the spinal cord and contribute to form a concave dose distribution component with avoidance of the spinal cord. Figure 5a shows dose-volume histograms of PTV1, PTV1wb, spinal cord and both parotid glands. Figure 5b shows the dose distribution in a transverse plane through the isocenter. Five percent of the volume of PTV1wb received less than 95% of the prescription dose. This underdosed volume was located partially at the posterior edge of lymph node area II left and right and partially at regions of PTV1wb close to the skin surface. The dose maximum of 49.9 Gy was located inside PTV1wb. 0.5% of the volume of PTV1wb received more than 107% of the prescription dose. Delivery on a phantom took 10 minutes for a 200 cGy fraction, calculated from the start of radiation delivery of the first beam to the end of radiation delivery of the sixth beam. The treatment room had to be entered twice during treatment to place the couch angle for the non-coplanar beams.

Figure 4

Fig.4a
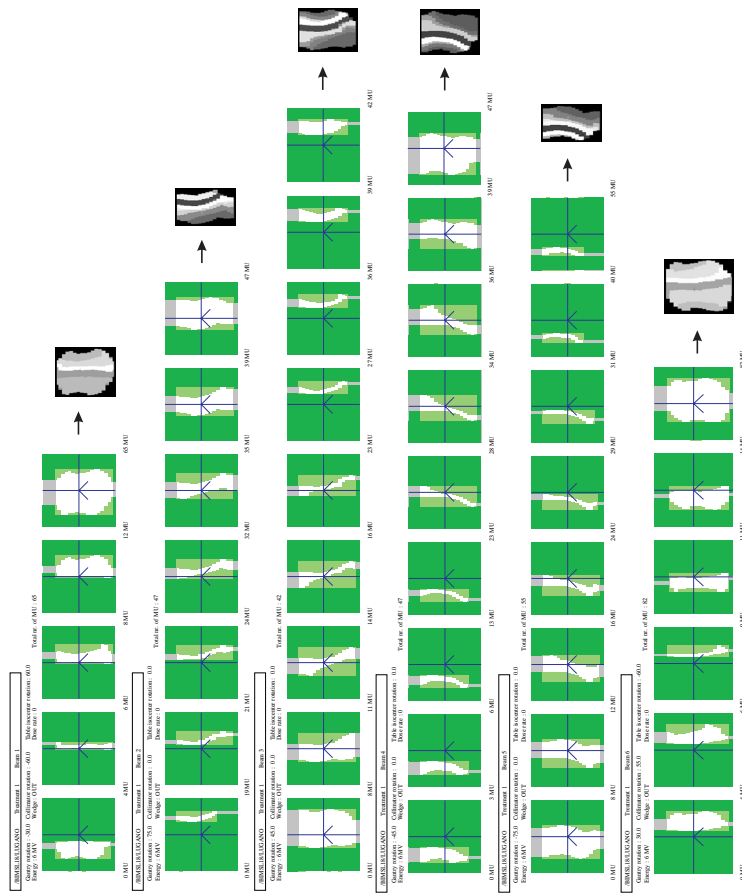
Fig.4b
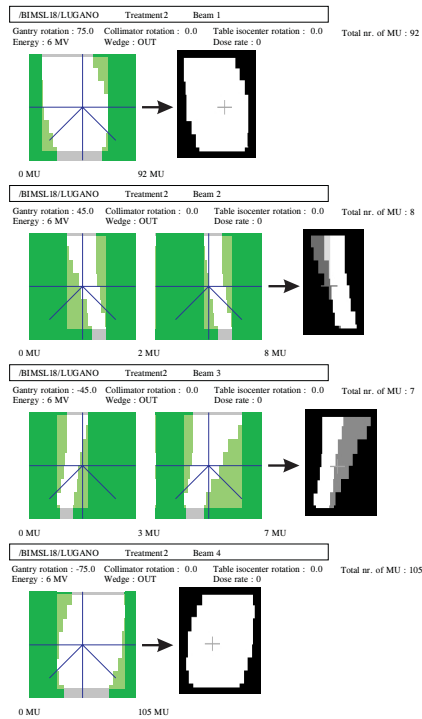
Legend : Graphical printout of the sequences of segments for each IM-beam used during phase 1 (4a) and phase 2 (4b). From left to right, the MLC configurations of the segment sequences to be delivered during an IM-beam are displayed. The numbers below each row of segments represent the cumulative monitor unit count reached at the end of the segments. At the far right, the resulting intensity profiles, as negative gray values, are shown right to the arrows. From top to bottom, the sequence of IM-beams as delivered during treatment is represented.

Figure 5
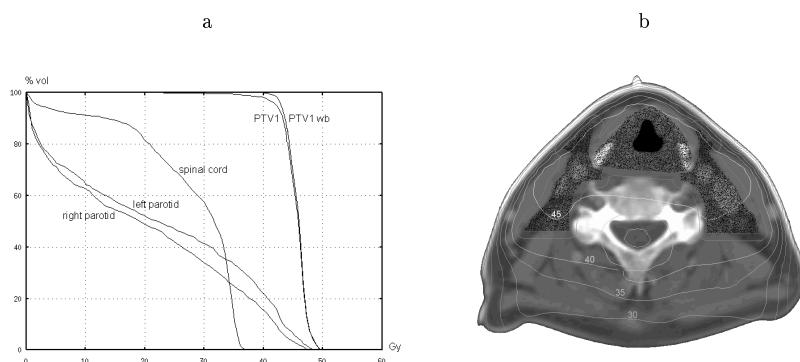
Legend : Treatment phase 1.
a: dose-volume histograms of PTV1, PTV1wb, spinal cord and both parotid glands.
b: dose distribution in a transverse plane through the isocenter for treatment phase 1. The spotted areas are the CTV that includes the elective nodal area III left and right and the CTV that represents the macroscopical tumor (mid-anterior spotted area).

Second phase of treatment

A total number of 14 segments was created by the ABST procedure. Segment weight optimization was done by constrained matrix inversion [7], using the objective function

$$F = \sum_{i=1}^{n} \left(D_{PTV2wb,i} - 24 \right)^2 + \sum_{j=1}^{n} D_{spinal\ cord,j}$$

where $D_{PTV2wb,i}$ is the dose at voxel i of PTV2wb, 24 is the wanted dose in Gy for the second phase of treatment at all n voxels of PTV2wb and $D_{spinal\ cord,j}$ is the dose at voxel j of the spinal cord. The parotids glands were not included in the objective function, since these structures are, unlike in phase 1, not close to the PTV. Only 6 segments were retained by the optimization. The graphical printout of the segment sequence is shown in figure 4b as well as the intensity map for each beam.

Integrated plan

A total plan was constructed by addition of both planning phases. Dose-volume histograms of PTV1, PTV1wb, PTV2, PTV2wb, spinal cord and both parotid glands are shown in figure 6a. Figure 6b shows the dose distribution in a transverse plane through the isocenter. The dose maximum of 72.9 Gy was located inside PTV2wb. Less than 2 % of the volume of PTV2wb received less than 95% of the prescription dose. This underdosage was found only in regions of PTV2 close to the skin surface and was caused by buildup. The mean dose to the right and left parotid was 20.1 and 23.3 Gy, respectively. The lower part of the parotid glands, close to lymph node area II left and right, is not well spared (figure 6c). Figure 6d illustrates a sufficiently low dose in the upper parts of the parotid glands, to have a mean dose to the parotid gland below 26 Gy [15] for maintaining the parotid function.

4. Discussion

In inverse planning, the shape of segments is inferred from fluence maps obtained by optimizing weights to bixels. The possible locations of intensity gradients in the beam are a function of the size and location of the bixels. By inferring the segment-shapes directly from the geometry of the planning target volumes and the patient's anatomy, ABST allows millimeter-precise control about the location of dose gradients in the planned dose distribution. In the head and neck region, portal imaging and radiographic studies have shown a random error of positional uncertainty in the range of 2 mm for mask-type immobilization [16]. The positional accuracy is of 1 mm or less for relocatable [17] or invasive [18] frame immobilization. Therefore, precise control on the location of dose gradients in the planned dose distribution can be exploited in the head and neck region, especially to spare critical organs of small size.

Figure 6

a

b

c

d
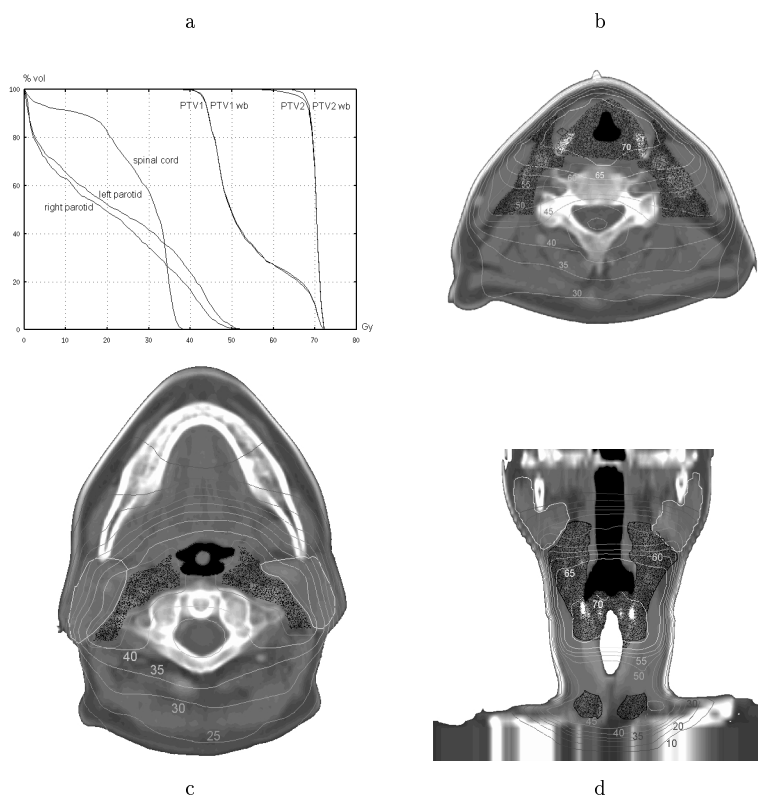
Legend : Integrated plan.

a. dose-volume histograms for PTV1, PTV1wb, PTV2, PTV2wb, spinal cord, left parotid gland, right parotid gland.

b. transverse dose distribution plot.

c. transverse dose distribution plot at the lower half of the parotid glands, showing little parotid sparing.

d. coronal dose distribution illustrating the sparing of the upper halves of both parotid glands.

By inferring the segment-shape from contoured structures without performing a dose computation, ABST is fast. In clinical practice, a typical number of segments created by ABST ranges from 20 for prostate to 60 for paranasal sinus tumors, generated in 1 to 4 minutes. As the segmentation grid does not need to be an intensity profile, a simple function which increases grid values towards the edges of the BEV of critical organs was used in step 5. The division by one plus the distance to the OAR results in an equal transformation for each grid point at the same distance from the OAR. If only one OAR is provided to ABST, this gives rise to segment edges parallel to this OAR; for multiple OARs, the transformation results in a higher number of superposing segments at closer distance to the OARs. Further, a small correction is done in step 6 to take extra tissue traversed by incoming rays into account. Because the idea of ABST is based on a method described by Brahme [2], who reports the calculation of an optimal intensity profile, it is not surprising that the segmentation grid resembles optimized intensity maps resulting from inverse planning. The segmentation grid used by ABST is however determined for each beam orientation separately and without dose computation, and the values of the grid are not optimized. Consequently, the segmentation grid is not an intensity profile, but only serves to derive segments. The method to derive the segments from the segmentation grid in steps 7-9 is comparable to leaf sequencing methods used by inverse planning implementations. The key points of ABST are the conformal avoidance of OARs and the increasing intensity towards the OARs. The implemented method ensures a fluent profile, except at the interfaces with critical organs.

In IMRT planning of little complexity, like the clinical example, acceptable plans can be generated by weighting the segments generated by ABST without further optimization of their shapes. In fact, the plan was competitive to plans obtained by inverse techniques as reported by P. Levendag et al. [19] Nevertheless, it is highly likely that the plan can be improved by segment geometry optimization (see figure 1). At the time when the planning comparison was made by Levendag and coworkers, segment geometry optimization [20] was still in a preclinical stage of development. The planning comparison was restricted to technology that was already in clinical use. Segment geometry optimization is now routinely used to optimize the shapes of segments generated by ABST for the treatment of more complicated head and neck cases. A paper that describes the implementation of IMRT for paranasal sinus cancer is submitted to the Int J Radiat Oncol Biol Phys.

Conclusion: ABST is a fast procedure used at Ghent University Hospital to generate a set of segments during IMRT planning. The plan is finalized by assigning weights to the segments or by further optimization of segment shapes and weights. ABST allows us to avoid the step of translating complicated intensity maps to sequences of segments.

Acknowledgements

References

1. Webb S. Intensity-Modulated Radiation Therapy. Bristol (UK): Institute of Physics Publishing; 2001.

2. Brahme A, Roos JE, Lax I. Solution of an integral equation encountered in rotation therapy. Phys Med Biol 1982;27:1221-9.

3. Lax I, Brahme A. Rotation therapy using a novel high-gradient filter. Radiology 1982;145:473-8.

4. De Neve W, De Wagter C, De Jaeger K, et al. Planning and delivering high doses to targets surrounding the spinal cord at the lower neck and upper mediastinal levels: static beam-segmentation technique executed by a multileaf collimator. Radiother Oncol 1996;40:271-9.

5. Khan FM. A system of dosimetric calculations. In: The Physics of Radiation Therapy. Baltimore; 1985. p. 182-204.

6. Sherouse GW, Thorn J, Novins K, et al. A portable 3D radiotherapy treatment design system. Med Phys 1989;16:466.

7. De Wagter C, Colle CO, Fortan LG, et al. 3D-conformal intensity modulated radiotherapy planning: interactive optimization by constrained matrix inversion. Radiother Oncol 1998;47:69-76.

8. Webb S, Nahum AE. A model for calculating tumour control probability in radiotherapy including the effects of inhomogeneous distributions of dose and clonogenic cell density. Phys Med Biol 1993;38:653-66.

9. Lyman JT. Complication probabilities as assessed from dose-volume histograms. Radiat Res 1985;104(Suppl.):513-9.

10. Kutcher GJ, Burman C. Calculation of complication probability factors for non-uniform normal tissue irradiation: the effective volume method. Int J Radiat Oncol Biol Phys 1989;16:1623-30.

11. Burman C, Kutcher GJ, Emami B, et al. Fitting of normal tissue tolerance data to an analytic function. Int J Radiat Oncol Biol Phys 1991;21:123-35.

12. Brent RP. Algorithm for minimization without derivatives. Book:, Prentice-Hall, Englewood Cliffs (NJ) (1973).

13. De Neve W, De Gersem W, Derycke S, et al. Clinical delivery of intensity modulated conformal radiotherapy for relapsed or second-primary head and neck cancer using a multileaf collimator with dynamic control. Radiother Oncol 1999;50:301-14.

14. Derycke S, De Gersem W, Van Duyse B, et al. Conformal radiotherapy of stage III non-small cell lung cancer: a class solution involving non-coplanar intensity modulated beams. Int J Radiat Oncol Biol Phys 1998;41:771-7.

15. Eisbruch A, Ten Haken RK, Kim HM, et al. Dose, volume and function relationships in parotid salivary glands following conformal and intensity-modulated irradiation of head and neck cancer. Int J Radiat Oncol Biol Phys 1999;45:577-88.

16. De Neve W, De Gersem W, Fortan L, et al. Clinical implementation of electronic portal imaging: correction strategies and setup errors. Bull Cancer Radiotherapie 1996;83:401-5.

17. Rosenberg I, Alheit H, Beardmore C, et al. Patient position reproducibility in fractionated stereotactic radiotherapy: an update after changing dental impression material. Radiother Oncol 1999;50:239-40.

18. Yeung D, Palta J, Fontanesi J, et al. Systematic analysis of errors in target localization and treatment delivery in stereotactic radiosurgery (SRS). Int J Radiat Oncol Biol Phys 1994;28:493-8.

19. Levendag P, Wijers O, van Sörnsen de Koste J, et al. Intensity-modulated radiation therapy: preliminary multi-institutional experience in head and neck cancer. Abstract of ICTR 2000 Int J Radiat Biol Phys 2000;46:Abstract 56:709-10.

20. De Gersem W, Vakaet L, Claus F, et al. MLC leaf position optimization using a biophysical objective function. Radiother Oncol 2000;56(suppl. 1):S96-S97 abstract 348.

4.3 **Intensity modulation techniques for improvement of normal tissue tolerance. W. De Neve, F. Claus, et al. Front Radiat Ther Oncol Basel Karger 2001;37:163-73.**

topics discussed :	→ IMRT and normal tissue tolerance
	→ clinical results for IMRT re-irradiations
	→ IMRT and low-dose hypersensitivity
key question :	How can IMRT affect normal tissue
	complication probabilities ?

paper 4.3

Intensity modulation techniques for improvement of normal tissue tolerance.

Wilfried De Neve, Filip Claus, Wim Duthoy, Gert De Meerleer and Carlos De Wagter.

Division of Radiotherapy
Ghent University Hospital

Abstract

Background and Purpose : Intensity modulated radiotherapy (IMRT) is arguably the hot topic in radiotherapy physics translational research. Avoidance of complications is achieved by lowering to organs at risk the total physical dose (physical selectivity), the fraction dose (fractionation selectivity) or by controlling the dose distribution inside organs at risk according to their respective dose / volume / function relationships.

Material and Methods : Between 01/9/1996 and 31/10/1999, 32 patients with cancer in the head and neck region were treated using segmental IMRT at Ghent University Hospital. Eleven of these patients were reirradiated for relapse or metachronous tumor in a previously irradiated region, eight patients received IMRT for paranasal sinus cancer, and in selected patients with pharyngeal cancer, parotid sparing was performed.

Results : The possibilities offered by physical selectivity are illustrated by IMRT applied for reirradiation of head and neck cancer where extreme dose reduction to spinal cord and brainstem was required. Fractionation selectivity was exploited to preserve functional optical pathways in IMRT of paranasal sinus tumors. The possible effect of hypersensitivity of the parotid gland to low doses per fraction, is calculated for a parotid-sparing IMRT plan.

Conclusion : IMRT allows us to customize dose distributions to maximize the probability of uncomplicated local control by incorporating organ specific dose / volume / function relationships in the plan optimization. It also allows us to design strategies for therapy optimization that secure safety against low-dose hypersensitivity.

1 Introduction

In the 80s, Brahme computed fluence patterns that were useful to form homogeneous concave dose distributions by arc therapy [1][16]. The interest to use these fluence patterns -in what were later called intensity modulated (IM) beams- was shown also for multiple static beams. Organs at risk (OARs) surrounded by tumor could now be spared. For a given tumor prescription dose, intensity modulated radiotherapy (IMRT) can be exploited to improve normal tissue tolerance by physical selectivity i.e. the physical dose is larger in the tumor than in invaginating normal tissues. With fractionation, the therapeutic gain is greater than expected from the degree of physical selectivity. Indeed, by lowering the dose to OARs for each fraction, physical selectivity is complemented by biological (fractionation)

selectivity when the ratios of α/β-values between tumor and OARs have a value larger than 1. Some IMRT applications using multiple convergent beams or arc therapy are characterized by spreading out the dose over large volumes. Regions receiving a dose per fraction below 0.5 Gy occur and the issue of low-dose hypersensitivity may have to be considered. The aim of this paper is to illustrate the use of IMRT for improvement of normal tissue tolerance by exploiting physical and biological selectivity. The potential drawback of low-dose hypersensitivity and the possible precautions to minimize the risk of its toxicity are also discussed. IMRT treatments selected from a database of patients treated for head and neck cancer are taken to illustrate the arguments.

2 Materials and methods

2.1 Patient treatments

Between 1/9/1996 and 31/10/1999, 32 patients with cancer in the head and neck region were treated using segmental IMRT. Table 1 shows the distribution of patients according to the site of the primary.

Table 1 : Patients treated with IMRT for head and neck cancer between 1/9/1996 and 31/10/1999, ranked accord ing to the site of the primary tumor (column 1), the number of patients for each site (column 2) and the number of re-irradiations (column 3).

H&N IMRT: 1/9/96 - 31/10/99

Site	Number	Re-irradiation
Nasopharynx	8	3/8
Oropharynx	3	2/3
Hypopharynx	2	1/2
Larynx	4	3/4
Oral cavity	2	1/2
Parotid	1	1/1
Thyroid gland	4	0/4
Paranasal sinus	8	0/8

Eleven of these patients were re-irradiated for relapse or metachronous tumor in a previously irradiated region (table 1, column 3). Permission from the hospital's Ethical Committee was obtained to use IMRT for re-irradiation in symptomatic patients with inoperable disease.

IMRT dose distributions were required that could achieve a large difference between the dose delivered to the malignancy and the dose delivered to anatomical structures that had previously been irradiated to doses close to tolerance. Thus the key mechanism that we aimed for was physical selectivity. Re-irradiation by IMRT was performed from September 1996 on.

From August 1998 till the end of October 1999, eight patients received IMRT for paranasal sinus cancer. In all patients, regions of the clinical target volume were at close distance (within 0-3 mm) from optical structures and pathways. As a result, the planning target volumes (PTVs) intersected optical structures (retina) and/or pathways (optic nerves, optic chiasm). In all patients, conventional radiotherapy techniques would have involved the delivery of total doses exceeding 60 Gy to optical organs at risk which would be more than the tolerance levels of these structures. In standard radiotherapy practice unilateral blindness is a feared complication of radiotherapy for such cases. The treatment planning often involves the sinister choice of "which eye to offer". The challenge for IMRT is to save binocular vision. The key mechanism is combined physical and biological selectivity. Follow up being too short, we aim to show that IMRT allows us to achieve dose distributions that are suitable to pursue this mechanism.

In selected patients with pharyngeal cancer, parotid sparing was performed. The treatment of one of these patients is taken to discuss the potential adverse effects of low-dose hypersensitivity when using forms of IMRT that lead to large areas that are irradiated at low doses per fraction. The patient was an eight year old boy, diagnosed with a nasopharyngeal embryonal rhabdomyosarcoma. The patient was treated by induction chemotherapy (ifosfamide, vincristine, adriamycine: 3 cycles) followed by radiotherapy (56 Gy in 2 Gy fractions, prescribed to planning target volume (PTV) based on the pre-therapeutic extension of the gross tumor volume (GTV)). The first five fractions were delivered by a 3D conformation technique while the remaining 23 fractions were delivered by IMRT. The 3D conformation technique did not allow us to spare a parotid gland but was applied to enable us to start radiotherapy in due time i.e. according to the protocol guidelines. After 5 fractions, the IMRT plan and its dosimetrical verification was finished. This practice to start with conventional radiotherapy until a sophisticated IMRT plan is finished and preclinically verified is not uncommon. To discuss the issue of low-dose hypersensitivity, a number of assumptions are made. First, it is assumed that low-dose hypersensitivity occurs in the parotid gland, that it occurs at fraction doses of 50 cGy/fraction or lower and that for 45 cGy/fraction, the biological equivalent dose is 2.0 times the physical dose. We also assume that a rival IMRT plan is available in which the right parotid would receive a mean and homogeneous dose of 45 cGy/fraction. We want to stress the fact that low-dose hypersensitivity has recently been reported for parotid glands 15. However, the exact quantitative hypersensitivity data are not known to us. Therefore the proposed dose modifying factor of 2.0 for a fraction dose of 0.45 Gy and the critical dose of 0.5 Gy below which hyper sensitivity would occur have to be considered in the context of a further theoretical discussion only.

2.2 Equipment

Software distributed by Sherouse (GRATIS) [19] was used as a platform for IMRT planning. In-house developed tools were added to translate field edges to multileaf collimator settings [24]; to perform beam segmentation for IMRT [7]; and to optimize beam weights [8][3]; to optimize collimator angles and individual MLC leaf positions (W. De Gersem, unpublished). Treatments were delivered by means of 6 MV photons of a SL20-MLCi or a SL25-MLCi (Elekta, Crawley, UK) linear accelerator equipped with a dynamic multi-leaf collimator (DMLC). The DMLC control software was described previously [6]. An extensive system for preclinical dosimetrical verification and clinical quality control is in place [9][2][23].

3 Results

3.1 Re-irradiation

Plans were constructed with the aim to achieve the maximum possible sparing of previously irradiated OARs like spinal cord, brainstem and mandibular bone. Figure 1 shows a typical plan. Maximal sparing of the brainstem and the spinal cord results in a dose distribution showing a low-dose tube matching brainstem and spinal cord. In any transverse direction away from brainstem and spinal cord, a sharp dose gradient exists. Patient setup and immobilization is critical. There are 2 reasons for dose inhomogeneity in the PTV. First, underdosage is observed where the minimal distance between PTV and spinal cord or brainstem is of the order of 1 cm or less i.e. the same order of magnitude as the beam penumbra. The beam penumbra sharpness determines the maximal dose gradient that can be achieved around an invaginating structure. Second, when a concave dose distribution must be created, with the aim to deliver zero dose to the invaginating structure, the maximal dose homogeneity that can be achieved depends on the number of incident static beams. If the number of beams is n, the dose homogeneity greater than $(n-1)/n$ is difficult to obtain. Table 2 shows the location of the primary tumor (column 1), the dose delivered initially (column 2) and for re-irradiation (column 3), the response to treatment (column 4) and the events observed during follow up (column 5).

Figure 1
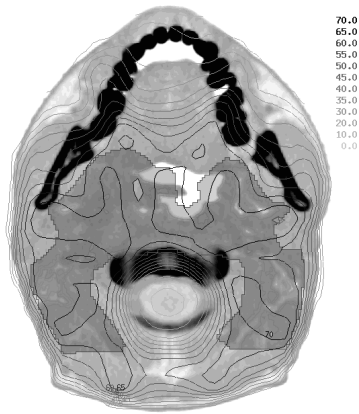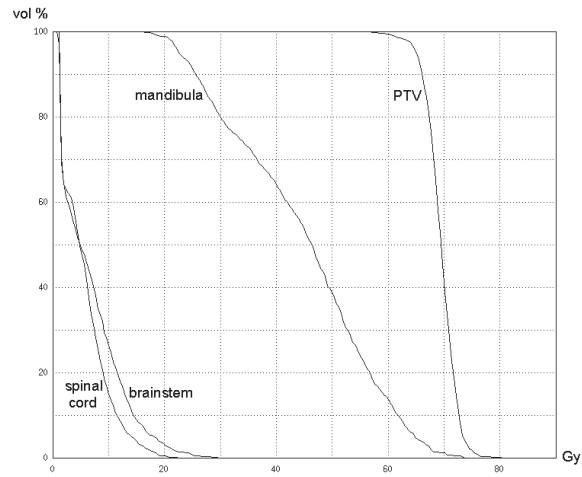
Legend : Dose-volume histogram and transverse isodose line plot of IMRT for a large horseshoe shaped relapse from a nasopharyngeal cancer. The PTV is shaded on the transverse plot. A dose gradient is shown, running from 20 Gy to 60 Gy over a distance of about 1 cm in the centrifugal direction from the spinal cord. The dose to two thirds of the mandible is lower than 55 Gy.

Filip Claus

For 8 of 10 evaluable patients palliation was achieved. Median duration of response was 9 months (figure 2). Median survival calculated from the onset of re-irradiation was 15 months (figure 2). The cause of death was intercurrent (intestinal hemorraghe) in one patient and related to disease progression in five patients. Subcutaneous fibrosis was reported in seven patients. Temporo-mandibular joint impairment and laryngeal edema each in one patient. In spite of cumulative doses as high as 136 Gy, no cases of cranial nerve palsy, arterial rupture or bone necrosis were observed.

Table 2 : Patients re-irradiated with IMRT for head and neck cancer, ranked according to the site of the primary tumor (column 1), the dose delivered initially (column 2), the dose delivered with IMRT for re-irradiation (column 3), the response to treatment (column 4) and the events observed during follow up (column 5).

H&N re-irradiation

Site	RT (Gy)	IMRT (Gy)	RESPONSE	FU (months) / outcome
Nasopharynx	66	60	CR[1]	7 / no evidence of disease
Nasopharynx	66	70	CR	8 / relapse
Nasopharynx	64.8	70	CR	7 / no evidence of disease
Parotid gland	64	60	PR[2]	14 / no evidence of disease
Oropharynx	70	60	PR	23 / relapse
Hypopharynx	64.8	60	PR	3 / relapse
Oropharynx	66	70	CR	10 / relapse
Oral cavity	50	66	PD[3]	0 / relapse
Larynx	66	60	PR	2 / relapse
Larynx	70	44*	?	4 / *stopped RT
Larynx	70	40*	?	0 / *Died during RT

[1]: complete response   [2]: partial response   [3]: persistent disease

Figure 2

H&N IMRT: re-irradiation
1/9/96 - 31/10/99
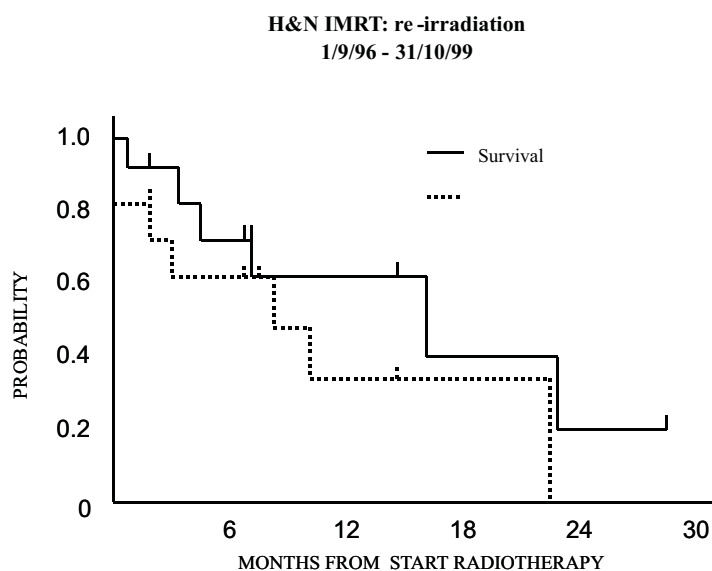
Legend : Probability of survival and progression-free survival for patients (n = 11) re-irradiated for head and neck cancer. Date of analysis: 15 January 2000.

3.2 Intentionally inhomogeneous dose distributions

In paranasal sinus cancer (especially ethmoid cancer), tumor edges adjacent to one or more of the numerous OARs (eyes, optic nerves and chiasm, brainstem, frontal lobes) are common. Conformal avoidance techniques of small-size OARs must take into account motion and setup uncertainty, not only of the tumor but also of the OARs. Indeed, when creating sharply increasing dose gradients in the vicinity of structures like the optic nerves (4 mm diameter) or optic chiasm (7 mm diameter), setup errors may expose the full thickness of the structure above tolerance. Applying margins for motion and setup uncertainty to CTV as well as to OARs adds safety. The resulting PTV often intersects the expanded OARs. The maximal dose to the region of intersection is determined by the tolerance of the respective OARs, while the dose to the non-intersecting PTV-part can be prescribed to a higher value. IMRT allows to irradiate with an inhomogeneous dose distribution so that at each fraction the PTV portion that intersects with or is close to the OAR(s) is slightly underdosed. If the tumor has a larger α/β than the OAR(s) (often the case if the OAR is nerve tissue),

a radiobiological advantage can be exploited by the smaller fraction size at the OAR. As a result of the smaller fraction size to OARs, the tolerance dose is increased. In figure 3, the dose gradient between optic nerves, chiasm and tumor runs through a small portion of the tumor. In none of eight patients treated between February 1999 and October 31st of 1999, blindness developed. Duration of follow up however is insufficient.

3.3 Low-dose hypersensitivity: an unforeseen obstacle for IMRT?

Avoiding xerostomia became another issue in IMRT of head&neck cancer, typically for the pharyngeal site. Dose/volume/function relationships in the parotid glands were found to be characterized by dose and volume thresholds, steep dose/response relationships when the thresholds were reached, and a high volume dependence in NTCP models. Eisbruch et al. [10] concluded that a parotid gland mean dose of $\leq$ 26 Gy should be a planning goal if substantial sparing of the gland function is desired. In our experience, a free space of 1-1.5 cm between the PTV and the parotid gland was sufficient to achieve this planning goal for a PTV-prescription dose up to 70 Gy.

For the irradiation of the nasopharyngeal rhabdomyosarcoma, we assumed that a theoretical plan was developed that spared the right parotid gland. At a PTV dose prescription of 2 Gy/fraction, the right parotid mean physical dose would be 0.45 Gy/fraction. Following the assumption of low-dose hypersensitivity as described in the Materials and Methods section, the corresponding biological equivalent dose BED' would be 0.9 Gy/fraction. For a PTV dose prescription of 28 x 2.0 Gy, the BED' to the right parotid would be 28 x 0.9 = 25.2 Gy and thus below the planning goal (i.e. a total physical dose below 26 Gy) to spare the parotid gland. Since there was no parotid sparing during the initial 5 fractions, a dose of 10 Gy (physical) or 16.7 Gy (BED, $\alpha/\beta = 3$ Gy) was accumulated. Applying the theoretical plan after 5 fractions would add a BED' of 23 x 0.9 = 20.7 Gy. The BED' for the total treatment would be 37.4 Gy, thus violating the planning goal, while the physical total dose would be 10 + 23 x 0.45 = 20.35 Gy mean dose to the right parotid i.e. in compliance with Eisbruch's planning goal but misleading.

Figure 3
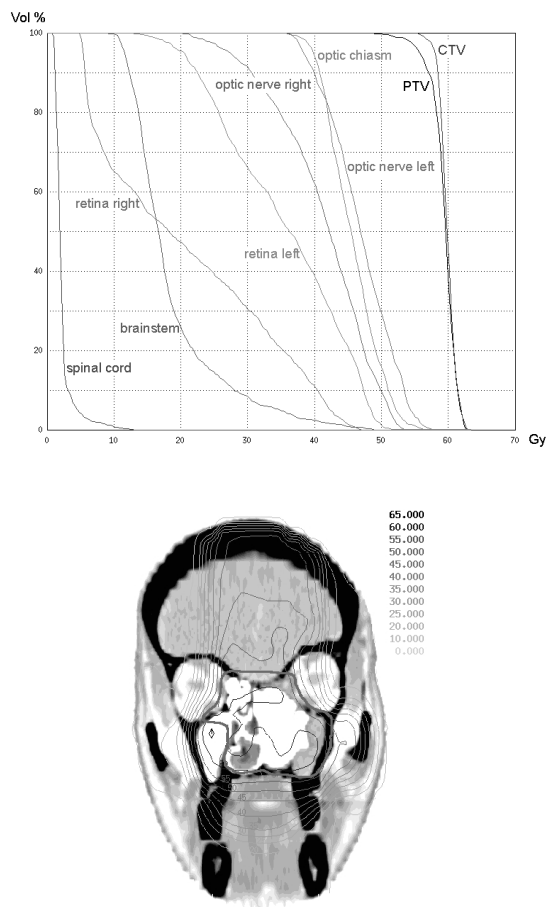
Legend : Dose-volume histogram and coronal isodose line plot of postoperative IMRT for ethmoid sinus cancer. PTV in solid gray line on the coronal plot. PTV prescription dose was 30 x 2.0 Gy. Left and right optic nerves passing through dose gradient. Doses above 50 Gy in optic nerves and chiasm are in regions that are intersected by the PTV (not shown on the coronal plot but consistent with the difference in dose minimum between PTV and CTV).

4 Discussion

For patients with inoperable locoregional relapse or new primary after high dose radiotherapy for head and neck cancer, the prognosis is poor. In the absence of distant metastases, cure can be attempted by re-irradiation. Most of the patients referred to our center suffer from advanced relapses. IMRT offers a sufficiently large window of possibilities to perform re-irradiation for large tumors that encompass OARs with limited remaining tolerance to radiation. The dose to such OARs can be limited to values that are close to the lowest values physically achievable with the present photon technology. When different OARs are inside the volume of re-irradiation, priorities must be assigned as a function of the severity and likelihood of toxicity. Data about normal tissue tolerance for re-irradiation are scarce. In practice, plan optimization aims at delivery of the lowest possible dose to OARs like brainstem and spinal cord since complications would be invalidating or lethal. Our preliminary data suggest that IMRT is a safe alternative to palliative care in advanced inoperable patients. Palliation of symptoms by induction of tumor response is the preferred and logical approach and was achieved in 8/9 evaluable patients. Median duration of response was 8 months. We plan to apply re-irradiation for less advanced cases.

The prime example of successful application of intentionally inhomogeneous dose distributions is prostate [17]. The rectal wall, in close vicinity of the posterior portion of the prostate and seminal vesicles, is dose limiting. When accounting for motion, the resulting PTV intersects the anterior rectal wall. The maximal homogeneous dose, that can be given to the PTV, is then directly determined by the intersected portion of the rectal wall. Escalating the dose above the rectal tolerance level can only be attempted safely to the non-intersecting PTV-part. Although this strategy has not yet been shown conclusively to produce higher cure rates, it looks promising and does seem to limit side effects [11]. In cancer of the paranasal sinuses, a problem with similar flavor occurs. Cancers at this site(s) are often diagnosed in an advanced stage with invasion of one or both orbits , the anterior and middle fossae of the skull. Tumors in close vicinity or even displacing the optical pathways are often seen. Data regarding tolerance doses of optic nerves, chiasm and retinae with the use of segmental IMRT for advanced paranasal sinus tumors were published by Martel [18]. He concluded that a maximal dose of 60 Gy in 1.8-2.0 Gy/fraction to the optic nerves is a suitable planning goal if visual function should be preserved. Of the optic pathway structures, the optic nerves seemed to have the lowest tolerance doses. For a PTV-prescription dose of 70 Gy in 2.0 Gy/fraction, an underdosage of 20% to the optic tract (e.g 1.6 Gy/fraction) would result in a physical dose of 56 Gy and a BED of 51.5 Gy at 2 Gy/fraction ($\alpha/\beta = 3$ for optic pathway structures). Accurate control of the maximal dose to optical pathways in the vicinity of sharp dose gradients (running from low in the optic pathways to high in the PTV) is a challenge even for modern high-precision techniques. The penumbras of the best collimation techniques (3-4 mm for the distance between the 20% and the 80% isodose) as well as the leaf width of mini-multileaf collimators are about as large as the diameter of the optic nerves. The sharpest gradients inside an IMRT dose distribution are created by segment edges and the penumbra limits the maximal gradient steepness. A

gradient running from 1.6 Gy to 2.0 Gy can be created over a distance of 4 mm (C. De Wagter, unpublished). Assume that the 1.6 Gy isodose surface is positioned at the edge of the optic nerve. Non-invasive patient setup and immobilization in the head and neck region is characterized by random setup errors around 2 mm [5]. With a systematic error of zero, the maximal dose to the the optic nerve would be 2.0 Gy for 2.5 % of the setups. In clinical practice, IMRT may create an underdosed tube at the optic nerves. Setup errors in any direction would overdose the optic nerves. Although random errors tend to overdose different regions for different fractions, systematic errors would overdose the same region repeatedly. For radiotherapy of paranasal sinus tumors, we reach the limits that are achievable with the present photon technology and patient setup methods.

During the last decade, hypersensitivity of exponentially growing cells exposed to radiation doses below 0.5 Gy has been observed [21]. As underlying hypothesis, it was suggested that a dose of 0.5 Gy or less is not sufficient to trigger an inducible repair mechanism. If this effect is present in irradiated cells it would be of considerable clinical significance. In pulse dose brachytherapy, hyperfractionated radiotherapy, multi-beam conformal therapy or tomotherapy, critical normal tissues often receive doses in the range of 0.5 Gy/fraction or lower. The evaluation of rival plans based on physical doses and comparisons using the LQ-model might lead to erroneous selection. Optimization algorithms involving NTCP computations based on the LQ-model [3][4] might lead to misleading predictions. Normal tissues showing low-dose hypersensitivity would impact on the choice of beam directions, number of beams and intensity profiles. The much debated issue of the best beam assembly in IMRT would become even more complicated and the arguments in favor of tumor-site dependent class solutions would be strengthened. Clinical IMRT applications using hyperfractionation and two-phase plans (non-IMRT followed by IMRT) would be dysfavored. Hypofractionation could be advantageous .

Most publications involve observations in the laboratory. Not all observations using cell lines support that, in fractionated schedules, low-dose hypersensitivity would lead to surviving fractions that would be ill predicted by the well documented utility of the LQ approach for estimating iso-effect doses for alternative fractionation schemes [20]. In mice, low-dose hypersensitivity was shown for acute skin damage and late kidney effects [13][14]. Clinical data are scarce. Hamilton found that the LQ-model significantly underpredicted peak skin erythema values at doses of less than 1.5 Gy /fraction [12]. Turesson also found evidence of low dose hypersensitivity in human skin exposed to fractionated radiotherapy [22]. Hypersensitivity in cell kill for doses up to 0.2-0.4 Gy/fraction was followed by less cell kill between 0.45 and 1.1 Gy/fraction. Hypersensitivity did not seem to disappear as a function of cumulative doses and could be observed after 15 and 20 fractions at 3 and 4 weeks of radiotherapy respectively. Lambin reported low-dose hypersensitivity in parotid glands [15]. Turesson pointed out that low dose hypersensitivity is not encountered in all cell types or organs [21]. Neither the list of organs nor the quantitative degree of hypersensitivity is known. Nevertheless, low dose hypersensitivity has to be taken into account when planning IMRT.

Acknowledgements

References

1. Brahme A, Roos JE, and Lax I. Solution of an integral equation encountered in rotation therapy. Phys Med Biol 1982;27:1221-9.

2. De Deene Y, De Wagter C, Van Duyse B, et al. Validation of MR-based polymer gel dosimetry as a preclinical three-dimensional verification tool in conformal radiotherapy. Magnetic Resonance in Medicine 2000;43:116-25.

3. De Gersem, W, Derycke S, Colle C, et al. Inhomogeneous target-dose distributions: a dimension more for optimization ? Int J Radiat Oncol Biol Phys 1999;44:461-8.

4. De Gersem W, Derycke S, Colle C, et al. Optimization of beam weights in conformal radiotherapy planning of stage III NSCLC: effect on therapeutic ratio. Int J Radiat Oncol Biol Phys 2000;47:255-60.

5. De Neve W, De Gersem W, Fortan L, et al. Clinical implementation of electronic portal imaging: correction strategies and set-up errors. Bull Cancer Radiother 1996;83:401-5.

6. De Neve W, De Gersem W, Derycke S, et al. Clinical delivery of intensity modulated conformal radiotherapy for relapsed or second-primary head and neck cancer using a multileaf collimator with dynamic control. Radiother Oncol 1999;50:301-14.

7. Derycke S, Van Duyse B, De Wagter C, et al. Non-coplanar beam intensity modulation allows large dose-escalation in stage III lung cancer. Radiother Oncol 1997;45:253-61.

8. De Wagter C, Colle CO, Fortan L, et al. 3D-conformal intensity modulated radiotherapy planning: interactive optimization by constrained matrix inversion. Radiother Oncol 1998;47:69-76.

9. De Wagter C, Martens C, De Deene Y, et al. Dosimetric verification of intensity modulation executed by a conventional accelerator equipped with a multileaf collimator. Cancer Radiother 1999;3(Suppl.1):171-82.

10. Eisbruch A, Ten Haken RK, Kim HM, et al. Dose, volume and function relationships in parotid salivary glands following conformal and intensity-modulated irradiation of head and neck cancer. Int J Radiat Oncol Biol Phys 1999;45:577-88.

11. Garnick MB and Fair WR. Combating prostate cancer. Scientific American 1998;Dec :45-53.

12. Hamilton CS, Denham JW, O'Brien M, et al. Underprediction of human skin erythema at low doses per fraction by the linear quadratic model. Radiother Oncol 1996;40:23-30.

13. Joiner MC, Denekamp J and Maughan RL. The use of 'top-up' experiments to investigate the effect of very small doses per fraction in mouse skin. Int J Radiat Oncol Biol 1986;49:565-80.

14. Joiner MC and Johns H. Renal damage in the mouse: the response to very small doses per fraction. Radiat Res 1988;114:385-98.

15. Lambin Ph, Van Mellaert L, Van Acker F, et al. Direct evidence of hypersensitivity and induced radioresistance in human systems. Int J Radiat Oncol Biol Phys 2000;46:692.

16. Lax I and Brahme A. Rotation therapy using a novel high-gradient filter. Radiology 1982;145:473-8.

17. Ling CC, Burman C, Chui C, et al. Conformal radiation treatment of prostate cancer using inversely-planned intensity-modulated photon beams produced with dynamic multileaf collimation. Int J Radiat Oncol Biol Phys 1996;35:721-30.

18. Martel MK, Sandler HM, Cornblath WT, et al. Dose-volume complication analysis for visual pathway structures of patients with advanced paranasal sinus tumors. Int J Radiat Oncol Biol Phys 1997;38:273-84.

19. Sherouse GW, Thorn J, Novins K, et al. A portable 3D radiotherapy treatment design system. Med Phys 1989;16:466.

20. Smith LG, Miller RC, Richards M, et al. Investigation of hyper sensitivity to fractionated low-dose radiation exposure. Int J Radiat Oncol Biol Phys 1999;45:187-91.

21. Turesson I and Joiner MC. Clinical evidence of hypersensitivity to low doses in radiotherapy. Radiother Oncol 1996;40:1-3.

22. Turesson I, Flogegard M, Johansson KA, et al. Use of in-situ assays and molecular markers to measure individual human tissue response to radiotherapy: evidence of low dose hypersensitivity and proliferation dependent radiosensitivity. Int J Radiat Oncol Biol Phys 2000;46:737.

23. Vakaet L, Bate MT, Fortan LG, et al. Off-line verification of the day-to-day three-dimensional table position variation for radiation treatments of the head and neck region using an immobilization mask. Radiother Oncol 1998;47:49-52.

24. Van Duyse B, Colle C, De Wagter C, et al. Modification of a 3D-planning syste m for use with a multileaf collimator. In: Conformal Radiotherapy: Physics, Treatment Planning and Verification, 1995:39-48 Belgian Hospital Physicist Association, Gent.

4.4 Evaluation of a leaf position optimization tool for IMRT of head and neck cancer. F. Claus, W. De Gersem, et al. Radiother Oncol 2001;61:281-6.

topics discussed :	→ an IMRT planning platform
	→ an IMRT leaf position optimization tool
	→ implementation of the tool for head and neck ca
key question :	What can we expect of direct leaf position
	optimization for head and neck IMRT planning ?

paper 4.4

Evaluation of a leaf position optimization tool for IMRT of head and neck cancer

Filip Claus, Werner De Gersem, Ilse Vanhoutte, Wim Duthoy, Vincent Remouchamps, Carlos De Wagter and Wilfried De Neve

Division of Radiotherapy
Ghent University Hospital

Abstract

Background and purpose : Since 1996, patients are treated at Ghent University Hospital with a multi-segment technique using MultiLeaf Collimators (MLC). The segments were obtained by using the Beam's Eye View projections of the Planning Target Volume (PTV) and the Organs At Risk (OARs), after which the segments weights were optimized. To investigate if optimization of the leaf positions would further improve the IMRT plans, a tool optimizing leaf positions and segment weights simultaneously, was developed. This tool is called SOWAT, which is the acronym for Segment Outline and Weight Adapting Tool.

Material and Methods : The tool evaluates the effects of changing the position of each collimating leaf of all segments on the value of the objective function. Only changes that improve the value of the objective function are retained. Between December 1999 and January 2001, 30 head and neck patients were treated with IMRT. Two patient groups were distinguished : pharyngeal and laryngeal tumors (n=17) and sinonasal tumors (n=13). A specific set of physical endpoints was evaluated for each group. Dose statistics of the treatment plans without and with SOWAT were analyzed.

Results : When using SOWAT for the pharyngeal and laryngeal cases, the PTV dose homogeneity increased with a median of 11% (range 2-27%), while the maximum dose to the spinal cord was decreased for 14 of the 17 patients. In 4 plans where parotid function preservation was a goal, the parotid mean dose was lower than 26 Gy in 1 plan without SOWAT, and in 4 plans with SOWAT. For the sinonasal tumors, the PTV dose homogeneity increased with a median of 7% (range 1-14%). SOWAT lowered the mean dose to 53 of the 63 optic pathway structures (retina, optic nerve and optic chiasm). SOWAT leaves the number of segments unchanged and has little or no effect on the delivery time.

Conclusions : SOWAT is a powerful tool to perform the final optimization of IMRT plans, without increasing the complexity of the plan or the delivery time.

Keywords: intensity modulated radiation therapy, head and neck, leaf position optimization

1 Introduction

Clinical implementation of Intensity Modulated Radiation Therapy (IMRT), using Multi-Leaf Collimators (MLC), started in 1996 at Ghent University Hospital (GUH). Patients were

treated by a multi-segment technique as described previously [8][6]. Before December 1999, IMRT plans were generated as shown in the left panel of figure 1. The total number and shape of the segments for each beam incidence was defined by an Anatomy Based Segmentation Tool (ABST) [4]. ABST generated segment outlines that are line contours related to the Beam's Eye View (BEV) projections of the planning target volume (PTV) and organs at risk (OARs). The MLC collimated segments were obtained by positioning of the leaves and jaws in relation to these line contours. The weights of the MLC collimated segments were obtained by a Segment Weight Optimization Tool (SWOT). To investigate if optimization of the leaf positions would further improve the IMRT plans, a tool optimizing leaf positions and segment weights simultaneously, was developed. This tool is called SOWAT, which is the acronym for Segment Outline and Weight Adapting Tool. Plans with and without the use of SOWAT were generated as shown in figure 1 to evaluate the clinical value of the new tool. In this paper, dose statistics for both plans are compared.

Figure 1 : The IMRT planning platform at Ghent University Hospital.
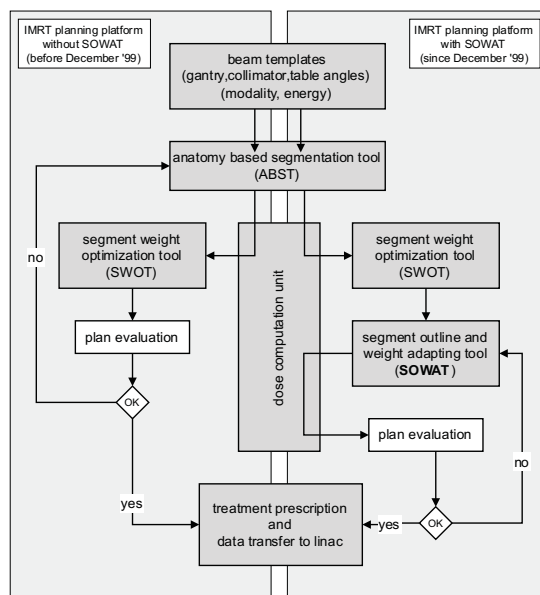
legend : The platform consists of several modular units, including tools to generate segments, compute doses, optimize plans and generate treatment prescriptions. An anatomy based segment generation tool (ABST) gives segments as output. Before December 1999

(left panel), weights were assigned to the segments by a segment weight optimization tool (SWOT) and an evaluation of the plan was performed. If the plan met the clinical objectives, a treatment prescription was generated, if not, new segments were added, again followed by segment weight optimization. Since December 1999 (right panel), both segment outlines and weights were optimized by SOWAT after the execution of SWOT. If the plan passes evaluation a treatment prescription is generated, if not a new SOWAT cycle is started. In the study plans finalized by the procedure without SOWAT were compared with plans finalized by the procedure with SOWAT.

2 Material and Methods

2.1 Patients

The study involves 30 patients, treated with IMRT for head and neck cancer between December 1999 and January 2001. Planning CT-scans were made in treatment position, with a slice thickness of 2 mm in the PTV region and 5 mm elsewhere. Two different patient groups can be distinguished.

The first group consists of 17 patients, irradiated for a pharyngeal or laryngeal tumor. For 10 patients IMRT was used to re-irradiate a locoregional in-field relapse. The dose to the spinal cord by the previous radiotherapy treatment ranged between 40 and 50 Gy. For the re-irradiation, the aim was to keep the dose to the spinal cord as low as possible. For the other 7 patients, IMRT was implemented to preserve parotid gland function or to avoid electron/photon matchlines. For both subgroups, the PTV-prescription dose ranged between 60-70 Gy, except for one patient where 50 Gy was delivered to re-irradiate a rhabdomyosarcoma. The endpoint analyzed for the PTV, was the dose homogeneity u, calculated as $\left(\frac{D_{max}-D_{min}}{D_{median}}\right)$ with D_{max} the maximum dose, D_{min} the minimum dose and D_{median} the median dose. The endpoint for the spinal cord was its D_{max}. If preservation of the parotid function was a treatment goal, the mean parotid dose [9][2] was used as endpoint.

The second group of 13 patients was irradiated for sinonasal tumors. The hypothesis to implement IMRT was to increase tumor control, while maintaining binocular vision. MRI datasets in treatment position were fused with the CT datasets, in order to delineate more accurately the optic nerves and the optic chiasm, further called optic pathway structures. The treatment protocol [3] prescribed a median dose of 70 Gy to the PTV, while only 5 % of the volume of each optic pathway structure was allowed to receive more than 60 Gy [13][12]. An underdosage of the PTV in the overlap zone between the optic pathway structures and the PTV was accepted. Therefore, we analyzed the $u_{95/5}$ instead of u to evaluate the target dose homogeneity, calculated as $\left(\frac{D_{95}-D_5}{D_{median}}\right)$, with D_5 the 5th percentile dose and D_{95} the 95th percentile dose. For the optic pathway structures, the D_{mean} and D_{95} were analyzed.

2.2 IMRT Planning platform

Figure 1 illustrates the planning platform for IMRT at GUH. The beam templates were de-

fined by class solutions, specific for each of the two patient groups. For each beam incidence, ABST generated multiple superposed segments [4]. The beam templates used for group 1 consist of 6 coplanar beams, as reported previously [8][6]. For group 2, a non-coplanar set of 7 beams was used [3]. In addition to the beam templates, the class solution specifies parameters for ABST, SWOT and SOWAT. For ABST, these parameters include : the definition of the PTV and its block margin, the different OARs and the margin to exclude them from the beam aperture, the minimal segment area, the possible incremental segment areas and a parameter to compensate for different pathlengths from the skin surface to the PTV. A detailed description of ABST is previously reported [4]. For SWOT and SOWAT, parameters related to the objective function and to the optimization process are given by the class solution.

The output of ABST was a set of segments which were provided as separate MLC collimated beams to the dose computation unit (the convolution-superposition algorithm of the ADAC Pinnacle system or the differential SAR algorithm of GRATIS [14]). Dose computation was performed on points randomly seeded in PTV, OARs and other contoured volumes (SURs), which defined the surrounding of the PTV. Dose to SURs was limited to prevent the deposit of high doses in tissues which surround the PTV but were not contoured as OAR, as described previously [3]. The number of seeded points per contoured volume was specified by the class solution and was related to the volume of the OAR. For each segment, a dose matrix, containing the dose distribution per volume and per seeded point in each volume, was computed using a unity weight.

2.3 The objective function used by SWOT and SOWAT

The biophysical objective function, used by SWOT and SOWAT, assigns weights by minimizing (conjugate gradient method) the function -B.P consisting of a biological factor B and a physical factor P.

2.3.1 Biological factor of the objective function

The factor B imposes dose constraints to contoured volumes of normal tissues and organs and is a product of factors, each of them computed as :

$$\left(1 - NTOF_{name\ of\ volume}\right)^a$$

where NTOF is the "normal tissue optimization factor" calculated according to the DVH-reduction scheme by Lyman [11], Kutcher [10] and Burman [1] (used for calculating NTCP : normal tissue complication probability). The exponent a is a weighting parameter. NTOF is usually different from NTCP since, for optimization purposes, the TD50 values were often adapted. Therefore NTOFs are not NTCP predictions anymore but only formulas which provide values useful to optimize plans. For a detailed discussion regarding our use of biological models for plan optimization we refer to a letter to the editor in the Int. J. Radiat. Biol. Phys. by Vaarkamp [15] and the response by De Neve [7].

2.3.2 Physical factor of the objective function

The factor P imposes the wanted PTV prescription dose and is a product of factors, one for each PTV. Each factor consists of a factor P_r that sets the prescription dose, and a factor P_h that limits the dose inhomogeneity to a predefined maximal percentage :

$$P = \prod_i \left(P_{r,i}^{r_i} \right) \cdot \left(P_{h,i}^{s_i} \right)$$

$$P_r = \left(\frac{\sqrt{\sum_{k=1}^{n} (d_k - D)^2}}{\sqrt{n} . d_{mean}} \right)$$

$$P_h = e^{-x \cdot \left(\frac{x_{max}}{x_{tol}} - 1 \right)} . (x_{max} - x)^{-x_{max} \cdot \left(\frac{x_{max}}{x_{tol}} - 1 \right)}$$

with the volume-related parameters

r_i , s_i	:	importance factors assigned to a volume i
n	:	number of seeded points in a volume
d_k	:	dose in point k
D	:	prescription dose to a volume
$x = \frac{d_{max} - d_{min}}{d_{mean}}$	:	inhomogeneity
d_{max}	:	maximum dose
d_{min}	:	minimum dose
d_{mean}	:	mean dose of all points of a volume
x_{max}	:	maximum inhomogeneity
x_{tol}	:	expected inhomogeneity

2.4 Plans finalized by SWOT

SWOT assigns weights to segments by minimizing the biophysical objective function -B.P. All plans were optimized to an accuracy of 0.01 MU, with a limitation of the maximal optimization time to 60 minute-equivalents CPU-time on a Compaq XP900 AlphaStation (466 MHz). In practice, all plan optimizations are finished in less than 30 minute-equivalents.

2.5 Plans finalized by SOWAT

The segments, the corresponding weights and the dose matrices of plans finalized by SWOT, are used as input for SOWAT.

SOWAT involves 41 cycles of adaptations of all collimating leaf positions and weights of the segments. Each leaf position adaptation cycle evaluates the effects of changing each individual leaf position by a specified distance (± 1 to ± 8 mm, dependent on the cycle number) on the objective function. Only leaf position changes that comply with the Elekta-MLC constraints [16] are evaluated. At each evaluation, the segment-specific dose matrix is

---

adapted using a fast dose computation tool specially designed to compute dose differences due to a leaf position change. To calculate this dose difference, the original dose matrix of the segment is divided by the tissue phantom ratio (TPR), a contribution for the leaf position adaptation is added (leaf opening) or subtracted (leaf closing), and the result is multiplied by the recomputed TPR value. The dose differences are computed in a way that the resultant segment-specific dose distributions are mathematically independent from the way the segment shapes are obtained. The weighted sum of all segment-specific dose matrices provides the new dose distribution and allows to compute the value of the objective function. The changes that decrease the value of the objective function are retained. The software implementation for leaf position optimization has no specific measures to avoid trapping in local minima. As the optimal monitor units are dependent on the segment shapes, each leaf position optimization cycle is followed by a monitor unit optimization. At the end of the optimization, the output factors of the segments are recomputed, and the monitor units are adapted according to the output factor changes. The optimization takes 30-45 minute-equivalents CPU-time on a Compaq XP900 AlphaStation (466 MHz).

After all 41 cycles, the resulting dose distribution is recomputed using the dose computation unit of Gratis and considered final if it meets the protocol objectives. Otherwise, it is the starting point for a new session of SOWAT. Figure 2 illustrates the changes in leaf positions by SOWAT for the segments of one beam incidence of a head and neck plan.

Figure 2 : Changes in leaf positions by using the Segment Outline and Weight Adapting Tool.

figure 2a   figure 2b

legend : Fluence profiles of 3 segments for one beam incidence of a patient of the group of sinonasal tumors. In the left panel (figure 2a), the resulting fluence pattern without the use of SOWAT, in the right panel (figure 2b) with SOWAT.

3 Results

Tables 1 and 2 report the differences in dose statistics between the treatment plans with and without SOWAT for the two patient categories. The patients are ranked according to their start date of radiotherapy, i.e. case 1 of each table is the first patient treated in this category.

Table 1 shows the increase in terms of percentage in dose homogeneity (u) of the PTV by using SOWAT for the first group. The improvement showed a median of 11 % (range 2-27 %). The D_{max} of the spinal cord was lower for 14 of the 17 cases. Potential preservation of the contralateral parotid function by limiting the mean parotid dose to 26 Gy was a treatment objective for 4 patients. This treatment goal was achieved for all the SOWAT plans, and only for one of the non-SOWAT plans.

For the sinonasal cases of group 2, the median improvement in PTV dose homogeneity ($u_{95/5}$) by SOWAT was 7 % (range 1-14 %), as shown in table 2. The table also reports changes of endpoints for a total of 63 optic pathway structures. The D_{mean} improved for 53 structures and remained unchanged for 1 structure. SOWAT worsened D_{mean} for 9 structures. The D_{95} exceeded 60 Gy for 14 optic pathway structures without the use of SOWAT and for 5 structures with SOWAT.

Table 1 : Changes in dose statistics by using SOWAT for pharyngeal and laryngeal tumors.

	re-irradiations				primary radiotherapy			
case	PTV		spinal cord		case	PTV		spinal cord	
	u	%	Dmax	D (Gy)		u	%	Dmax	D (Gy)
1	+	2	+	$19 \rightarrow 10$	1	+	5	+	$55 \rightarrow 49$
2	+	27	-	$17 \rightarrow 18$	2	+	14	+	$55 \rightarrow 53$
3	+	4	+	$36 \rightarrow 28$	3	+	14	+	$39 \rightarrow 34$
4	+	6	+	$19 \rightarrow 18$	4	+	11	-	$50 \rightarrow 51$
5	+	20	+	$20 \rightarrow 14$	5	+	4	+	$55 \rightarrow 51$
6	+	8	+	$30 \rightarrow 12$	6	+	11	+	$54 \rightarrow 48$
7	+	13	+	$30 \rightarrow 16$	7	+	18	-	$42 \rightarrow 49$
8	+	19	+	$26 \rightarrow 18$					
9	+	2	+	$42 \rightarrow 22$					
10	+	14	+	$31 \rightarrow 14$					

legend :

for the PTV

u = dose homogeneity $\frac{Dmax - Dmin}{Dmedian}$ (+ : better result with SOWAT)

Dmax = maximum dose in Gy, Dmin = minimal dose in Gy

Dmedian = median dose in Gy

% : ($u_{without\ SOWAT}$ - $u_{with\ SOWAT}$) expressed in %

for the spinal cord

Dmax = maximum dose

+ : lower Dmax with SOWAT, - : higher Dmax with SOWAT

$< dose > \rightarrow < dose > =$

maximum dose in Gy respectively without and with SOWAT

Table 2 : Changes in dose statistics by using SOWAT for sinonasal tumors.

case	PTV		chiasm		nerve left		nerve right		retina left		retina right	
	u 95/5	%	Dmean	Gy	Dmean	Gy	Dmean	Gy	Dmean	Gy	Dmean	Gy
1	+	9	-	49 → 50	-	52 → 53	+	48 → 45	+	41 → 39	-	21 → 24
2	+	5	-	44 → 46	=	54 → 54	+	55 → 48	+	44 → 31	+	36 → 23
3	+	4	+	44 → 38	+	57 → 44	+	53 → 41	+	51 → 23	+	29 → 15
4	+	8	+	54 → 50	+	50 → 46	+	50 → 48	+	38 → 27	+	32 → 24
5	+	11	-	34 → 41	+	56 → 49	+	52 → 43	+	49 → 34	+	50 → 35
6	+	7	-	27 → 28	+	44 → 38	+	55 → 49	+	43 → 34	+	49 → 39
7	+	7	+	45 → 41	+	55 → 52	+	46 → 36	+	46 → 38	+	31 → 23
8	+	14	+	42 → 38	+	53 → 47	+	47 → 42	+	38 → 28	+	30 → 23
9	+	12	+	50 → 43	+	50 → 39	+	52 → 38	+	37 → 27	+	31 → 21
10	+	8	+	38 → 35	-	47 → 48	+	41 → 39	+	39 → 32	+	27 → 25
11	+	2	+	42 → 35	+	27 → 25	+	54 → 46	+	27 → 24	+	53 → 39
12	+	1	+	45 → 41	resected		+	47 → 44	resected		+	38 → 31
13	+	4	-	27 → 28	-	29 → 31	+	53 → 48	+	20 → 18	+	42 → 34

for the PTV

u 95/5 = dose homogeneity $\frac{D95 - D5}{Dmedian}$ (+ : better result with SOWAT)

D95 = 95th percentile dose in Gy, D5 = 5th percentile dose in Gy, Dmedian = median dose in Gy

% : (u $95/5_{without\ SOWAT}$ - u $95/5_{with\ SOWAT}$) expressed in %

for the optic pathway structures

Dmean : mean dose

+ : lower Dmean with SOWAT, - : higher Dmean with SOWAT, = : Dmean unchanged by SOWAT

$< dose > \to < dose >$ = Dmean in Gy respectively without and with SOWAT

4 Discussion

SOWAT only retains a new segment outline or segment weight status if this is associated with a better outcome of the value of the objective function. However, comparing different treatment plans generated for a case may be difficult, certainly if multiple organs at risk are involved. For the first group (table 1) the value of SOWAT was obvious. For only three patients there was an increase in D_{max} for the spinal cord, two of them with a dose of 1 Gy and one with a dose of 7 Gy. The PTV dose homogeneity however, increased for the three cases with respectively 27, 11 and 18 %. For all the other cases both target coverage and sparing of OARs was better for the SOWAT plans. For the sinonasal cases (group 2), the high number of organs at risk and their different toxicity thresholds make comparisons of the outcome of different treatment plan optimizations less obvious. However, the PTV dose homogeneity was higher for all SOWAT plans, and this was combined with a lower dose for 84 % of the optic pathway structures. For the 30 cases (group 1 and 2), the plans optimized with and without SOWAT were evaluated by a clinical staff. None of the plans optimized without SOWAT was found to be better. As a result, all SOWAT treatment plans were clinically delivered.

In the forward planning strategy at GUH, segment geometries are defined prior to any optimization. As a result, the segment outlines are likely to be suboptimal. If the treatment planning outcome after segment weight optimization is not compliant with the clinical objectives, segment outlines can be adapted or additional segments can be generated, followed by new cycles of segment weight optimization. Direct leaf position optimization improves the plan by making better use of an existing number of segments, without the need for extra segments. By finetuning the position of leaves, SOWAT can place dose gradients at the optimal location between the PTV and OARs and adapt the shape of segments for one beam direction, dependent on the shape of segments for another beam direction. This can result in an erosion of the margins around the PTV and an increase of the number of intensity levels in a beam for a fixed number of segments. Target dose homogeneity can be increased by repositioning leaves that are in BEV close to hot or cold spots. As the use of SOWAT does not change the beam incidences and does not generate additional segments, treatment delivery time remains almost unaffected.

In conclusion, SOWAT is a powerful tool to perform the final optimization of IMRT plans, without increasing the complexity of the plan or the delivery time.

Acknowledgements

References

1. Burman C, Kutcher G, Emami B, et al. Fitting of normal tissue tolerance data to an analytic function. Int J Radiat Oncol Biol Phys 1991;21:123-35.

2. Chao K, Deasy J, Markman J et al. A prospective study of salivary function sparing in patients with head-and-neck cancers receiving intensity-modulated or three-dimensional radiation therapy: initial results. Int J Radiat Oncol Biol Phys 2001;49:907-16.

3. Claus F, De Gersem W, De Wagter C, et al. An implementation strategy for IMRT of ethmoid sinus cancer with bilateral sparing of the optic pathways. Int J Radiat Oncol Biol Phys 2001;51:318-31.

4. De Gersem W, Claus F, De Wagter C, et al. An anatomy based beam segmentation tool for intensity modulated radiation therapy and its application to head and neck cancer. Int J Radiat Oncol Biol Phys 2001;51:849-59.

5. De Gersem W, Vakaet L, Claus F, et al. MLC leaf position optimization using a biophysical objective function. Radiother Oncol 2000;56(suppl.1):S96-S97 abstract 348.

6. De Neve W, De Gersem W, Derycke S et al. Clinical delivery of intensity modulated conformal radiotherapy for relapsed or second-primary head and neck cancer using a multileaf collimator with dynamic control. Radiother Oncol 1999;50:301-14.

7. De Neve W, De Gersem W, De Meerleer G, et al. Reduction of target dose inhomogeneity in IMRT treatment planning using biological objective functions. Int J Radiat Oncol Biol Phys 2001;49:1519-20.

8. De Neve W, De Wagter C, De Jaeger K et al. Planning and delivering high doses to targets surrounding the spinal cord at the lower neck and upper mediastinal levels: static beam-segmentation technique executed by a multileaf collimator. Radiother Oncol 1996;40:271-9.

9. Eisbruch A, Ten Haken R, Kim H, et al. Dose, volume, and function relationships in parotid salivary glands following conformal and intensity-modulated irradiation of head and neck cancer. Int J Radiat Oncol Biol Phys 1999;45:577-87.

10. Kutcher G and Burman C. Calculation of complication probability factors for non-uniform normal tissue irradiation: the effective volume method. Int J Radiat Oncol Biol Phys 1989;16:1623-30.

11. Lyman J. Complication probabilities as assessed from dose-volume histograms. Radiat Res 1985;104(Suppl.):513-9.

12. Martel M, Sandler H, Cornblath W et al. Dose-volume complication analysis for visual pathway structures of patients with advanced paranasal sinus tumors. Int J Radiat Oncol Biol Phys 1997;38:273-84.

13. Parsons J, Bova F, Fitzgerald C, et al. Radiation optic neuropathy after megavoltage external-beam irradiation: analysis of time-dose factors. Int J Radiat Oncol Biol Phys 1994;30:755-63.

14. Sherouse G, Thorn J and Novins K. A portable 3D radiotherapy treatment design system. Med Phys 1989;16:466.

15. Vaarkamp, J. and Krasin, M. Reduction of target dose inhomogeneity in IMRT treatment planning using biological objective functions. Int J Radiat Oncol Biol Phys 2001;49:1518-20.

16. Webb S. Issues in delivering IMBs via the DMLC technique. In: Intensity-Modulated Radiation Therapy. Bristol (UK), Institute of Physics Publishing; 2001;96-170.

4.5 **Intensity modulated radiation therapy for oropharyngeal and oral cavity tumors : clinical use and experience. F. Claus, W. Duthoy, et al. Oral Oncol 2002;in press.**

topics discussed :	→ IMRT for oropharyngeal and oral cavity tumors
	→ clinical results for head and neck IMRT
	→ feasibility of IMRT to preserve parotid function
key question :	How to implement IMRT for oropharyngeal and oral cavity tumors ?

paper 4.5

Intensity modulated radiation therapy for oropharyngeal and oral cavity tumors : clinical use and experience

Filip Claus[1], Wim Duthoy[1], Tom Boterberg[1], Werner De Gersem[1], John Huys[1], Hubert Vermeersch[2] and Wilfried De Neve[1]

[1]Division of Radiotherapy
Ghent University Hospital

[2]Department of Head and Neck Surgery
Ghent University Hospital

Abstract

Background and purpose : Intensity modulated radiation therapy (IMRT) offers an opportunity to generate dose distributions highly conformal to the target volume. Head and neck cancer patients, referred for radiotherapy, may be good candidates to benefit from IMRT. This paper discusses the clinical implementation of IMRT for oropharyngeal and oral cavity tumors, and reports the clinical results of the 14 patients treated with this technique at Ghent University Hospital (GUH).

Patients and Methods : Between May 1999 and May 2001, 14 patients were treated with IMRT at GUH for oropharyngeal or oral cavity tumors. Two groups of patients can be distinguished. The first group consists of 8 patients re-irradiated with IMRT for a locoregional relapse. The second group of 6 patients were treated with IMRT for a primary tumor. For the first group, IMRT was used to treat the relapse by generating a concave dose distribution, i.e. to combine a homogeneous target re-irradiation with a dose to the spinal cord as low as possible. For the second group, IMRT was applied in order to achieve a more homogeneous dose distribution inside the PTV and to preserve parotid gland function.

Results : The majority of the patients of group 1 (6/8) relapsed in field within 4 months after the end of the re-irradiation, with a median overall survival of 7 months. For group 2, two patients died shortly after the end of the IMRT treatment, the other 4 patients are free of tumor relapse with a median follow-up of 5 months (1-13 months). The acute toxicity due to radiation was acceptable for both patient groups. Dysphagia and pain was more present in group 1. Regarding late complications for the group of re-irradiations (group 1), no myelitis, carotid rupture or cranial nerve palsy was observed. One patient of group 1 developed osteoradionecrosis of the mandible and feeding tube dependency was present for another patient. No fatal late complications were observed in this group. For the first two patients of group 2, sparing of the parotid function was not a treatment objective. For the other patients of group 2, the mean dose to the contralateral parotid gland ranged from 17 to 25 Gy, which resulted in a decrease of subjective symptoms of xerostomia compared to patients treated with conventional radiotherapy.

Conclusions : The implementation of IMRT for oropharyngeal and oral cavity tumors results in a homogeneous target irradiation and allows to re-irradiate locoregional relapses with acceptable adverse effects. Sparing of the parotid gland by

IMRT is feasible, although this may be significantly influenced by the delineation method of the elective lymph node regions.
Keywords : cancer, oral cavity, oropharynx, radiotherapy, IMRT

1 Introduction

Head and neck cancer patients may be good candidates to benefit from intensity modulated radiation therapy (IMRT). IMRT offers the opportunity to improve the planning target volume (PTV) dose homogeneity by omitting photon-electron matchplanes, and in selected cases, to decrease xerostomia by sparing one or more of the major salivary glands. However, due to the complexity of implementing IMRT for this region, few clinical results are reported yet, and most of the data consist of very small patient series [1][3][8][9][10][13][16][22]. IMRT is often delivered in combination with conventional techniques [15], or its use is restricted to a boost to the primary tumor region [21].

By May 2001, 85 head and neck patients were treated with IMRT at Ghent University Hospital (GUH). Initially, IMRT was the treatment modality of choice to re-irradiate locoregional relapses or second primary head and neck cancers [10]. In a second phase, IMRT was applied as primary treatment. For pharyngeal and oral cavity tumors, the rationale to use IMRT was to increase the dose homogeneity inside the target volume and to preserve parotid function.

This paper discusses a clinical implementation of IMRT for oropharyngeal and oral cavity tumors.

2 Patients and Methods

Between May 1999 and May 2001, 14 patients were treated with IMRT at GUH for oropharyngeal or oral cavity tumors. Two groups of patients can be distinguished. The first group consists of 8 patients re-irradiated with IMRT for a locoregional relapse. The second group of 6 patients was treated with IMRT for a primary tumor.

2.1 group 1 : IMRT for locoregional relapses

2.1.1 Treatment objectives

For all patients, the dose to the spinal cord by the first radiotherapy treatment ranged between 40 and 50 Gy, delivered by 2 Gy fractions (5 days/week). IMRT was used to treat the relapse by generating a concave dose distribution, i.e. to combine a homogeneous target re-irradiation with a dose to the spinal cord as low as possible.

The maximal dose to the spinal cord imposed by the IMRT plan was 15 Gy. The PTV dose prescription ranged between 64 and 70 Gy. For the dose homogeneity within the PTV, the ICRU (International Commission on Radiation Units and Measurements) guidelines were followed, i.e. a maximal underdosage of 5 % and maximal overdosage of 7 %. In case of

overlap or close vicinity of the PTV and the spinal cord, the dose constraint to the spinal cord was respected, at the cost of the PTV dose homogeneity. Dose to the mandible was penalized by plan optimization, but no dose constraints were specified upfront as treatment objectives.

2.1.2 Planning strategy

Our IMRT planning strategy for locoregional relapses of head and neck cancer is previously reported [9][10]. The IMRT plans consisted of six non-opposed coplanar 6 MV photon beams, for which the individual multileaf collimated beamparts (segments) were optimized by adapting leaf positions and segment weights [7], using a biophysical cost function [11]. Treatments were delivered within a time slot of 15 minutes on an Elekta Sli-plus accelerator.

2.2 group 2 : IMRT as primary radiotherapy

2.2.1 Treatment objectives

Conventional radiotherapy for elective node irradiation of head and neck cancer patients at GUH consisted of two lateral fields and an anterior supraclavicular field, delivered with a single isocenter technique [20]. At a dose of 44 Gy, the spinal cord was blocked, and the target region not covered by the photon beams was boosted with electron beams. Figure 1 shows the location of the matchplane (dotted line) between a lateral photon and electron beam in a transverse plane through the body of the second cervical vertebra. The matchplane is situated in the middle of the upper jugular lymph node chain. Initially, IMRT was used to avoid electron-photon matching. In a second phase, preservation of the parotid gland function was also intended.

For the part of the PTV that is located outside build-up regions and outside regions where PTV overlaps with organs at risk (OARs), the ICRU guidelines for dose homogeneity were followed. The region of the PTV that extends close to the skin in the build-up region, is carefully analyzed. If underdosage is clinically unacceptable, bolus material is used. A clinical decision is also made regarding overlap areas of PTV and OARs. If the OAR function is to be preserved, a PTV underdosage restricted to the overlap zone which is consistent with OAR function preservation, is accepted. When parotid gland function had to be preserved, the mean dose to the contralateral parotid gland was limited to 26 Gy. This dose threshold was based on previous data published by Eisbruch et al. [12].

Figure 1

1 mandible

2 submandibular gland

3 sternocleidomastoid muscle

4 internal jugular vein

5 carotid artery

6 paraspinal muscles

7 vertebral body C2

Legend : Drawing of a transverse section through the bottom level of the second cervical vertebral body, illustrating the photon-electron match line (black dotted line), located in the middle of the upper jugular lymph node chain, outlined in solid black.

2.2.2 Current planning strategy

2.2.3.1 Entrance criteria for patients included

Since December 2000, following entrance criteria are specified to include patients for IMRT. For oropharyngeal cancer, stages T1-3 N0-2b M0 are included, for oral cavity cancer, the stages T1-T4 N0-2b M0. The expected median survival has to exceed 1 year, and the Karnofsky performance status has to be more than 50.

2.2.3.3 Treatment protocol

Table 1 specifies the selection of lymph node target volumes, and the prescribed dose to these volumes, as used for the IMRT plans. The terminology for lymph node regions as

proposed by Robbins et al. [19] is used in the table.

The clinical target volume is 3D-isotropically expanded with a margin of 3 mm to a PTV, to take into account setup-inaccuracies during treatment delivery. A reduced PTV, excluding the region within a distance of 6 mm from the skin outline, is used for plan optimization and dose prescription. By excluding the build-up region from the PTV, conflicts during plan optimization and a potential impossibility to achieve the ICRU guided PTV dose homogeneity are avoided. Dose is reported for the complete as well as for the reduced PTV.

Before December 2000, dose prescriptions were made on a patient-individual basis (patients 1-4 in table 3). Since December 2000, a treatment protocol was applied.

Three PTVs with corresponding dose prescriptions are specified :

PTV-70 :
- ▷ the primary tumor and lymph nodes containing clinical
    or radiological evidence of disease, treated to 70 Gy
- ▷ the median PTV-70 dose is used for dose prescription
- ▷ the tolerated dose range inside this PTV-70 is 66 to 75 Gy
- ▷ the 3D-maximum dose has to be located inside this PTV-70

PTV-60 :
- ▷ elective lymph node regions treated to a dose of 60 Gy
- ▷ the selection criterion is specified in table 1
- ▷ the median PTV-60 dose is used for dose prescription
- ▷ the tolerated dose range inside this PTV-60 is 57 to 65 Gy

PTV-50 :
- ▷ elective lymph node regions treated to a dose of 50 Gy
- ▷ the selection criterion is specified in table 1
- ▷ the minimum PTV-50 dose is used for dose prescription
    (i.e the minimum PTV-50 dose is 50 Gy)

When we elected to spare a parotid gland, it was a planning goal to keep its mean dose below 26 Gy [12]. The dose constraints for the spinal cord and brainstem were respectively set to 50 and 60 Gy, with a maximum daily fraction size of 2 Gy.

The IMRT treatment is delivered in two consecutive phases. The first phase consists of 27 fractions of 1.85 Gy to PTV-50 and 2.22 Gy to PTV-60 and PTV-70. In a second phase, 5 fractions of 2 Gy were delivered to PTV-70.

The beam setup consists of six non-opposed coplanar 6 MV photon beams, for which the individual multileaf collimated segments are computer-generated [6] and optimized by adapting leaf positions and segment weights [7], using a biophysical cost function [11]. Treatments are delivered within a time slot of 15 minutes on an Elekta Sli-plus accelerator.
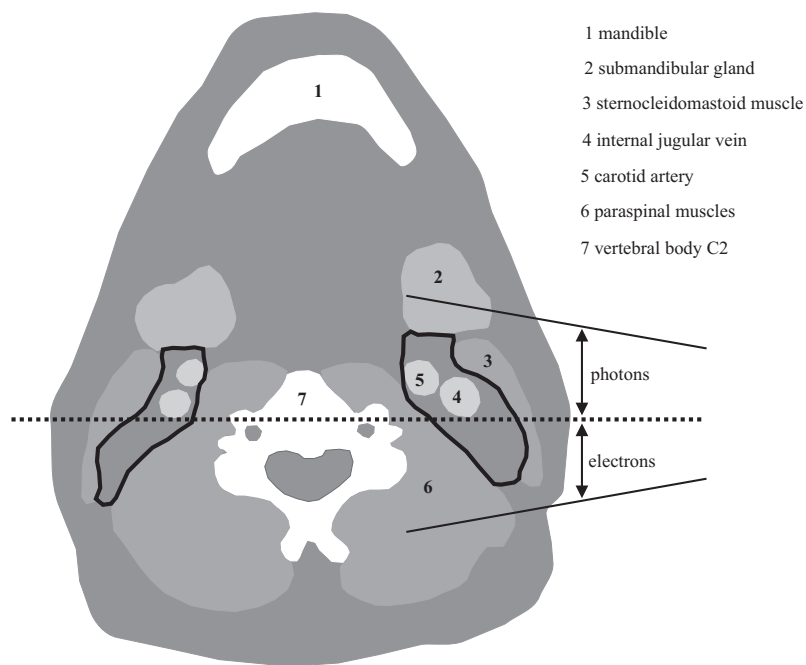
2.3 Patients

Table 2 and 3 list the 14 patients. All of them were treated with curative intent.

Table 1

Selection and dose prescription of lymph node target volumes			
lymph node region	**selection criterion**	**ipsi-bilateral**	**dose (Gy)**
Ia	if evidence clinical invasion floor of mouth or region Ib	ipsilateral*	60
Ib	target in all cases	ipsilateral*	60
II	target in all cases	bilateral	60
III	target in all cases	bilateral	50-60**
IV	target in all cases	bilateral	50-60**
V	if clinical evidence invasion regions II or III or IV	ipsilateral	60
retropharyngeal	target in all cases	bilateral	60

* : bilateral if tumor crosses the midline

** : 60 Gy if first elective station, 50 Gy if second or third elective station

Table 2 part1

case	age*	subsite primary	TNM stage	histology	surgery	start	dose**
	y		primary	grade (G)	/ chemo	radio R/	Gy
1	56	floor of mouth	pT4pN0M0	squam. cell G3	y / n	01/10/97	50
2	51	retromolar area	pT3pN0M0	squam. cell G2	y / n	23/10/98	60
3	51	floor of mouth tongue	cT2cN0M0	squam. cell G3	n / n	24/01/99	65
4	52	uvula	cT1cN0M0	squam. cell G3	n / n	01/03/99	70
5	55	floor of mouth	pT1pN0M0	squam. cell G1	y / y	03/05/96	56
6	40	cheek mucosa	pT4pN0M0	muco-epiderm.	y / n	08/04/99	60
7	59	floor of mouth	cT1cN0M0	squam. cell G2	n / n	07/07/99	84***
8	49	floor of mouth tongue	pT2pN0M0	squam. cell G3	y / n	27/09/99	50

Table 2 (part1) : Group 1 : IMRT for relapses

* at time of analysis (July 2001) **dose to the primary tumor site ***includes brachytherapy dose

Table 2 part2

	Table 2 (part2) : Group 1 : IMRT for relapses				
case	subsite relapse	TNM stage relapse	surgery / chemo	start IMRT	dose** (Gy)
1	soft palate	r cT4cN0M0	n / n	18/05/99	66
2	retromolar area, tongue, tonsil	r cT4cN0M0	n / y	13/12/99	64
3	retromolar area, submandibular nodes	r pT4pN2bM0	y / n	21/12/99	64
4	cranial jugular nodes, retropharyngeal nodes	r cTxcN3M0	n / n	27/01/00	66
5	floor of mouth, tonsil, cranial jugular nodes	r cT4cN3M0	n / y	10/03/00	66
6	cheek mucosa, posterior wall, submandibular nodes	r pT4pN1M0	y / n	13/03/00	70
7	floor of mouth, tonsil, retromolar area, tongue	r pT4pN0M0	y / n	05/09/00	70
8	floor of mouth, tongue	r cT3cN2cM0	n / n	19/03/01	70

* at time of analysis (July 2001) **dose to the primary tumor ***includes brachytherapy dose

Table 3

Table 3 : Group 2 : patients treated with IMRT for primary lesions

case	age y*	subsite primary	TNM stage primary	histology grade (G)	surgery /chemo	start radioR/	dose Gy**	parotid ***
1	43	tonsil posterior wall	cT4cN2cM0	squam. cell G2	n / y	24/12/99	70	no
2	58	retromolar	pT2pN2bM0	squam. cell G3	y / n	03/02/00	60	no
3	53	tonsil tongue	cT3cN2bM0	squam. cell G1	n / n	17/03/00	70	yes
4	47	tonsil	pT2pN1M0	squam. cell G3	y / n	06/11/00	66	yes
5	67	tonsil soft palate	pT3pN1M0	squam. cell G1	y / n	14/12/00	70	yes
6	61	tonsil	pT2pN1M0	squam. cell G2	y / n	20/03/01	70	yes

*time of analysis (July 2001) **dose to the primary tumor ***parotid sparing is treatment goal

3 Results

Table 4 reports the clinical results for the 14 patients. The follow-up was recorded from the end of the IMRT treatment till the time of analysis (July 2001).

The first 6 patients of group 1 relapsed in field within 4 months after the end of the re-irradiation. For patients 4 and 5, residual disease was present at the end of the IMRT treatment. Patients 7 and 8 of group 1 are still free of disease. The median overall survival for the patients of this group (measured as the time after the end of the treatment) is 7 months.

For group 2, two patients (patient 1 and 2) died shortly after the end of the IMRT treatment. Patient 1 died one month after the end of the concomittant chemo-radiotherapy treatment, due to a candida sepsis. Patient 2 developed a tumor relapse in the contralateral lymph node region II, which was not treated by the previous radiotherapy (the patient was treated before December 2000, and thus not according to the current IMRT treatment protocol). He died four months after the end of the radiation treatment. Patients 3-6 are free of tumor relapse, with a median follow-up of 5 months (1-13 months).

To score the acute toxicity due to radiation, the Common Toxicity Criteria (CTC) of the NIH (The US National Institutes of Health) were used (information on http://ctep.info.nih.gov/CTC3). Weight loss was less than 10 % for all patients, except for the second patient of group 1 (15 %). Radiation dermatitis was mild (dry desquamation) to moderate (patchy moist desquamation) for 13 patients, and confluent moist for the first patient of group 1. Pain due to radiation was more present in group 1. Pain due to radiation was mild and not interfering with function for 2 patients, moderate for 8 patients and severe (interfering with activities of daily living) for 4 patients. Mucositis was mild (erythema) for only 2 patients, patchy pseudomembranous for 6 patients and confluent pseudomembranous for 6 patients. Pharyngeal dysphagia was mild (patient could eat regular diet) to moderate (requiring predominantly pureed, soft, or liquid diet) for 12 patients. Two patients suffered from severe dysphagia, requiring feeding tube and IV hydratation.

Regarding late complications for the group of re-irradiations (group 1), no myelitis, carotid rupture or cranial nerve palsy was observed. Patient 7 of group 1 developed osteora-dionecrosis of the mandible. Feeding tube dependency was present for patient 7. All patients had neck fibrosis and two of them suffered from hearing loss. No fatal late complications were observed in this group.

Table 4

Table 4 : Results of the IMRT treatments for group 1 and 2

category / case	group 1 : relapses								group 2 : primaries					
	1	2	3	4	5	6	7	8	1	2	3	4	5	6
common toxicity criteria : peak score (grade)														
weight loss	0	2	0	1	0	1	1	0	1	1	1	1	1	0
dermatitis*	1	1	2	1	1	2	1	2	3	2	1	1	3	2
pain*	3	3	3	3	2	2	2	2	2	2	1	1	2	2
mucositis*	1	3	3	2	2	2	2	2	3	3	2	1	3	3
dysphagia*	2	3	2	2	2	2	3	1	2	1	1	1	2	1
(second) relapse / survival														
relapse	yes	yes	yes	yes	yes	yes	no	no	no	yes	no	no	no	no
in field relapse	yes	yes	yes	yes	yes	yes	no	no	no	no	no	no	no	no
# months between IMRT → relapse	1	2	4	0**	0**	4	/	/	/	1	/	/	/	/
cancer-related death	yes	yes	yes	yes	yes	yes	no	no	no	yes	no	no	no	no
non-cancer related death	no	no	no	no	no	no	yes	no	yes	no	no	no	no	no
# months between IMRT → relapse	12	3	11	7	7	7	/	/	1	4	/	/	/	/

** : residual disease   *related or due to radiation

For the first two patients of group 2, sparing of the parotid function was not a treatment objective. For patients 3-6, the mean dose to the contralateral parotid gland ranged from 17 to 25 Gy, which resulted in a decrease of subjective symptoms of xerostomia compared to patients treated with conventional radiotherapy. No functional tests or saliva flow measurements were performed. Figure 2 shows the dose distribution in a coronal plane of the treatment plan for patient 6 of group 2, illustrating the intended sparing of the left parotid gland.

Figure 2
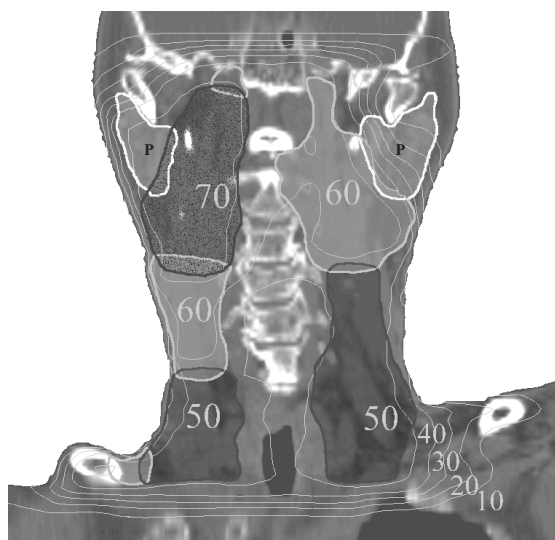
Legend : Dose distribution in a coronal plane of the IMRT treatment plan for patient 6 of the second group, illustrating the intended sparing of the left parotid gland. The isodose lines, expressed in Gy, represent the cumulative dose for the two treatment phases. The PTV-50 is coloured in transparent dark grey, the PTV-60 in transparent light grey and the PTV-70 in black speckles. The parotid glands are outlined in white and designated with the capital P.

4 Discussion

As previously reported [5], the overall survival for high dose re-irradiations of head and neck

---

cancer remains poor, and is associated with a lower rate of local tumor control compared to tumors of similar stage treated with primary radiotherapy. Although re-irradiations for locoregional relapses are associated with a poor prognosis, IMRT is a good technique to combine a high tumor dose with acceptable toxicity grades. The osteoradionecrosis of the mandible observed in patient 7 of group 1, may be explained by the high cumulative dose (154 Gy) of both treatment plans and the use of brachytherapy for the first radiation treatment.

For primary radiotherapy, IMRT allows a higher dose homogeneity inside the PTV by avoiding photon-electron matching. Another advantage is the possibility and feasibility of IMRT to preserve uni- or bilateral parotid gland function [12][4][23].

A strategy to treat 3 dose prescription levels with 2 consecutive treatment phases reduces the planning workload and results for the macroscopically invaded regions and the first elective lymph node stations in a radiobiological advantage, because of a higher fraction size (2.22 Gy) with shortening overall time [17].

The use of a fixed beam-setup and a fixed set of parameters for beam segmentation and plan optimization, allows to automate the generation of IMRT plans and guarantees a plan deliverable within a specified time slot.

The bottle-neck of the treatment planning process is the delineation of the clinical target volumes. The implementation of IMRT for head and neck cancer has lead to an increased interest in guidelines for delineation of lymph node regions. Especially the definition to outline lymph node region II may affect, or even determine the feasibility to preserve the parotid function by conformally irradiating this lymph node region. Figure 3 displays the difference in delineation guidelines for this region in a transverse plane, as proposed by Gregoire et al. [14] (solid white line) and Nowak et al. [18] (dashed white line). In a coronal plane, the difference is even more striking, as illustrated by figure 4. The cranial border of lymph node region II, as defined by Gregoire, is the bottom edge of the body of the first cervical vertebra (C1), whereas Nowak defines the cranial border as the cranial CT-slice (in a transverse plane) through C1. These differences in contouring may affect cure rates of the radiation treatment, but certainly affect the plantechnical feasibility to limit dose to a certain volume of the parotid gland. The validity of the two proposed guidelines needs to be confirmed in larger patient series. For our IMRT implementation, we follow the guidelines proposed by Gregoire, except for the cranial border of lymph node region II, which we define at the middle of the body of C1.

Dawson et al. [4] reported the patterns of locoregional recurrence following parotid-sparing radiotherapy. This sparing was achieved by limiting the dose to the contralateral parotid gland. The superior extent of the contralateral lymph node region II, was defined as the axial CT image in which the posterior belly of the digastric muscle crosses the jugular vein. This corresponds to the superior extent of a radical neck dissection. The ipsilateral superior extent was set at the base of the skull. They examined 58 patients, and the eligibility criteria for the parotid-sparing protocol were patients who required radiotherapy to the primary tumor and bilateral neck lymph nodes. Patients with suspicion of contralateral neck disease were included as long as the jugulodigastric and higher neck nodes did not contain metastases. The median time from treatment to follow-up was 27 months. They

found that the majority of locoregional relapses after parotid-sparing radiotherapy were in-field, and none of the relapses occurred in the contralateral high level of lymph node region II. These data support a rationale to implement IMRT to preserve salivary gland function by sparing the contralateral parotid gland.

Chao et al. [2] reported 27 patients treated with IMRT, most of them nasopharyngeal and oropharyngeal cases. Bilateral sparing of the parotid glands was a treatment objective, and the average dose to the parotid gland was 28 Gy for the postoperative cases and 30 Gy for the patients receiving IMRT as definitive treatment. The jugular chain (level II-IV) was target volume for all cases, but there was no specification with regard to their lymph node delineation method. Disease free survival rates were not reported.

Figure 3

1 mandible
2 medial pterygoid muscle
3 parotid gland
4 digastric muscle
5 internal jugular vein
6 internal carotid artery
7 sternocleidomastoid muscle
8 paraspinal muscles
9 vertebral body C2
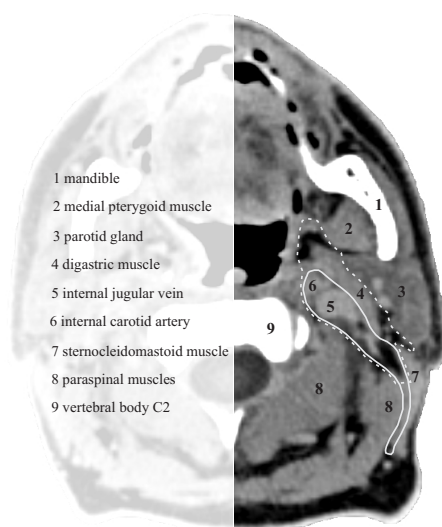
Legend : Transverse CT-slice through the second cervical vertebral body illustrating two different approaches to delineate lymph node region II. In white solid line the delineation as defined by Gregoire et al., in white dashed line the guidelines proposed by Nowak et al.

Figure 4
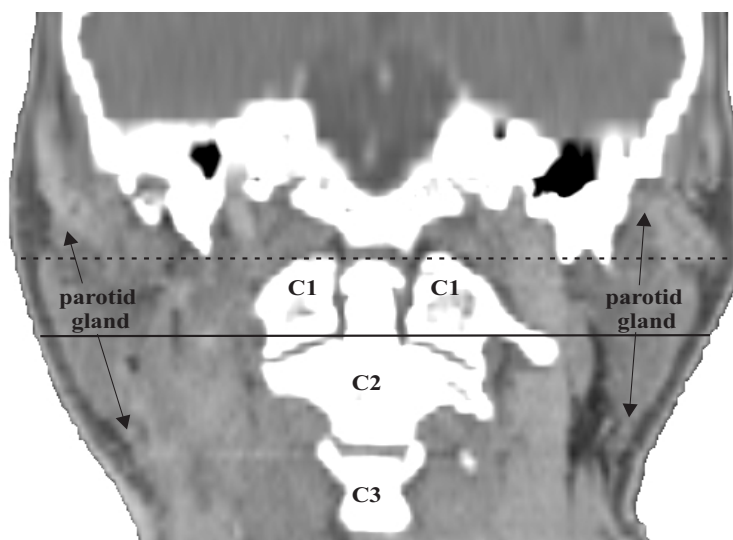
Legend : A coronal reconstructed CT-image through the cervical vertebral bodies 1, 2 and 3 (C1,C2,C3). The black lines represent the cranial edge of the target volume for lymph node region II, as respectively defined by Gregoire et al. (solid line) and Nowak et al. (dashed line). The black solid lines with arrows indicate the craniocaudal extent of the parotid glands.

In conclusion, the implementation of IMRT for oropharyngeal and oral cavity tumors results in a homogeneous target irradiation and allows to re-irradiate locoregional relapses to high doses with acceptable adverse effects. Sparing of the parotid gland by IMRT is feasible, although this may be significantly influenced by the delineation method of the elective lymph node regions. Sparing of the ipsilateral gland remains a topic of debate.

Acknowledgements

FWO. The Ghent University Hospital is a member of the Elekta IMRT Consortium.

References

1. Butler EB, Teh BS, Grant WH, et al. Smart (simultaneous modulated accelerated radiation therapy) boost: a new accelerated fractionation schedule for the treatment of head and neck cancer with intensity modulated radiotherapy. Int J Radiat Oncol Biol Phys 1999;45(1):21-32.

2. Chao KS, Deasy J, Markman J, et al. A prospective study of salivary function sparing in patients with head-and-neck cancers receiving intensity-modulated or three-dimensional radiation therapy: initial results. Int J Radiat Oncol Biol Phys 2001;49:907-16.

3. Chao KS, Low DA, Perez CA, et al. Intensity-modulated radiation therapy in head and neck cancers: The Mallinckrodt experience. Int J Cancer 2000;90(2):92-103.

4. Dawson LA, Anzai Y, Marsh L, et al. Patterns of local-regional recurrence following parotid-sparing conformal and segmental intensity-modulated radiotherapy for head and neck cancer. Int J Radiat Oncol Biol Phys 2000;46(5):1117-26.

5. Dawson LA, Myers LL, Bradford CR, et al. Conformal re-irradiation of recurrent and new primary head-and-neck cancer. Int J Radiat Oncol Biol Phys 2001;50(2):377-85.

6. De Gersem, W, Claus F, De Wagter C, et al. An anatomy based beam segmentation tool for intensity modulated radiation therapy and its application to head and neck cancer. Int J Radiat Oncol Biol Phys 2001;51:849-59.

7. De Gersem W, Vakaet L, Claus F, et al. MLC leaf position optimization using a biophysical objective function. Radiother Oncol 2000;56(suppl.1):S96-S97 abstract 348.

8. De Neve W, Claus F, Van Houtte P, et al. Intensity modulated radiotherapy with dynamic multileaf collimator. Technique and clinical experience. Cancer Radiother 1999;3(5):378-92.

9. De Neve W, De Wagter C, De Jaeger K, et al. Planning and delivering high doses to targets surrounding the spinal cord at the lower neck and upper mediastinal levels: static beam-segmentation technique executed by a multileaf collimator. Radiother Oncol 1996;40:271-9.

10. De Neve W, De Gersem W, Derycke S, et al. Clinical delivery of intensity modulated conformal radiotherapy for relapsed or second-primary head and neck cancer using a multileaf collimator with dynamic control. Radiother Oncol 1999;50:301-14.

11. De Neve W, De Gersem W, De Meerleer G, et al. Reduction of target dose inhomogeneity in IMRT treatment planning using biological objective functions. Int J Radiat Oncol Biol Phys 2001;49:1519-20.

12. Eisbruch A, Ten Haken RK, Kim HM, et al. Dose, volume, and function relationships in parotid salivary glands following conformal and intensity-modulated irradiation of head and neck cancer. Int J Radiat Oncol Biol Phys 1999;45:577-87.

13. Fraass BA, Kessler ML, McShan DL, et al. Optimization and clinical use of multisegment intensity-modulated radiation therapy for high dose conformal therapy. Semin Radiat Oncol 1999;9(1):60-77.

14. Gregoire V, Coche E, Cosnard G, et al. Selection and delineation of lymph node target volumes in head and neck conformal radiotherapy. Proposal for standardizing terminology and procedure based on the surgical experience. Radiother Oncol 2000;56(2):135-50.

15. Hunt MA, Zelefsky MJ, Wolden S, et al. Treatment planning and delivery of intensity-modulated radiation therapy for primary nasopharynx cancer. Int J Radiat Oncol Biol Phys 2001;49(3):623-32.

16. Kuppersmith RB, Greco SC, Teh BS, et al. Intensity-modulated radiotherapy: first results with this new technology on neoplasms of the head and neck. Ear Nose Throat J 1999;78(4):238, 241-6, 248 passim.

17. Mohan R, Wu Q, Manning M, et al. Radiobiological considerations in the design of fractionation strategies for intensity-modulated radiation therapy of head and neck cancers. Int J Radiat Oncol Biol Phys 2000;46(3):619-30.

18. Nowak PJ, Wijers OB, Lagerwaard FJ, et al. A three-dimensional CT-based target definition for elective irradiation of the neck. Int J Radiat Oncol Biol Phys 1999;45(1):33-39.

19. Robbins KT, Medina JE, Wolfe GT, et al. Standardizing neck dissection terminology. Arch Otolaryngol Head Neck Surg 1991;117:601-5.

20. Sohn JW, Suh JH, Pohar S. A method for delivering accurate and uniform radiation dosages to the head and neck with asymmetric collimators and a single isocenter. Int J Radiat Oncol Biol Phys 1995;32(3):809-13.

21. Sultanem K, Shu HK, Xia P, et al. Three-dimensional intensity-modulated radiotherapy in the treatment of nasopharyngeal carcinoma: the University of California-San Francisco experience. Int J Radiat Oncol Biol Phys 2000;48(3):711-22.

22. Verellen D, Linthout N, van den Berge D, et al. Initial experience with intensity-modulated conformal radiation therapy for treatment of the head and neck region. Int J Radiat Oncol Biol Phys 1997;39(1):99-114.

23. Wu Q, Manning M, Schmidt-Ullrich R, et al. The potential for sparing of parotids and escalation of biologically effective dose with intensity-modulated radiation treatments of head and neck cancers: a treatment design study. Int J Radiat Oncol Biol Phys 2000;46(1):195-205.

4.6 **Postoperative radiotherapy for paranasal sinus tumours : a challenge for intensity modulated radiotherapy. F. Claus, L. Vakaet, et al. Acta Oto-Rhino-Laryngol Belg 1999;53:263-9.**

topics discussed :	→ IMRT for ethmoid sinus cancer
	→ different steps of the IMRT process
	→ an IMRT ethmoid sinus example case
key question :	Is IMRT for ethmoid sinus ca feasible ?

paper 4.6

Postoperative radiotherapy of paranasal sinus tumours: a challenge for intensity modulated radiotherapy.

Filip Claus[1], Luc Vakaet[1], Werner De Gersem[1], Marc Lemmerling[2], Ilse Vanhoutte[1], Stefaan Vermael[1], Robert Van Severen[1], Bart Van Duyse[1], Hubert Vermeersch[3], Mieke Moerman[3] and Wilfried De Neve[1]

[1]Division of Radiotherapy
Ghent University Hospital

[2]Department of Radiology
Ghent University Hospital

[3]Department of Head and Neck Surgery
Ghent University Hospital

Abstract

Background and purpose : Intensity modulated radiotherapy (IMRT) is used in our department for treatment of paranasal sinuses. We describe the methodology that was developed together with the clinical implementation, illustrated by a case report.

Material and methods : Patient history, treatment and short follow-up are described. An IMRT, obtained by superposition of static beam segments was implemented. Electronic portal images, compared to digitally reconstructed radiographs (DRR) were used to evaluate and adjust patient positioning.

Results, discussion and conclusion : IMRT is an appropriate and feasible treatment technique for head and neck cancer in this anatomical regions that are difficult to treat. A high tumour dose can be combined with a good sparing of the surrounding organs at risk (OAR's).

Keywords : paranasal cancer, ethmoid cancer, conformal, intensity modulated radiotherapy

1 Introduction

Primary or postoperative conformal irradiation of head and neck tumours is a challenge, especially in the paranasal site [1], because of the difficulty to spare the different organs at risk (OAR's) located nearby the clinical target volume (CTV). The CTV is defined as the volume, anatomically defined, thought to harbour residual tumour or micro-invasion.

Segmental IMRT (intensity modulated radiotherapy) treatments have been used in our department since early 1997. IMRT is based on beam intensity modulation (BIM) meaning that inside one beam, the radiation fluence (intensity) is not equal inside the field. This

enables maximal sparing of OAR's, while retaining good coverage of the planning target volume (PTV). (The PTV is an expansion of the CTV, taking into account physiologic organ motion during treatment, and daily set-up inaccuracy). By using IMRT, we want to increase the chance of local tumour control and decrease the possibility of normal tissue complication, or both.

Implementation examples of IMRT include: i) PTV's with concave surfaces (paraspinal tumours) [2][3], ii) anatomical regions with restricted spatial range of feasible beam incidences [4] and iii) the delivery of dose distributions that are intentionally inhomogeneous (prostate, paranasal, brain).

The anatomy of the paranasal sinuses is very complex. Bony partitions between the different structures are thin and of little resistance to cancer spread. Moreover there is the presence of different important structures: the optic chiasm, optical nerves, retinae, anterior cranial fossa, pituitary gland and the brainstem. Complete surgical resection of malignant lesions located in this region is rare. Therefore, postoperative irradiation is advised, even in those cases where resection margins are negative [5].

We illustrate IMRT for paranasal sinus tumours by a case report. Until now, we treated five similar cases, using this technique.

2 Material and Methods

A 57-year-old carpenter consulted an otorhinolaryngologist for swelling in his nose. Computed tomography revealed a lesion of the nasal cavity and paranasal sinuses. Investigation by MRI showed the following tumour localisation: lesion of the left ethmoid sinus, extending to the nasal cavity without invasion of the left orbit (normal status of the medial rectus muscle and the surrounding fat). Cranially invasion of the lamina cribrosa was seen and laterally the tumour extended to the cranial part of the medial wall of the left maxillary sinus. The posterior part of the lesion was located in the left nasal choana. Caudally the lesion reached the inferior turbinate. There was no invasion of the nasopharynx and hard palate. Biopsy of the lesion revealed a poorly differentiated adenocarcinoma.

A cranio-facial resection of the tumour was performed (bilateral ethmoidectomy and resection of the medial wall of the maxillary sinus, resection of dura mater). Reconstruction was done with a free radialis-forearm flap.

The man was referred for postoperative irradiation of the tumour bed.

3 Results and Discussion

Planning was performed using the GRATIS planning system, developed by Sherouse [6]. Adaptations were made for the use of multileaf collimation, beam segmentation and optimisation of beam weights and are described elsewhere [7][8].

The treatment was delivered by an SL18-MLC (Elekta, Crawley, UK) linear accelerator, equipped with a dynamic multileaf collimator, with 6 MV photon beams. The patient was

immobilised with a thermoplastic cast (SINMED BV, Netherlands), in supine position.

First, a planning CT was taken, with consecutive 2 mm thick slices. On these 85 CT scans the skin, OAR's (optic chiasm, optic nerves, retinae, brainstem, spinal cord, parotid glands, pituitary gland, mandible and temporo-mandibular joint) and the CTV were contoured on each slice by a physician. The delineation of the CTV was based on radiological examinations (MRI and CT), and the surgeon's findings. The CTV had a volume of 47 cc (fig. 1).

Figure 1 : CTV and optic structures (eyes, optic nerves, optic chiasm) in beam's eye view in the Virtual Simulator; 1a: anterior, 1b: lateral, 1c: vertex.
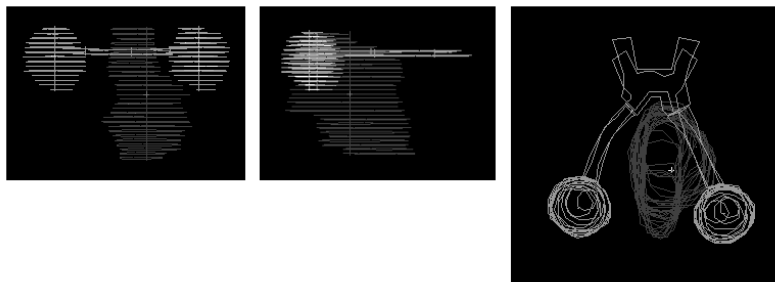
During virtual simulation, the isocenter of the treatment was located in the centre of the target. All beam incidences were in a sagittal plane. For each beam direction, a beam (open segment) with a margin of 1 cm around the CTV was planned. Inside the open segment, further segmentation was based on the exclusion of the optic structures (optic chiasm, optic nerves and retinae) and the brainstem. Segments were created in beam's eye view (BEV) manually for each beam incidence separately. The principle of segmentation was described previously [2][3]. After the design of the segments, optimisation of the segment weights was done interactively with a tool based on constrained matrix inversion (time: 30 minutes) [9]. This resulted in a significant reduction of the number of segments (70 % decrease). The computer plan was then transferred to the real world by a physical simulation with the help of digitally reconstructed radiographs (DRR's). The machine data obtained by planning, were translated to a machine instruction file, (containing the necessary information to deliver the treatment), and transferred to the accelerator by network using in-house written software.

Patient set-up was based on the isocentre. Control of the positioning was performed with an electronic portal imager iView (Elekta, Crawley, UK) once or twice a week (fig. 2). Daily set-up inaccuracy was within 2 millimetres. The duration of irradiation varied between 5 and 6 minutes which is comparable to a conventional treatment. The overall treatment time varied between 9 to 13 minutes. The radiographers were trained specifically for these high precision techniques.

Figure 2 : DRR and portal image: isocenter control; 2a:anterior, 2b:lateral.
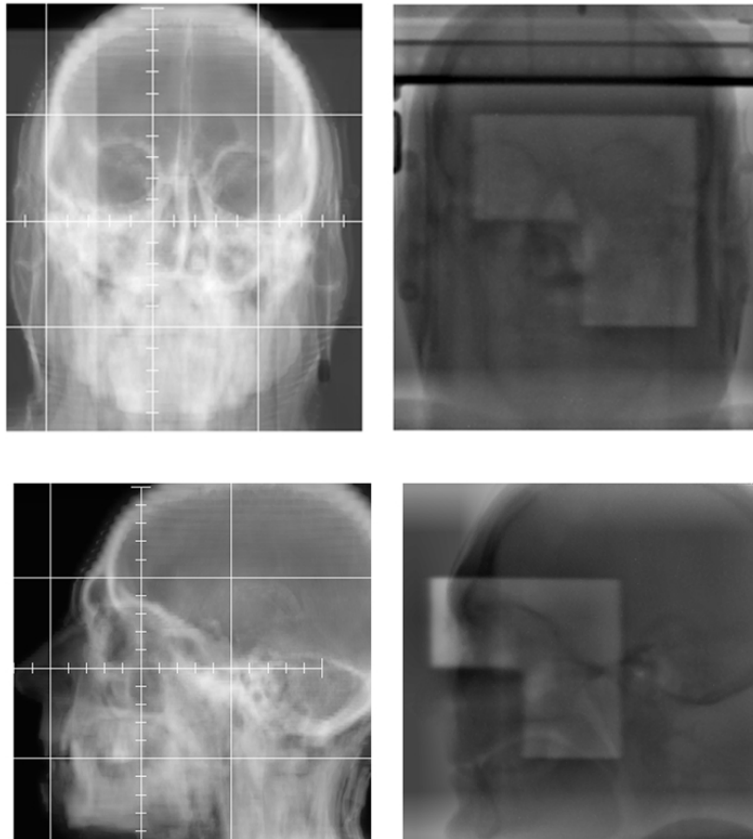
A total dose of 66 Gy in 33 fractions of 2 Gy (5 days a week) was delivered, using 6 MV photon beams. There was an interruption of 1 day because of an acute gastro-enteritis. Acute side effects were fatigue, slime and crusts in the nose, watering of the left eye, bad taste and a moderate swelling of the left cheek. Medication during radiotherapy treatment: physiologic solution for nose cleaning, natrium valproate (900 + 500 mg / day), artificial tears and paracetamol sporadically.

The visual display of the dose distribution is demonstrated in fig.3. Maximum, mean and minimum doses for target and OAR's are summarised in table 1. The dose-volume-histogram (fig 4) shows a mean target dose of 65 Gy, with a minimum dose of 55.9 Gy and maximum dose of 69.9 Gy. Maximum doses of the left and right optic nerve and the optic chiasm did not exceed 54 GY, what is considered as a safe dose level, regarding late ocular complications [10]. Of course the volume of the OAR irradiated to a certain dose-level is also important, what can be estimated by the dose volume histograms. Maximum left and right retinal doses did not exceed 46 and 37 GY respectively, for a mean dose of 19 and 7 Gy. Referring to data of Takeda et al. [11], no retinal complications should be expected.

The patient is actually free of tumour and no ocular complications have been reported (follow-up period of 3 months) until now.

Table 1 : Dose statistics

Contoured structure	Dose (Gy)		
	min	mean	max
target	55.9	65	69.9
left optic nerve	19.9	39	53.8
left retina	0.79	19	45.5
optic chiasm	29.1	40	52.2
right optic nerve	5.03	30	50.2
right retina	0.44	7	36.9
brainstem + medulla spinalis	0.70	20	49.6

Figure 3 : Dose distributions; 3a: transverse, 3b: coronal, 3c: sagittal.
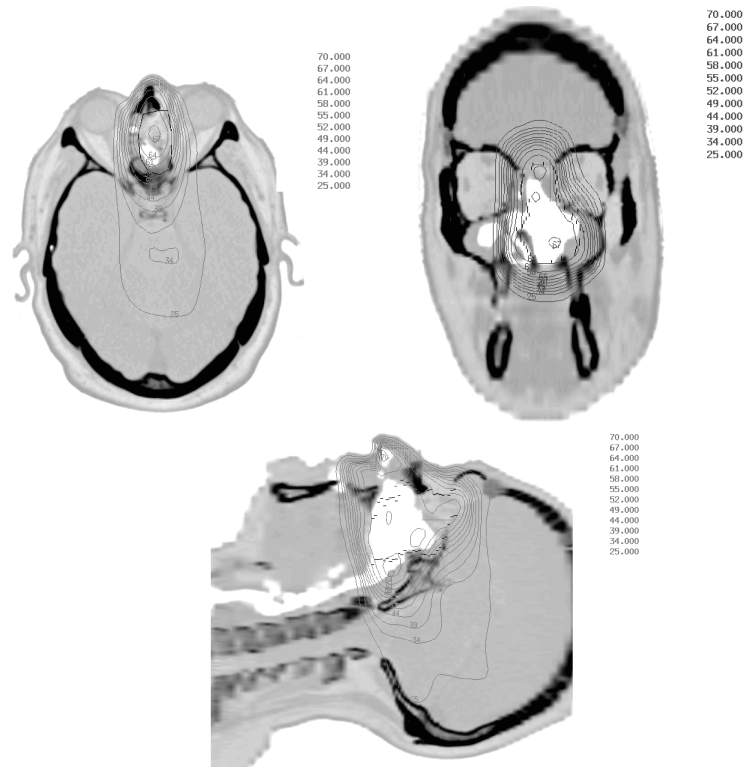
Figure 4 : Dose-Volume-Histograms for target optic structures, brainstem and spinal cord.
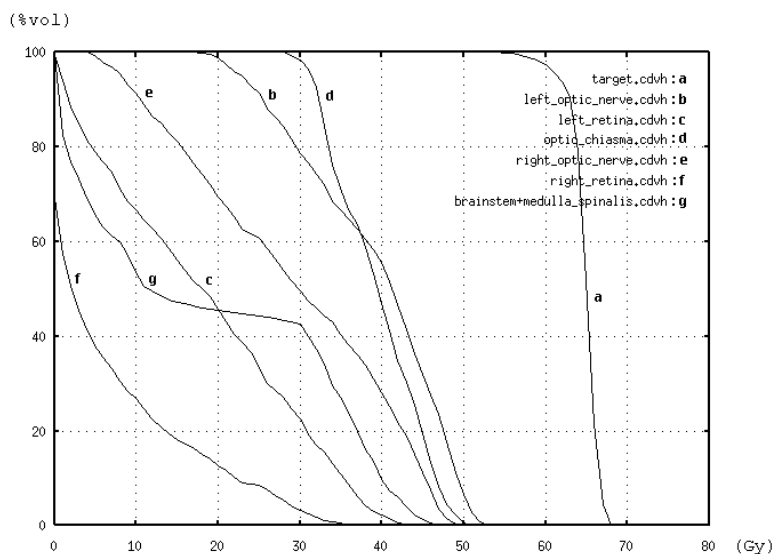
4 Conclusion

Postoperative irradiation of the paranasal sinuses is a good indication for intensity modulated radiotherapy. IMRT enables a high tumour dose and good sparing of the surrounding OAR's. This treatment can be executed in a fast way which is comparable to normal treatment. The planning however still remains very time-consuming. Steep dose-gradients require a very accurate and rigorous patient positioning.

Acknowledgements

Special thanks to the radiographers Franck S. and Speleers B. for their daily effort to deliver high precision treatments.

References

1. Brizel DM, Light K, Zhou SM, et al. Conformal radiation therapy treatment planning

reduces the dose to the optic structures for patients with tumors of the paranasal sinuses. Radiother Oncol 1999;51:215-9.

2. De Neve W, De Wagter C, De Jaeger K, et al. Planning and delivering high doses to targets surrounding the spinal cord at the lower neck and upper mediastinal levels: static beam segmentation technique executed by a multileaf collimator. Radiother Oncol 1996;40:271-9.

3. De Neve W, De Gersem W, Derycke S, et al. Clinical delivery of intensity modulated conformal radiotherapy for relapsed or second-primary head and neck cancer using a multileaf collimator with dynamic control. Radiother Oncol 1999;50:301-14.

4. Derycke S, Van Duyse B, De Gersem W, et al. Non-coplanar beam intensity modulation allows large dose escalation in stage III lung cancer. Radiother Oncol 1997;45:253-61.

5. Perez CA, Brady LW. Principles and Practice of Radiation Oncology, 3e edition, 1997.

6. Sherouse GW, Thorn J, Novins K, et al. A portable 3D radiotherapy treatment design system. Med Phys 1989;16:466.

7. Van Duyse B, Colle C, De Wagter C, et al. Modification of a 3D-planning system for use with a multileaf collimator. Conformal Radiotherapy: Physics, Treatment Planning and Verification. Gent: Belgian Hospital Physicist Association, 1995;39-49.

8. De Wagter C, Colle C, Fortran L, et al. 3D conformal intensity-modulated radiotherapy planning: interactive optimization by constrained matrix inversion. Radiother Oncol 1999;47:69-76.

9. De Gersem W, Derycke S, Colle C, et al. Inhomogeneous target-dose distributions: a dimension more for optimization? Int J Radiat Oncol Biol Phys 1999;44:461-9.

10. Martel M, Sandler H, Cornblath W, et al. Dose-volume complication analysis for visual pathway structures of patients with advanced paranasal sinus tumors. Int J Radiat Oncol Biol Phys 1997;38:273-84.

11. Takeda A, Shigematsu N, Suzuki S, et al. Late retinal complications of radiation therapy for nasal and paranasal malignancies: relationship between irradiated-dose area and severity. Int J Oncol Biol Phys 1999;44:599-605.

4.7 **An implementation strategy for IMRT of ethmoid sinus cancer with bilateral sparing of the optic pathways. F. Claus, W. De Gersem, et al. Int J Radiat Oncol Biol Phys 2001;51:318-31.**

topics discussed :	→ IMRT for ethmoid sinus ca
	→ pitfalls in IMRT planning
	→ preliminary results for ethmoid sinus IMRT
key question :	How to implement IMRT for ethmoid sinus ca ?

paper 4.7

An implementation strategy for IMRT of ethmoid sinus cancer with bilateral sparing of the optic pathways

Filip Claus[1], Werner De Gersem[1], Carlos De Wagter[1], Robert Van Severen[1],
Ilse Vanhoutte[1], Wim Duthoy[1], Vincent Remouchamps[1], Bart Van Duyse[1], Luc Vakaet[1],
Marc Lemmerling[2], Hubert Vermeersch[3] and Wilfried De Neve[1]

[1] Division of Radiotherapy
Ghent University Hospital

[2] Department of Radiology
Ghent University Hospital

[3] Department of Head and Neck Surgery
Ghent University Hospital

Abstract

Purpose: to develop a protocol for the irradiation of ethmoid sinus cancer, with the aim to spare binocular vision; to develop a strategy of intensity modulated radiation therapy (IMRT) planning which produces dose distributions which i) are consistent with the protocol prescriptions ii) are deliverable by static segmental IMRT techniques within a 15 minute time slot; to finetune the implementation strategy to a class solution approach that is sufficiently automated and efficient to allow routine clinical application; to report on the early clinical implementation, involving 11 patients between February 1999 and July 2000.
Patients, methods and material: Eleven consecutive T1-4N0M0 ethmoid sinus cancer patients were enrolled in the study. For patients 1-8 a first protocol was implemented defining a PTV prescription dose of 60-66 Gy in 30-33 fractions and a maximum dose (Dmax) to optic pathway structures and spinal cord limited to 50 Gy and to 60 Gy for brainstem. For patients (9-11) an adapted (now considered mature) protocol was implemented defining a PTV prescription dose of 70 Gy in 35 fractions and a Dmax to optic pathway structures and brainstem limited to 60 Gy and to 50 Gy for spinal cord.
Results: The class solution-directed strategy, developed during this study, reduced the protocol translation process from a few days to about 2 hours of planner time. The mature class solution involved the use of 7 beam incidences (20-37 segments), which could be delivered within a 15 minute time slot. Acute side effects were limited and mild. None of the patients developed dry-eye syndrome or other visual disturbances. The follow-up period for detection of retinopathy or optic nerve and chiasm toxicity is too short.
Discussion and conclusion: Conventional radiotherapy of ethmoid sinus tumors is associated with serious morbidity, including blindness. We hypothesize that IMRT has the potential to save binocular vision. The dose to the optic pathway

structures can be reduced selectively by IMRT. Further enrollment of patients and longer follow up will show whether the level of reduction tested by the clinical protocol is sufficient to save binocular vision. An adaptive strategy of IMRT planning was too inefficient for routine clinical practice. A class solution-directed strategy improved efficiency by eliminating human trial and error during the IMRT planning process.
Keywords : radiotherapy, ethmoid sinus, IMRT, optic, clinical implementation

1 Introduction

Ethmoid sinus cancer is often diagnosed in a locally advanced stage with extensions through the bony walls of the paranasal sinuses, the orbit, the sphenoid and the anterior skull base. In most patients, volumes of the tumor are at close distance (within 0-3 mm) to optic structures such as the retinae, the optic nerves and the optic chiasm. Surgical resection is usually followed by local relapse, in spite of the use of wide-field excision by a team of head-and-neck, neuro- and reconstructive (plastic) surgeons [1][2]. The degree of mutilation and morbidity of such surgery, which may involve enucleation of the eye and removal of head facial bones and parts of the skull, is substantial.

Conventional radiotherapy either as primary treatment or in a postoperative setting is unable to produce local control rates above 50% in T2-4 tumors [3]. Radiochemotherapy is investigational according to the actual (02/2001) Physician Data Query (PDQ) of the National Cancer Institute (NCI) for treatment of paranasal sinus and nasal cavity cancer (http://cancernet.nci.nih.gov/pdq.html). The radiotherapy prescription dose typically exceeds the tolerance of the optic pathways and conventional radiotherapy often involves the decision on which eye to sacrifice. At the Ghent University Hospital, conventional radiotherapy was typically given by an anterior and a (bi-)lateral wedged beam arrangement to a tumor prescription dose of 60-66 Gy in 30-33 fractions. Blindness (uni- or bilateral) is a known side effect of the delivery of such doses to the eyes and optic pathways [4].

We hypothesized that an anatomy based planning technique to obtain intensity modulated radiotherapy (IMRT) would allow us to customize the dose distribution to spare the optic pathways and in this way increase the likelihood of uncomplicated local control. We designed a protocol, setting the tumor prescription dose in the early phase of the study to 60-66 Gy and finally to 70 Gy in 2-Gy fractions, while simultaneously limiting the maximal dose (Dmax) to optic chiasm, optic nerves and retinae to a dose of 50 Gy (early phase) and finally to 60 Gy (second phase). Taking into consideration the data published by Martel et al. [5] and others [6][7], the lower fraction size at the level of the optic structures (maximally 60 Gy would be delivered in 35 fractions) and the small volume that would receive doses close to Dmax, we hypothesized that 60 Gy Dmax would preserve binocular vision in most patients. After the protocol was accepted, a strategy for planning and delivering IMRT that would meet the protocol prescriptions, had to be investigated. This paper reports these investigations, which resulted in a mature strategy, involving a class solution approach for planning IMRT of ethmoid sinus cancer.

2 Patients, Materials and Methods

2.1 Patients

Between February 1999 and July 2000, 11 patients with node negative (clinical examination, CT and MRI imaging) ethmoid sinus tumors were referred to the Division of Radiotherapy, Ghent University Hospital and were treated by IMRT. Patient, tumor and treatment characteristics are given in table 1. All patients were men and IMRT was given either as definitive (n=1) or as postoperative (n=10) treatment. Median age was 62 (range 46 - 70). Histology was adenocarcinoma in seven patients, squamous cell carcinoma in three patients, and transitional cell carcinoma in one patient. T-stage was T1 for one patient, T2 for three patients, T3 for one patient and T4 for six patients. Elective nodal irradiation was not performed. All patients were staged as clinical M0 (no evidence for distant metastasis). In nine out of ten patients who underwent surgery, the resection was macroscopically complete. Microscopic invasion of the resection margins was observed in patient 3.

2.2 Contouring of target volumes

Patients 1-10 underwent surgery. Gross Tumor Volume (GTV) was present in patient 11. The clinical target volume (CTV) definition evolved from the radiotherapist's impression (patients 1-6) to a "compartment related CTV definition" used for patients 7-11. The compartment related CTV was defined as follows:

In the non-operated patient (patient 11), the CTV was based on the MRI-imaging of the GTV. In those regions where GTV was flanked by intact bone or by cranial nerves, no margin was added. In those regions where GTV invaded compartments enclosed by bone, like other paranasal sinuses or extended up to their ostia, the whole compartment was included in the CTV contours. In those regions where GTV invaded radiologically defined spaces [8] known to resist poorly to invasion by malignant tumors (e.g. masticator or parapharyngeal spaces), and where GTV invaded the orbit or extended intracranially, either the entire space or a margin of 0.5-1.0 cm was added to the GTV edge.

For patients 7-10, who had undergone macroscopically complete surgical resection of the tumor, the above principles were applied to the edges of resection as if the edges of resection delineated the GTV. Thus, the post-operative CTV consisted of the edges of resection plus a variable margin, according to the principles of a "compartment related CTV" as described in the previous paragraph.

By in-house developed tools, a 3-mm isotropic expansion margin was applied to the CTV to obtain the planning target volume (PTV), further named PTV_3mm.

Table 1 : Overview of the IMRT implementation process for patients with N0M0 ethmoid sinus cancer

Table 1 : part 1

patient	age	histology	T stage	surgery/complete	start date IMRT	expansion of OARs	number of beams
1	65	adenoca	pT2	yes / yes	22/02/1999	no	4
2	56	adenoca	pT4	yes / yes	03/03/1999	no	5
3	66	transitional cell ca	pT4	yes / no	10/05/1999	no	9
4	60	adenoca	pT2	yes / yes	08/07/1999	no	8
5	56	squamous cell ca	pT4	yes / yes	19/07/1999	no	7
6	46	adenoca	pT4	yes / yes	23/09/1999	no	7
7	62	adenoca	pT1	yes / yes	07/03/2000	yes	7
8	63	adenoca	pT2	yes / yes	11/04/2000	yes	7
9	70	squamous cell ca	pT3	yes / yes	11/04/2000	yes	7
10	65	adenoca	pT4	yes / yes	06/06/2000	yes	7
11	51	squamous cell ca	cT4	no / no	06/07/2000	yes	7

Table 1 : part 2

patient	segment generation	# segments(a)	dose PTV Gy	optimization	onstr	SOWAT(b)
1	manual / IPAB(c)	45 / 12	66	CMI(e)	no	no
2	manual / IPAB	59 / 19	66	CMI	no	no
3	manual / IPAB	185 / 31	66	CMI	no	no
4	manual / IPAB	141 / 27	60	CMI	no	no
5	manual	39 / 15	60	CMI	no	no
6	manual / IPAB	89 / 27	60	CMI	no	no
7	ABST(d)	85 / 31	60	BP-SWOT(f)	no	no
8	ABST	48 / 20	66	BP-SWOT	yes	yes
9	ABST	71 / 24	70	BP-SWOT	no	yes
10	ABST	65 / 37	70	BP-SWOT	yes	yes
11	ABST	51 / 27	70	BP-SWOT	yes	yes

(a) : generated / delivered : for patients 1-6 "generated" means ythe segments used by CMI during the last cycle

(b) : SOWAT : Segment Outline and Weight Adapting Tool

(c) : IPAB : IsoPathlength Beam Segment

(d) : ABST : Anatomy Based Segmentation Tool

(e) : CMI : Constrained Matrix Inversion

(f) : BP-SWOT : BioPhysical-Segment Weight Optimization Tool

2.3 Contouring of organs at risk (OARs)

The following anatomical structures were contoured as a standard set of OARs: the optic chiasm, the optic nerve(s), the retina(e), the brainstem, the spinal cord, the brain, the mandible and both parotids.

To account for setup uncertainty, for patients 7-11 the contours of the optic chiasm, the left and right optic nerve and the respective retinae were isotropically expanded by 2 mm (structure_name_2mm) and the brainstem by 3 mm (brainstem_3mm). The spinal cord itself was contoured and not the content of the vertebral canal; considering that NTCP data for spinal cord were based on conventional radiotherapy and thus rather on the edges of the vertebral canal than on the anatomical edge of the spinal cord, a 5-mm expansion was applied (2 mm to approach the edge of the vertebral canal and 3 mm for setup uncertainty) to obtain spinal_cord_5mm.

For the last three patients, two additional contoured structures were generated as follows: the CTV was isotropically expanded by respectively 20 mm and 50 mm and the resulting volumes were subtracted from the volume enclosed by the patient's surface contours. The remaining structures were named onstr_20mm and onstr_50mm, as shown in figure 2. The prefix "onstr" is an abbreviation for "Overdosed Normal STRucture". By using the onstr concept in the objective function for plan optimization, we aimed at a substantial gain in conformality, i.e. isodose surfaces of intermediate and high dose values should be pushed outside the respective onstrs and towards the PTV.

Figure 2
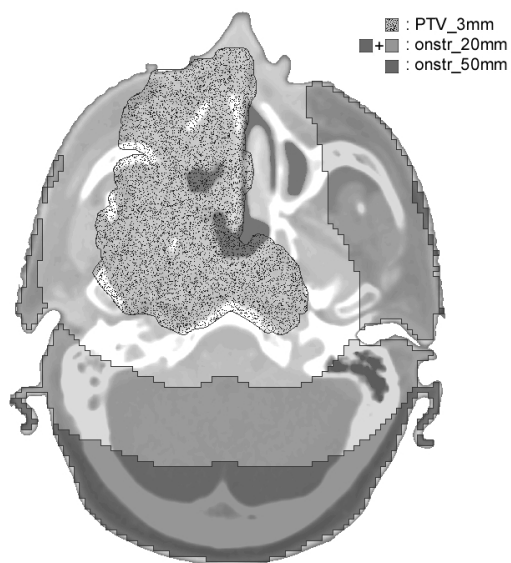
Legend : PTV and onstr's (Overdosed Normal tissue STRuctures) generated for plan optimization.
Transverse CT slice for patient 11 with the PTV in black dots, the onstr_20mm in transparent light grey and the onstr_50mm in transparent dark grey.

2.4 Treatment protocol

For patients 1-8, the maximum dose to the optic nerves, optic chiasm, retinae (further called optic structures) and the spinal cord was 50 Gy and 60 Gy to the brainstem. This was an intended dose limit for optic structures, but was rigidly imposed for spinal cord and brainstem. The median PTV prescription dose was 60-66 Gy delivered in 2 Gy fractions. For patients 9-11, the dose to the 2mm-expanded optic structures was set by the meanwhile

updated treatment protocol to a maximum of 60 Gy. This intended dose limit for optic structures was set to 95 % of the volume of each structure i.e. 5 % of the expanded optic structures was allowed to receive more than 60 Gy. The maximum dose to brainstem_3mm and spinal_cord_5mm was 60 Gy and 50 Gy respectively. The median PTV prescription dose was 70 Gy delivered in 35 fractions. An underdosage of more than 5 % (ICRU) of the PTV_3mm was accepted in the regions adjacent to or overlapping with the 2mm-expanded optic structures, as well as in PTV_3mm regions close to the patient's surface i. e. in the build-up region of the 6 MV photon beams. With regard to PTV overdosage, the ICRU guideline of 7% was followed. The three dimensional maximum dose had to be located inside the PTV_3mm. The final decision to accept the treatment plan was taken by the clinical staff.

2.5 Protocol implementation strategy

The protocol implementation strategy is graphically represented in figure 1 which depicts the IMRT planning platform that was developed at Ghent University Hospital. The planning platform consisted of several modular units, including image processing, IMRT planning and dose computation units. For patients 7-11, the ADAC Pinnacle system was a component of the image processing unit and is currently being used for MRI-CT image fusion and contouring of CTV and OARs.

2.5.1 Patient individualized approach

For patients 1-4, beam incidences were defined by a physician and located in the sagittal plane. Beam angles were equallly spaced and ranged from $-45°$ to $90°$. Segments were drawn by a physician using beams eye view (BEV). More levels of segments were designed with closer distance to optical structures according to a rationale explained previously [9]. Segment weights were assigned by an interactive optimization tool called constrained matrix inversion (CMI) [10][11]. A physical objective function was used, containing intended doses to PTV, while minimizing doses to optic pathway structures and other OARs. Repeated trials involved changing the weighting factors of different terms of the objective function followed by evaluation of the dose volume histograms (DVHs). If unwanted inhomogeneities in the dose distribution persisted and were caused by missing tissue effects (not taken into account by segmentation), additional segments were created inside the existing segments by a tool called IPAB (IsoPAthlength Beam segment, method unpublished), and CMI was executed again.

Figure 1

Flowchart:

- **clinical case**
  - ethmoid sinus cancer
  - T1-4 N0 M0
  - informed consent

- **image processing contouring - expansion**
  - CT — ADAC Pinnacle™ TPS
  - MRI — GRATIS™ TPS

- **anatomy based segmentation tool (ABST)**
  - beam templates
  - planning target volume
  - expanded organs at risk

- **dose computation for optimization**

- **SWOT-BP**
  - biophysical objective function

- **SOWAT**
  - MLC position adaptations
  - segment weight optimization

- **protocol prescription evaluation**
  - dose volume histograms

- OK? — No / Yes

- **dose computation**
  - GRATIS™ TPS
  - dose grid

- **plan evaluation**
  - protocol prescription
  - dose distributions
  - dose volume histograms

- OK? — No / Yes

- **treatment prescription**
  - segment sequencing
  - data transfer to linac
  - dummy run
  - dosimetric verification
  - treatment delivery

- **clinical follow-up**
  - tumor control
  - acute toxicity
  - chronic toxicity
  - protocol validation

Panel a: CT image

Panel b: beam arrangement diagram

Panel c: contour overlay

Panel d: dose volume histogram (vol% vs Gy)

Panel e: **protocol prescription**

PTV

median dose 70 Gy (35 x 2)
maximal overdosage 7% (ICRU)
3D D_{max} located inside PTV_3mm

OARs	D_{max} (Gy)
optic_chiasm_exp_2mm	60
optic_nerve_exp_2mm	60
spinal_cord_exp_5mm	50
brainstem_exp_3mm	60

Panel f: 3D head reconstruction

Panel g: Gantry : -30.0 Collimator : 30.0 Table isocenter : 90.0
Energy : 6 MV Wedge : OUT Total MU : 34
0 MU   21 MU   30 MU   34 MU

Legend :Translation strategy of the clinical protocol to IMRT

Eligible are patients with T1-4 N0 M0 ethmoid sinus cancer. Primary or postoperative IMRT.

Image processing unit involves 2 systems. The ADAC Pinnacle Treatment Planning System (TPS) is used for MRI-CT fusion, illustrated by panel a, and for contouring. All the contours are transferred by network to the GRATIS TPS as anastruct formatted files. Three-dimensional expansion of the anastructs by a margin of a magnitude as defined by the suffix of the anastruct name. The class solution defines the standard set of anastructs and their names.

The IMRT planning unit reads the anastructs, and executes ABST, the Anatomy Based Segmentation Tool. ABST selects consecutive beam incidences, shown in panel b, from the beam template of the class solution. For each beam incidence, ABST creates segments using BEV-projection of the following anastructs: PTV_3mm, skin, optic_chiasm_2mm, optic_nerve_left_2mm, optic_nerve_right_2mm, retina-_left_2mm and retina_right_2mm. The class solution defines the type of segments, which ABST must make (here: segments to create a concave (type 1 segments) and segments to create a convex (type 0 segments) dose distribution component). Panel c demonstrates the BEV of 3 segments generated by ABST for a given beam incidence (gantry rotation angle 60 degrees, collimator rotation 270 degrees and table isocenter rotation 90 degrees). The PTV is shown in grey, the optic pathway structures in black.

The dose computation unit seeds, in all anastructs, a number of dose points (see table 2), also defined by the class solution. For each segment, a (unity weighted) dose-point matrix is computed.

BP-SWOT, the Segment Weight Optimization Tool, uses the dose-point matrices to assigns weights to all segments by minimizing the objective function -B.P, described by the class solution. Segments weighted 1 MU or less are deleted.

SOWAT, the Segment Outline and Weight Adapting Tool, simultaneously optimizes the shape and weights of the segments. SOWAT also uses -B.P as objective function. When SOWAT has finished, segments weighted 1 MU or less are deleted. Using the remaining weight- and shape-optimized segments, DVHs (panel d : patient 11), are constructed and evaluated against the clinical protocol, summarized in panel e. If the DVHs do not pass this evaluation, the cycle is repeated. Otherwise, a voxel (0.5 x 0.5 x 0.5 cm^3 or smaller) based dose computation is performed, illustration of the size of the dose matrix in panel f, and dose distributions are evaluated. If the plan fails to pass evaluation, reiteration of SOWAT is done or user-interactive corrective measures are taken. If the plan passes, the segment delivery sequence is optimized and the prescription files are made. Panel g shows radiographer's printouts of the prescription file for the first beam incidence for patient 11. On the left side of the arrow the 3 segments for this beam incidence, on the right side the resulting fluence distribution (in negative grey values).

2.5.2 Anatomy based segmentation tool (ABST)

For patients 7-11, two new tools, ABST and a Segment Outline And Weight Adapting Tool (SOWAT), were used as shown in figure 1. For patients 5-11, a standard set of 7 beam incidences was used (see figure 1 panel b), and became later part of the class solution. The first 5 beam templates, with central axes located in the sagittal plane (table isocenter rotation angle of 90 degrees), were characterized by the following gantry rotation angles : 0, 30, 60, 90 and 330 degrees. This set was complemented by 2 beam templates with central axes in a transverse plane (table isocenter rotation angle : 0, gantry rotation angles : 75 and 285). The collimator rotation angles of beams 1-2 and beams 3-7 were respectively 30 and 270 degrees. The isocenter of all beams was located at the XYZ-midpoint of PTV_3mm. ABST generates for each beam template, segments from the BEV projections of the PTV_3mm and the 2mm-expanded optic structures, the basic principle of ABST being the creation of an increasing number of segments with decreasing distance to the 2mm-expanded optic structures and with increasing thickness of forelaying tissue (defined as the pathlength measured along rays from their entrance point through the patient's surface to the isocentric plane). The maximum number of segments is specified for each beam incidence by the class solution database (patients 9-11) or interactively by a human planner (patients 7-8). ABST generates segments which take into account the Elekta-specific MLC constraints [12].

2.5.3 Dose computation for optimization

When ABST has finished, all segments are provided as separate MLC collimated beams to the dose computation unit. For each contoured structure, a user-defined number of points (see table 2) are randomly seeded in the volume of the structure, and a dose matrix (dose contribution per segment and per seeded point) is computed using unity weights. Dose computation was performed for 6MV photons, using a 3D-differential scatter air ratio algorithm [13] distributed with the GRATIS 3D treatment planning system [14], without corrections for tissue-density heterogeneity.

Table 2 : Parameters of NTOF (Normal Tissue Optimization Factors) computation

	# dose points	volume n	slope m	imp factor	OTD50* (Gy)
optic chiasm	1000	0.25	0.14	3	55
optic nerve	1000	0.25	0.14	1	55
retina	1000	0.20	0.12	1	45
spinal cord	1000	0.05	0.175	5	55
brainstem	1000	0.16	0.14	5	55
brain	1000	0.25	0.15	1	60
mandible	1000	0.90	0.30	1	45
onstr_20mm	10000	0.03	0.07	0.1	60
onstr_50mm	10000	0.03	0.07	0.1	45
* : OTD50 : optimization TD50 value					

2.5.4 Biophysical segment weight optimization tool (BP-SWOT)

The BP-SWOT assigns weights to segments by minimizing, using a conjugate gradient method, a biophysical objective function -B.P consisting of a biological factor B and a physical factor P, which are explained further.We experienced that biophysical optimization was far more efficient in dealing with a high number of critical structures, compared to a purely physical model.

2.5.4.1 "Biological" factor of the objective function

The term B imposes dose constraints to normal tissues and organs and is a product of the factors computed for the volumes:
optic_chiasm_2mm,
optic_nerve_left_2mm, optic_nerve_right_2mm,
retina_left_2mm, retina_right_2mm,
spinal_cord_5mm, brainstem_3mm,
brain, mandible,
onstr_20mm and onstr_50mm.
Each of these factors was computed as:

$$\left(1 - NTOF_{name\,of\,volume}\right)^{a}$$

where NTOF is the "normal tissue optimization factor" calculated according to the DVH-reduction scheme by Lyman, Kutcher and Burman [15][16] (used for calculating NTCP: normal tissue complication probability), and the exponent a is a weighting parameter. Ta-

ble 2 shows the number of randomly seeded points (inside the respective contoured structure) on which the NTOF value is computed, the value of an importance factor (imp factor) and the NTOF fitting parameters for each of the factors. For optimization purposes, the TD50 values for several OARs were empirically adapted. Therefore they are not NTCP predictions anymore but only formulas which provide values useful to customize plans. For a discussion the reader is referred to a letter to the editor in the Int. J. Radiat. Oncology Biol. Phys. and to our reply (2001 : in press).

For brain, the NTOF fitting parameters were taken from Burman et al. [17], which makes NTOF parameters identical to NTCP. For optic_chiasm_2mm, optic_nerve_left(right)_2mm, retina_left(right)_2mm, spinal_cord_5mm and brainstem_3mm, the volume (n) and slope (m) parameters of NTCP were taken from Burman et al. [17] and used to compute NTOF but the TD50 values were decreased (table 2). Using these decreased values, the optimization algorithms customized the plans closely to the protocol constraints in a reproducible way (last 5 patients). These adapted TD50 values (OTD50 : optimization TD50) lead to NTOFs which are larger than the respective NTCP estimations. For mandible, parameters m,n and OTD50 were adapted because the goal was to avoid not only necrosis (endpoint of Burman et al. [17]) but also dental loss which was assumed to occur at substantially lower doses. The factors onstr_20mm and onstr_50mm are penalty scores for unwanted dose levels at distances of more than 20 mm and 50 mm from the PTV_3mm. Using a low volume (n = 0.03) and a high slope parameter (1/m = 1/0.07), these factors act as a "soft maximum dose constraint".

2.5.4.2 Physical factor of the objective function
The physical factor P imposes the wanted dose level of 70 Gy to PTV_3mm and deals with the accepted underdosages in the boundary regions, which were mentioned above in the protocol description. It is the product of the physical factors computed for the volumes CTV, PTV_3mm, PTV_3mm_whbu_6mm and PTV_3mm_whbu_6mm_whoars_6mm. The PTV_3mm_whbu_6mm is created by an "erosion tool" which displaces the edges of PTV_3mm that are closer than 6 mm to the patient's surface contours to a depth of 6 mm. The influence of buildup on the outcome of dose optimization is reduced when using voxels inside PTV_3mm_whbu_6mm (the abbreviation "whbu" is an acronym for "without buildup"). A similar procedure is followed to allow precise control of the wanted underdosage inside and close to the optic pathway region. The "erosion tool" displaces the edges of PTV_3mm_whbu_6mm that are closer than 6 mm from optic pathway contoured structures (unexpanded) to a distance of 6 mm, which results in the structure PTV_3mm_whbu_6mm_whoars_6mm (the abbreviation "whoars" is an acronym for "without organs at risk"). The PTV-related structures are illustrated in figure 3.

Figure 3
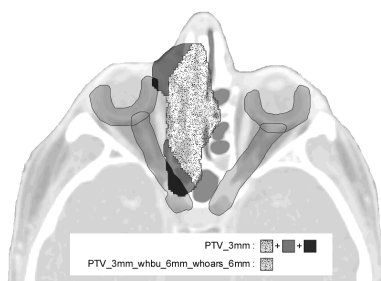
Legend : PTV related optimization structures. Transverse CT slice for patient 11 with the expanded optic nerves and retinae in transparent light grey. The PTV_3mm_whbu_6mm_ whoars_6mm in black dots. The black coloured region is the overlap region between the expanded optic pathway structures and the PTV_3mm. The PTV_3mm is the region defined by the black dots, the black overlap region and the dark grey region connecting the former two.

The physical factor for each volume consists of a factor P_r which imposes a prescribed dose D and a factor P_h which limits the dose inhomogeneity to a predefined maximal percentage:

$$P_r = \left(\frac{\sqrt{\sum_{i=1}^{n}(d_i - D)^2}}{\sqrt{n} . d_{mean}} \right)^a$$

$$P_h = e^{-b.x\left(\frac{x_{max}}{x_{tol}} - 1\right)} . (x_{max} - x)^{-b.x_{max}.\left(\frac{x_{max}}{x_{tol}} - 1\right)}$$

with the volume-related parameters

n	: number of seeded points (= 3000 for each target structure)
d_i	: dose in point i
D	: prescribed dose (= 70 Gy in the final treatment protocol)
d_{mean}	: mean dose
a	: importance factor
	value for all target structures : 0.5
$x = \frac{d_{max} - d_{min}}{d_{mean}}$	: inhomogeneity factor
d_{max}	: maximum dose
d_{min}	: minimum dose
x_{max}	: maximum inhomogeneity
	value for CTV and PTV_3mm_whbu_6mm_whoars_6mm : 0.3
	value for PTV_3mm_whbu_6mm : 0.35
x_{tol}	: tolerable inhomogeneity
	value for CTV and PTV_3mm_whbu_6mm_whoars_6mm : 0.2
	value for PTV_3mm_whbu_6mm : 0.25
b	: importance factor
	value for PTV_3mm : 0
	value for the other target structures : 1

2.5.5 Segment outline and weight adapting tool (SOWAT)

The use of ABST for each beam incidence, followed by BP-SWOT leads to n segments and weights, which make a starting set for the segment outline and weight adapting tool (SOWAT). The tool iteratively changes the individual leaf positions. Each resulting segment shape change is evaluated as follows: the dose distribution change resulting from each leaf position change is taken into account by adding or subtracting a dose distribution deposited by a narrow diverging beam representative for the change. The additional beam has rectangular cross section equal to the leaf width (reduced by the part blocked by the jaws in the case of outer leaves) times the (unsigned) leaf position change. The narrow-beam dose distribution is computed by a simplified but fast algorithm. The dose distributions before and after leaf position change are evaluated using -B.P, the biophysical objective function. The change is retained if -B.P is decreased. Weights are optimized after each leaf position optimization cycle. A cycle is completed when a new position for each leaf of each segment has been evaluated. After 15 cycles, the output factors are recomputed and DVHs are displayed. The proces is halted by the user when the DVHs meet the protocol prescriptions or, by the system, if no further improvements can be obtained.

2.5.6 Segment sequencing and treatment delivery

SOWAT tends to reduce the total number of segments by zero-weighting. Using the remaining segments and weights, the dose distribution is computed with a voxel size of 0.5x0.5x0.5 cm^3 or smaller. If the plan passes clinical evaluation, the segment delivery sequence is optimized by CRASH (Combine Re-order And Step and Shoot) as described previously [18] in order to ensure the shortest possible delivery time. Treatments were delivered by a SL18-MLCi (Elekta, Crawley, UK) linear accelerator. Patient setup was verified by on-line electronic portal imaging.

2.6 Patient follow-up

A LENT SOMA scale for the head and neck region to grade late effect toxicity [19] was modified to score for acute toxicity.

3 Results

During both phases, the clinical protocol was successfully translated into an appropriate IMRT delivery. Now, following the class solution strategy, the translation takes about 2 hours of operator time, counted from the start of ABST until the generation of the treatment prescription (figure 1). Table 1 shows, for patients 1-6, the number of segments weighted by CMI during the last cycle. For 2 patients (3 and 4), optimization weighted more than 100 segments and, by assigning weights of zero to segments optimized to a weight of less than 1 MU, over 80% of the segments were eliminated. The procedure used for patients 7 to 11 is far more efficient. The number of segments created by ABST for patients 7 to 11 was between 48 and 85. An option in the command line of ABST allows to set the number of superposed segments for each beam direction and allows to predict the number of segments that will be created. The further steps of planning (BP-SWOT and SOWAT) cannot create additional segments, but typically discarded about half of the number of segments created by ABST. For patients 7-11, between 20 and 37 segments were retained. Treatment delivery time (patient setup included) was 15 minutes or less.

Our method of segmental IMRT shows a relatively high MU-efficiency. To deliver a fraction dose of 2 Gy, 256-508 MU were delivered (the calibration of the accelerator at the isocenter corresponds to 1 cGy/MU at 5-cm depth in water for a 10x10 cm^2 field).

Table 3 reports the maximal dose (Dmax) to the non-expanded optic structures, to allow comparison between all patients. Patients 9-11 were treated according to the final treatment protocol and class solution strategy. The DVHs, the dose distribution displays and the step-and-shoot delivery sequence for patient 11 are illustrated in figures 4 and 5.

Table 3 : Maximal dose (Dmax) to the optic pathway structures

patient	optic chiasm Dmax in Gy	optic nerve left Dmax in Gy	optic nerve right Dmax in Gy	retina left Dmax in Gy	retina right Dmax in Gy
1	47	29	55	10	52
2	50	52	50	42	36
3	53	53	46	53	13
4	46	49	48	42	49
5	52	surgically removed	24	surgically removed	42
6	54	surgically removed	54	surgically removed	43
7	56	57	53	52	47
8	54	56	58	52	40
9	56	57	57	48	49
10	56	61	60	53	52
11	40	50	60	48	58

Figure 6 shows the DVHs for patients 9-11 of CTV and optic chiasm (panel a), optic nerves and PTV_whbu_6mm_whoars_6mm (panel b) and retinae and PTV_whbu_6mm-_whoars_6mm (panel c).

Patients were seen by a radiation oncologist, at least once a week during the radiotherapy course. Light sensitivity (grade 1) was observed in 8 patients. Tearing, cornea and lacrimation symptoms were observed in 10 patients, grade 1 (occasional) in 5 patients, and grade 2 (intermittent) in the other patients. Pain and dryness of the eyes was reported in 8 patients, occasional and minimal (grade 1) for 6 patients and intermittent and tolerable (grade 2) for 2 patients. For none of the patients evolution to dry-eye syndrome is observed.

Patient follow up reports no evidence of disease in 7 patients. Two patients died, one of a locoregional relapse (patient 2), the other of distant metastasis (patient 6). Meningitis carcinomatosa is diagnosed in patient 10. For patient 8 no recent follow up data are available. No unilateral or bilateral visual impairment has been observed yet, however follow-up to detect this is too short [6] to make a final report.

4 Discussion

The rationale to use IMRT for ethmoid sinus cancer was based on the hypothesis that binocular vision could be saved in these patients. During the 1.5 year period, shortcomings with regard to imaging, definition of target volumes, definition of organs at risk and planning techniques were identified and eliminated.

For patients 1-8, OAR contouring was based on CT-scan only. For patients 9-11 the contours of the optic chiasm were drawn using CT-scan information and electronically overlayed on the MRI images. It appeared that the contours were offset i.e. the chiasm visible on MRI was located more cranially and posteriorly than the contours. Similarly, the part of the optic nerve that is located in the optic canal, formed by the lesser wing of the sphenoid bone, is more clearly visible on MRI. The standard procedure now involves drawing of the optic chiasm and the posterior parts of the optic nerves on the MRI slices, followed by fusion with the CT-scans.

Before the use of SOWAT, OAR-contours were not expanded. Segment edges were placed by the planner or by ABST at a predefined distance from the OARs, usually 2-3 mm, to take into account setup uncertainty. For OARs that were used in SOWAT, expanded contours were implemented to account for setup uncertainty. We thought that a margin was needed because SOWAT tends to erode the distance between segment edges and OARs as much as possible. Thereby dose gradients come closer to OARs.

Figure 4
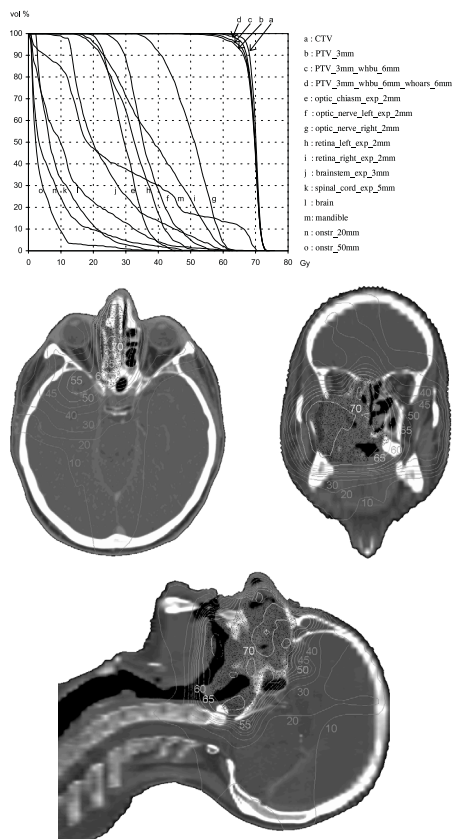
Legend : Dose volume histograms and dose distributions for patient 11.
A median dose of 70 Gy is prescribed to the PTV_3mm.
Figure 4a : Dose volume histograms.
Figure 4b : Transverse dose distribution at the level of the optic nerves. The PTV_3mm is shown in black dots.
Figure 4c : Coronal dose distribution at the level of the optic nerves. The PTV_3mm is shown in black dots.
Figure 4d : Sagittal dose distribution at the midline. The PTV_3mm is shown in black dots.

Figure 5

Legend : Segments and resulting beam fluence distributions (negative grey values) of the step-and-shoot delivery for patient 11. Each row represents a beam incidence, of which gantry, collimator and table isocenter rotation are indicated. The beam quality is 6 MV photons for all incidences. No wedges are used. The white space inside the grey rectangles represent the segment shapes. The cumulative MUs are indicated below each rectangle and are for the start of that segment. The black rectangle at the end of each row represents the resulting fluence distribution. Black color indicates no fluence, while white indicates the highest fluence inside the fluence map.

Figure 6
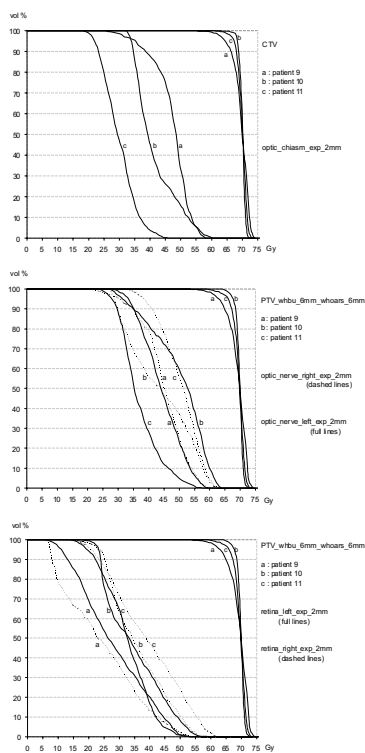
Legend : Dose volume histogram analysis for patients 9, 10 and 11. Patients 9, 10 and 11 are indicated by a, b and c respectively.

Figure6a : Dose volume histograms of the CTVs and the expanded optic chiasms. CTVs at the right side of the figure, optic chiasms in the middle.

Figure6b : Dose volume histograms of the PTV_whbu_6mm_whoars_6mm's and the expanded optic nerves. PTV_whbu_6mm_whoars_6mm's at the right side of the figure, optic nerves in the middle. Left optic nerves in solid lines, right optic nerves in dashed lines.

Figure6c : Dose volume histograms of the PTV_whbu_6mm_whoars_6mm's and the expanded retinae. PTV_whbu_6mm_whoars_6mm's at the right side of the figure, retinae in the middle. Left retinae in solid lines, right retinae in dashed lines.

Initially, the treatment protocol aimed to deliver 60-66 Gy to PTV, while keeping the maximum dose to the optic pathways below 50 Gy. The dose distributions that could be obtained led to discussion about the PTV prescription dose as well as the normal tissue constraints. Expansion of CTV to PTV resulted in overlap between PTV and optic pathway structures like retina, optic chiasm and nerves. In the light of the published data, the medical staff considered the dose limits to optical structures (Dmax of 50 Gy to retina, optic nerves and chiasm) as too severe, considering the close vicinity of gross tumor preoperatively, for most patients. The protocol was modified with the dose limit raised to 60 Gy, set to 95 % of the expanded volume of the optic structures. The tumor prescription dose was also raised from 60-66 Gy to 70 Gy (median PTV dose). This resulted in a higher maximal dose to the optic structures for patients 7-11 compared to patients 1-6, as illustrated in Table 3.

During the first period, the planning was performed as an adaptive forward procedure and patient-individualized. This method was too inefficient for routine planning and the quality of the final plan was highly dependent on the skills of the planner. We learned that a complex planning problem as IMRT for ethmoid sinus cancer needs a standardized protocol implementation strategy. By strategy, we mean a precise guideline, which can be followed to translate the protocol first to a matching dose distribution and second to a machine prescription file.

Consistency of the planning result was improved by limiting the optimization routines of the planning system, upfront and in a systematic way, in their freedom. It meant that almost the whole scanned volume of the patient had to be loaded with constraints to restrain the planning system to take the freedom e.g. to put relatively high doses in large volumes of normal tissue or place hot spots at distance from the PTV, even if by doing so indices of uncomplicated local control like P+ would show decreased values. This substantial gain in plan conformality was obtained by parametrization of almost the entire virtual volume of the patient in the objective function by the use of onstrs. With the use of onstrs, only a small rim of non-PTV tissue was free of dose constraints. In the planning phase for patient 11, even this small rim of tissue was used by the optimization process to deposit a hot spot, as illustrated in figure 7. As a result, we had to involve this hot spot region in the biophysical function and started a new optimization cycle. A third onstr, touching the PTV, is now included in the optimization process. This penalizes a dose higher than the prescribed PTV dose in the region outside the PTV. Efficiency was also gained by removal of conflicts in the PTV dose prescription. When PTV and expanded optic pathway structures or brainstem intersect, a conflictual dose prescription is present. Inside PTV, subvolumes were created and contoured as anastructs which were used in the biophysical objective function. By prescribing 70 Gy to the PTV part outside the overlap region and a dose >= 50 Gy or respectively >= 60 Gy to the total PTV, the conflict was removed. Underdosages in the PTV were planned and were not the result of optimization based on a conflictual prescription.

Figure 7
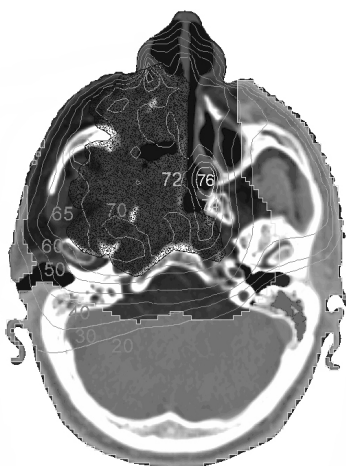
Legend : Unwanted hot spot situated between PTV_3mm and onstr_20mm. Transverse CT slice for patient 11 with the PTV_3mm in black dots, and the onstr_20mm in transparent grey.

The follow-up period of the treated patients is too short to confirm the hypothesis of bilateral sparing of the optic pathways. For optic chiasm, optic nerve and retina injuries, latency periods between one and several years are common [5][6][20]. Severe dry-eye syndrome develops much earlier, with most patients being symptomatic one month after the end of radiation therapy [21]. Acute eye toxicity was moderate or mild. In none of the patients dry-eye syndrome is observed.

Using the class solution, plans for different patients were customized closely to the protocol constraints. The class solution-directed strategy rewards with known value and predictable timing. This is preferred as timing is necessary to maintain the flow of patients. The value is expressed as the degree of compliance with a consistent clinical protocol. The preliminary toxicity profile of the treatment is encouraging.

Acknowledgements

References

1. Jiang G, Morrison W, Garden A, et al. Ethmoid sinus carcinomas : natural history and treatment results. Radiother Oncol 1998;49:21-7.

2. McCutcheon I, BlackLock J, Weber R, et al. Anterior transcranial (craniofacial) resection of tumors of the paranasal sinuses : surgical technique and results. Neurosurgery 1996;38:471-80.

3. Schantz S, Harrison L, Forastiere A. Tumors of the nasal cavity and paranasal sinuses, nasopharynx, oral cavity and oropharynx. In: Cancer: Principles and Practice of Oncology. 5th ed. Lippincott Raven 1997. p. 741-801.

4. Jansen E, Keus R, Hilgers F, et al. Does the combination of radiotherapy and debulking surgery favor survival in paranasal sinus carcinoma? Int J Radiat Oncol Biol Phys 2000;48:27-35.

5. Martel M, Sandler H, Cornblath W, et al. Dose-volume complication analysis for visual pathway structures of patients with advanced paranasal sinus tumors. Int J Radiat Oncol Biol Phys 1997;38:273-84.

6. Parsons J, Bova F, Fitzgerald, et al. Radiation optic neuropathy after megavoltage external-beam irradiation: analysis of time-dose factors. Int J Radiat Oncol Biol Phys 1994;30:755-63.

7. Parsons J, Bova F, Mendenhall W, et al. Response of the normal eye to high dose radiotherapy. Oncology (Huntingt.) 1996;10:837-847; discussion 847-848, 851-2.

8. Harsberger H. Handbook of Head and Neck Imaging 2nd ed. Mosby 1995.

9. De Neve W, De Wagter C, De Jaeger K, et al. Planning and delivering high doses to targets surrounding the spinal cord at the lower neck and upper mediastinal levels: static beam-segmentation technique executed by a multileaf collimator. Radiother Oncol 1996;40:271-9.

10. De Wagter C, Colle C, Fortan L, et al. 3D-conformal intensity modulated radiotherapy planning: interactive optimization by constrained matrix inversion. Radiother Oncol 1998;47:69-76.

11. Chriss T, Herman M, Wharam M, et al. Rapid optimalisation of stereotactic radio-surgery using constrained matrix inversion. In: 2nd Congress of the International Stereotactic Radiosurgery Society Boston June 14-16 1995.

12. De Gersem W, Claus F, De Wagter C, et al, An anatomy based segmentation tool for intensity modulated radiotherapy of head and neck cancer. Int J Radiat Oncol Biol Phys 2001;51:849-59.

13. Khan F. A system of dosimetric calculations. In: The Physics of Radiation Therapy. 1st ed. Williams&Wilkins 1984. p.182-204.

14. Sherouse G, Thorn J, Novins K. A portable 3D radiotherapy treatment design system. Med Phys 1989;16:466.

15. Lyman J. Complication probabilities as assessed from dose-volume histograms. Radiat Res 1985;104(Suppl.):513-519.

16. Kutcher G, Burman C. Calculation of complication probability factors for non-uniform normal tissue irradiation: the effective volume method. Int J Radiat Oncol Biol Phys 1989;16:1623-30.

17. Burman C, Kutcher G, Emami B, et al. Fitting of normal tissue tolerance data to an analytic function. Int J Radiat Oncol Biol Phys 1991;21:123-35.

18. De Neve W, De Gersem W, Derycke S, et al. Clinical delivery of intensity modulated conformal radiotherapy for relapsed or second-primary head and neck cancer using a multileaf collimator with dynamic control. Radiother Oncol 1999;50:301-14.

19. LENT SOMA scales for all anatomic sites. Int J Radiat Oncol Biol Phys 1995;31:1049-91.

20. Jiang G, Tucker S, Guttenberger R, et al. Radiation-induced injury to the visual pathway. Radiother Oncol 1994;30:17-25.

21. Parsons J, Bova F, Fitzgerald C, et al. Severe dry-eye syndrome following external beam irradiation. Int J Radiat Oncol Biol Phys 1994;30:775-80.

4.8   IMRT for sinonasal cancer : short term toxicity profile for 32 patients. F. Claus, T. Boterberg, et al. (submitted).

```
┌─────────────────────────────────────────────────────────┐
│  topics discussed :   → IMRT for sinonasal cancer         │
│                       → acute toxicity                    │
│                       → corneal and lacrimal toxicity     │
│                                                           │
│  key question : What is the short term toxicity profile   │
│                 of IMRT for sinonasal cancer ?            │
└─────────────────────────────────────────────────────────┘
```

paper 4.8

IMRT for sinonasal cancer : short term toxicity profile for **32** patients

Filip Claus, Tom Boterberg, Piet Ost and Wilfried De Neve

Division of Radiotherapy
Ghent University Hospital

Abstract

Intensity modulated radiation therapy (IMRT) was given for 32 patients with M0 sinonasal cancer, with a median follow-up of 15 months. Acute toxicity was mucositis grade 1-2 in 28 patients and grade 3 in 4 patients. No corneal injury was observed, except in one patient where it was present before the start of IMRT. Conjunctivitis and dry eye symptoms were mild (no grade 3-4 toxicity) and no evolution to dry eye syndrome was observed. We conclude that high dose conformality of IMRT results in mild acute toxicity and that IMRT allows to avoid dry eye syndrome by its ability to create concave dose distributions which avoid the main lacrimal glands. Follow-up it too short to evaluate local control, optic nerve or retinal toxicity.
Keywords : sinonasal, radiotherapy, IMRT, acute toxicity, dry eye

1 Introduction

Malignant tumors of the nasal cavity and paranasal sinuses are rare and often present in advanced disease stage [11][2]. Conventional radiotherapy either as primary or postoperative treatment is unable to produce local control rates above 50% in advanced stages (T3-T4) [16][13], and is associated with a significant risk of visual pathway complications [6][12]. Radiation-induced ocular and optic late injury can be divided in two groups according to the time of onset. The onset of retinopathy and optic/chiasmal neuropathy, is mainly between 2 and 5 years after radiotherapy [9][15][8][3]. Corneal and lacrimal injury, typically occur within the first 2 years after the radiation treatment [5][3][10].

Since February 1999, sinonasal tumors are treated with intensity modulated radiation therapy (IMRT) at Ghent University Hospital (GUH). The hypothesis to implement IMRT is to increase tumor control, while selectively reducing the dose to visual pathway structures in order to maintain binocular vision [1]. The acute toxicity profile as well as the occurrence of corneal and lacrimal injury for 32 IMRT treatments are discussed.

2 Material and Methods

2.1 Patients

Between February 1999 and November 2001, 32 patients were treated with IMRT at GUH

---

for sinonasal cancer. The sites of origin were ethmoid sinus (21), maxillary sinus (6) and nasal cavity (5). The histological types of the tumor were adenocarcinoma (17), squamous cell carcinoma (8), esthesioneuroblastoma (3), adenoid cystic carcinoma (2), transitional cell carcinoma (1) and lympho-epithelioma (1). Only two patients were staged as N-positive at the time of diagnosis and no patient had clinical evidence of distant metastasis at the start of the radiation treatment.

For tumors originating in the ethmoid and maxillary sinuses, staging was performed according to the TNM classification system of the International Union Against Cancer (UICC) [14]. No patient had T1, 8 patients T2, 7 patients T3 and 10 patients T4 disease. For nasal cavity tumors there is no UICC classification system available. For two patients, IMRT was used to re-irradiate a locoregional relapse of an ethmoid sinus tumor following surgery and conventional radiation therapy. Because of repeated surgery for these two cases, no rT-staging was possible. Radiotherapy was given as postoperative treatment in 31 cases, and as primary therapy for one patient. None of the 32 patients received chemotherapy. The median follow-up was 15 months (3-33 months). Overall survival data (endpoint = death by all causes) were measured from the start of radiation, using the Kaplan-Meier method.

2.2 Radiotherapy

For the first 10 patients treated with IMRT, the total dose ranged between 60 (n = 4) and 66 Gy (n = 6). For the remaining patients, a definitive treatment protocol was used, prescribing a median dose of 70 Gy to the planning target volume (PTV), while only 5 % of the volume of each optic pathway structure was allowed to receive more than 60 Gy. One patient died during the course of radiotherapy, reaching an end dose of 40 Gy. Patients diagnosed as N+ (n = 2) also received bilateral radiation for lymph node groups Ib, II, III, IV, V and the retropharyngeal nodes. All patients were treated with daily fractions of 2 Gy, five days a week. A detailed description of the IMRT implementation strategy is previously reported [1].

2.3 Toxicity scoring

To score the short term toxicity due to radiation, the Common Toxicity Criteria (CTC) of the NIH (The US National Institutes of Health) were used (information on http://ctep.info.nih.gov/CTC3). Apart from mucositis and weight loss, symptoms related to eye injury are reported, including conjunctivitis, dry eye, keratitis, tearing, blurred vision, double vision and photophobia. The CTC-scales distinguish 5 grades of toxicity, ranging between grade 0 (no toxicity present) and grade 4 (full blown toxicity : such as necrosis or total loss of function).

3 Results and Discussion

Overall survival is shown in figure 1. Table 1 summarizes the toxicity grade scores for the

32 patients treated with IMRT. The scores for the adverse effects are divided in two periods : (1) the acute toxicity, scored during or within one month after IMRT and (2) the corneal and lacrimal injury, scored one month after finishing IMRT until the last date of follow-up.

Figure 1 : Overall survival curve for the 32 sinonasal cancer patients treated with IMRT.
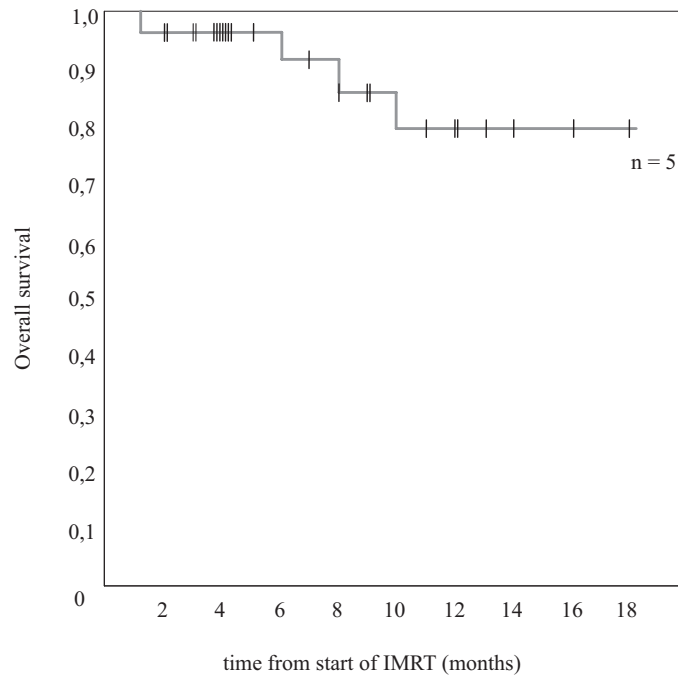
Table 1 : IMRT short term toxicity grade scores for 32 sinonasal cancer patients

CTC-scaling	grade 0	grade 1	grade 2	grade 3	grade 4
acute toxicity : highest score during or within 1 month after IMRT					
mucositis	0 % (0/32)	47 % (15/32)	41 % (13/32)	12 % (4/32)	0 % (0/32)
conjunctivitis	0 % (0/32)	84 % (27/32)	16 % (5/32)	0 % (0/32)	0 % (0/32)
dry eye	0 % (0/32)	88 % (28/32)	12 % (4/32)	0 % (0/32)	0 % (0/32)
keratitis	91 % (29/32)	6 % (2/32)	0 % (0/32)	3 % (1/32) [a]	0 % (0/32)
tearing	44 % (14/32)	31 % (10/32)	25 % (8/32)	0 % (0/32)	0 % (0/32)
blurred vision	91 % (29/32)	0 % (0/32)	9 % (3/32)	0 % (0/32)	0 % (0/32)
double vision	97 % (31/32)	0 % (0/32)	3 % (1/32) [b]	0 % (0/32)	0 % (0/32)
photophobia	94 % (30/32)	0 % (0/32)	6 % (2/32)	0 % (0/32)	0 % (0/32)
weight loss	78 % (25/32)	22 % (7/32)	0 % (0/32)	0 % (0/32)	0 % (0/32)
corneal and lacrimal injury : highest score $\geq$1 month after IMRT					
conjunctivitis	81 % (25/31)	16 % (5/31)	3 % (1/31) [a]	0 % (0/31)	0 % (0/31)
dry eye	65 % (20/31)	32 % (10/31)	3 % (1/31) [a]	0 % (0/31)	0 % (0/31)
keratitis	97 % (30/31)	0 % (0/31)	3 % (1/31) [a]	0 % (0/31)	0 % (0/31)
blurred vision	97 % (30/31)	0 % (0/31)	3 % (1/31)[a]	0 % (0/31)	0 % (0/31)
photophobia	97 % (30/31)	0 % (0/31)	3 % (1/31)[a]	0 % (0/31)	0 % (0/31)

[a] : already present before the start of IMRT (re-irradiation with cumulative dose of 136 Gy)

[b] : already present before the start of IMRT (medial wall of both orbits was surgically removed)

    With respect to the acute toxicity period, mucositis grade 3 was observed in 4 cases, and was located at the roof of the oral cavity (hard palate) for two patients, and at the oropharynx for the two N+ patients. For conjunctivitis, dry eye, tearing, blurred vision, double vision, photophobia and weight loss, no grade 3 acute toxicity was observed. Only one patient was diagnosed with keratitis grade 3, already present before the start of the IMRT treatment. The man was re-irradiated for a local relapse and received a cumulative

dose of 136 Gy. Grade 0 or 1 acute ocular toxicity was observed in 84 % of the patients, except for tearing, for which the rate dropped to 75 % (25 % of the patients suffered grade 2 toxicity). In more than half of the cases tearing was already present before the start of radiotherapy, due to extensive surgery, especially in those cases where tumoral invasion of the lacrimal canal was present.

With respect to corneal and lacrimal injury, scored after the acute toxicity period, grade 2 toxicity was observed in one patient who was re-irradiated. No keratitis, blurred vision or photophobia was observed in the other patients. Grade 1 dry eye and conjunctivitis was present in respectively 32 and 16 % of the cases. No grade 3 or 4 toxicity was observed.

The major lacrimal gland is located in the superolateral part of the orbit, as illustrated in figure 2a. Together with the accessory lacrimal glands, it produces the watery tear film. The sebacceous tarsal glands, embedded in the upper and lower eyelids, produce an oily secretion protecting this tear film. The main functions of the lacrimal apparatus are to prevent the conjunctiva and cornea from drying up, to form a natural barrier against particles, noxious fumes and micro-organisms, to increase the smoothness of the cornea in order to improve the visus, and to facilitate the movements of the eyelids [17]. Damage to this lacrimal apparatus may thus debilitate the natural host defense and increase the susceptibility of the conjunctiva and cornea to radiation damage.
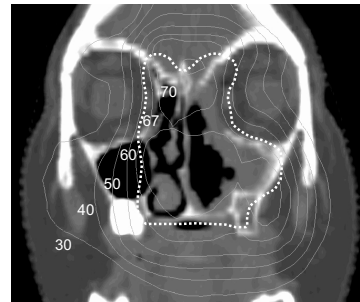
| Figure 2a | Figure 2b |

Legend : Figure 2a : Location of the lacrimal gland (white arrow) on a coronal MRI scan. The patient was diagnosed with a melanoma originating in the left ethmoidal sinus cells. Figure 2b : Dose distribution display in a coronal plane of the IMRT plan for the case illustrated in figure 1a. The isodose lines are expressed in Gy. Both major lacrimal glands are excluded by the isodose line of 30 Gy.

Dry eye syndrome symptoms start at 30 Gy to the structures located anteriorly in the orbit and it is observed in 100% of the cases at doses exceeding 55-60 Gy [7]. The onset of the symptoms of dry-eye syndrome usually starts within one month after radiotherapy, and is characterized by a red, painful and itchy eye, with photophobia, foreign body sensation

and hypersensitivity to wind. Secondary symptoms may give rise to corneal epithelial break-down with ulceration, surinfection, opacification and sometimes perforation. The treatment is symptomatic : ocular lubrication or ointments and occlusion of the lacrimal puncta (mechanical by silicone punctal plugs or surgical by cautery) in order to decrease the drainage of tear film. However in many instances of severe dry eye syndrome, enucleation of the eye is necessary to control the symptoms, resulting in a complete loss of function and a cosmetic disfiguring effect [10].

Patients with sinonasal cancer are good candidates to benefit from IMRT, given the close vicinity of the ocular and visual pathway structures. Free surgical margins are sometimes difficult to obtain, which necessitates high radiation doses to increase locoregional control. Even for cases with advanced disease and a very poor prognosis, much attention should be paid to short time complications such as dry eye syndrome, since it develops within one year after finishing radiotherapy. None of the 32 patients treated with IMRT, developed a dry eye syndrome, even the two cases where IMRT was used to re-irradiate a local recurrence (cumulative PTV-prescription doses of 120 and 136 Gy). The mean dose to the major lacrimal glands did not exceed 40 Gy for all treatment plans. Figure 2b illustrates the intended functional sparing of the major lacrimal glands. Even in cases where sparing of the optic tract is less indicated, because of tumoral invasion of the visual pathway structures, functional preservation of the lacrimal apparatus is recommended in order to prevent the painful complications of dry eye syndrome and for cosmetic reasons [7][4]. At the time of analysis, none of the 32 patients had developed retinopathy or neuropathy, although follow-up is too short to draw final conclusions.

In radiation therapy of sinonasal tumors, IMRT is able to deliver high doses with low acute toxicity and allows to avoid lacrimal gland and corneal injury. Longer follow-up is necessary to evaluate its potential to avoid retinopathy and optic neuropathy while maintaining locoregional tumor control.

Acknowledgements

References

1. Claus F, De Gersem W, De Wagter C, et al. An implementation strategy for IMRT of ethmoid sinus cancer with bilateral sparing of the optic pathways. Int J Radiat Oncol Biol Phys 2001;51:318-31.

2. Gospodarowicz M, Henson D, Hutter R, et al. (eds): Prognostic factors in cancer, 2nd ed. New York, Wiley-Liss, 2001.

3. Jiang G, Tucker S, Guttenberger R, et al. Radiation-induced injury to the visual pathway. Radiother Oncol 1994;30:17-25.

4. Karim A, KralendonkJ, Njo K, et al. Ethmoid and upper nasal cavity carcinoma : treatment, results and complications. Radiother Oncol 1990;19:109-20.

5. Letschert JG, Gonzalez-Gonzalez D, Oskam J, et al. Results of radiotherapy in patients with stage I orbital non-Hodgkin's lymphoma. Radiother Oncol 1991;22:36-44.

6. Martel M, Sandler H, Cornblath W, et al. Dose-volume complication analysis for visual pathway structures of patients with advanced paranasal sinus tumors. Int J Radiat Oncol Biol Phys 1997;38:273-84.

7. Million R, Parsons J. Radiation-induced eye injury from head and neck therapy. Front Radiat Ther Oncol Basel, Karger, 1999;32:21-33.

8. Parsons J, Bova F, Fitzgerald, et al. Radiation optic neuropathy after megavoltage external-beam irradiation: analysis of time-dose factors. Int J Radiat Oncol Biol Phys 1994;30:755-63.

9. Parsons J, Bova F, Fitzgerald, et al. Radiation retinopathy after external-beam irradiation: analysis of time-dose factors. Int J Radiat Oncol Biol Phys 1994;30:765-73.

10. Parsons J, Bova F, Fitzgerald C, et al. Severe dry-eye syndrome following external beam irradiation. Int J Radiat Oncol Biol Phys 1994;30:775-80.

11. Physician Data Query (PDQ) of the National Cancer Institute : Treatment options for health professionals. Paranasal Sinus and Nasal Cavity Cancer. CancerNet http://cancernet.nci.nih.gov.

12. Romestaing P, Hullo A. Late effects of radiation on the eye and ocular adnexa. Cancer Radiother 1997;1(6):683-91.

13. Schantz S, Harrison L, Forastiere A. Tumors of the nasal cavity and paranasal sinuses, nasopharynx, oral cavity and oropharynx. In: Cancer: Principles and Practice of Oncology. 5th ed. Lippincott Raven 1997. p. 741-801.

14. Sobin LH, Wittekind C, (eds): UICC TNM classification of malignant tumors, 5th ed. New York, Wiley-Liss, 1997.

15. Takeda A, Shigematsu N, Suzuki S, et al. Late retinal complications of radiation therapy for nasal and paranasal malignancies: relationship between irradiated-dose area and severity. Int J Radiat Oncol Biol Phys 1999;44:599-605.

16. Waldron JN, O'Sullivan B, Warde P, et al. Ethmoid sinus cancer: twenty-nine cases managed with primary radiation therapy. Int J Radiat Oncol Biol Phys 1998;41:361-9.

17. Williams PL. Gray's Anatomy. 38th ed. Churchill Livingstone 1995.

4.9 **Postoperative radiotherapy for adenocarcinoma of the ethmoid sinuses: treatment results for 47 patients. F. Claus, T. Boterberg et al. (submitted).**

topics discussed :	→ adenocarcinoma of the ethmoid sinuses
	→ patient and tumor characteristics
	→ results for postoperative radiotherapy
key question : What is the prognosis of postoperative radiotherapy for adenocarcinoma of the ethmoid sinuses ?	

paper 4.9

Postoperative radiotherapy for adenocarcinoma
of the ethmoid sinuses: treatment results for 47 patients

Filip Claus[1], Tom Boterberg[1], Piet Ost[1], John Huys, Hubert Vermeersch[2],
Sabine Braems[1], Katrien Bonte[2], Mieke Moerman[2], Christophe Verhoye[3]
and Wilfried De Neve[1]

[1]Division of Radiotherapy
Ghent University Hospital
[2]Department of Head and Neck Surgery
Ghent University Hospital

[3]Department of Otorhinolaryngology,
Sint Lucas Hospital, Bruges

Abstract

Purpose : Ethmoid sinus cancer is a rare malignancy. Treatment results are mostly reported together with other sinonasal tumors, grouping a wide range of different histologies and treatment approaches. This study reports on the treatment outcome of 47 patients diagnosed with adenocarcinoma of the ethmoid sinuses and treated with surgery and high dose postoperative radiation therapy.

Methods and Materials : Between September 1985 and October 2001, 51 patients with adenocarcinoma of the ethmoid sinuses were referred to the Ghent University Hospital. Four patients were treated with low dose palliative radiation because of very extended inoperable disease or distant metastasis at the time of diagnosis. They were not included in this analysis. The other 47 patients, all staged as N0M0, were treated with surgery and postoperative high dose radiation therapy. The median follow-up was 32 months. The T-stages were T1 for 2, T2 for 17, T3 for 11 and T4 for 17 patients. All 47 patients were staged as N0M0.

Results : The 3-year, 5-year and 7-year overall survival are respectively 71 %, 60 % and 38 %. The 3-year and 5-year disease free survival are respectively 62 % and 36 %. The 3-year and 5-year disease free survival for T1-T2 stages are respectively 87 % and 55 %, for T3 stages 57 % and 28 % and for T4 stages 41 % and 25 %. The locoregional tumor control was 70 % and 59 % at respectively 3 and 5 years. Patients presenting with intracranial tumor invasion at the time of diagnosis relapsed within 7 months after the end of radiotherapy. Radiation induced severe dry eye syndrome and optic neuropathy was observed in respectively 7 and 2 of the 47 cases.

Conclusion : Postoperative radiotherapy for adenocarcinoma of the ethmoid sinuses is associated with good local control rates. Crucial for a favorable prognosis is the absence of intracranial invasion. The rarity of these tumors makes it difficult to evaluate new therapeutic advances.

Keywords : ethmoid sinus, adenocarcinoma, postoperative radiotherapy

1 Introduction

Ethmoid sinus tumors account for less than 20 % of all paranasal sinus cancers and less than 1 % of all head and neck malignancies. Radiotherapy as primary or postoperative treatment for ethmoid sinus cancer is unable to produce local control rates above 50 % in advanced disease stages (T3-T4) [1]. Treatment results for ethmoid sinus tumors are mostly reported together with tumors located in the nasal cavity and other paranasal sinuses, designated as sinonasal tumors. However, a distinction as to the specific site of origin and to the histological type of sinonasal tumors does have an impact on prognosis [2]. Most of the series reported are small and very non-uniform with respect to histology, tumor staging system and treatment regimens.

This report includes 47 patients with adenocarcinoma of the ethmoid sinuses treated with surgery and postoperative radiotherapy between 1985 and 2001. All patients analyzed were node-negative and had no clinical evidence of distant metastasis at the time of diagnosis. Endpoints for the presented analysis are locoregional tumor control, disease-specific survival and overall survival.

2 Material and Methods

Between September 1985 and October 2001, 51 patients with adenocarcinoma of the ethmoid sinuses were referred to the Ghent University Hospital (GUH). Four patients were not treated with surgery and received low dose palliative radiation, because of very extended inoperable disease or distant metastasis at the time of diagnosis. They were not included in this analysis. The other 47 patients were all staged as N0M0 and treated with surgery and postoperative high dose radiation therapy. The median follow-up, recorded from the end date of radiation therapy, was 32 months (range 2-119). None of the patients received chemotherapy. Clinical staging was performed according to the TNM classification system of the International Union Against Cancer (UICC) [3]. For patients diagnosed before 1997, a retrospective clinical staging was performed based on the radiological, surgical and pathologic reports. Two patients had T1, 17 patients T2 , 11 patients T3 and 17 patients T4 disease. Cranial invasion with tumor growth into the brain tissue parenchyma was observed in eight cases. The male/female ratio was 46/1. The mean and median age at the time of diagnosis was respectively 59 and 60 year (range 28 - 79). Two patients were younger than 40 year, 5 patients were diagnosed in the 5th decade, 15 in the 6th decade, 20 in the 7th decade and 5 in the 8th decade. Professional wood dust exposure was documented in 81 % of the cases (38/47).

All patients underwent surgery, with a transfacial approach in 38 cases, an anterior craniofacial approach [4] in 8 cases and functional endoscopic sinus surgery (FESS) in one case. An unilateral orbital exenteration was performed in 4 cases.

The radiation dose prescribed to the target volume ranged between 60 and 70 Gy, except for one patient receiving a dose of 54 Gy. A conventional treatment technique [5], consisting of an anterior portal and two lateral wedged fields, was used for 19 patients, a non-coplanar

3D-conformal technique for 11 cases, and intensity modulated radiation therapy (IMRT) for 17 cases. The fraction size varied between 1.8 and 2 Gy and all patients were treated 5 days a week. No prophylactic neck irradiation was given. Irradiation was administered with ^{60}Cobalt γ-rays for 16 patients and with a linear accelerator (5 or 6 MV photon beams) for 31 patients.

The endpoints of the presented analysis are overall survival, disease free survival and locoregional tumor control, calculated using the Kaplan-Meier method. Overall survival rate was measured from the date of histological diagnosis. Disease free survival and locoregional tumor control were calculated from the start date of radiotherapy. All data were analyzed using the SPSS 9.0 software package. Endpoints for ocular and visual pathway toxicity were severe dry eye syndrome [6] and optic neuropathy [7][8].

3 Results

Figure 1 shows the survival and locoregional control plots for the 47 patients. The 3-year, 5-year and 7-year overall survival are respectively 71 %, 60 % and 38 %. The 3-year and 5-year disease free survival are respectively 62 % and 36 %. The 3-year and 5-year disease free survival for T1-T2 stages are respectively 87 % and 55 %, for T3 stages 57 % and 28 % and for T4 stages 41 % and 25 %. Distant metastasis was observed in 6 cases and local tumor recurrence in 15 cases. No nodal tumor recurrence was observed. Ethmoid cancer was the cause of death for 15 patients, cardiovascular disease for 3 patients and an astrocytoma for one patient.

The locoregional tumor control was 70 % and 59 % at respectively 3 and 5 years. The 2-year locoregional tumor control for T1-T2, T3 and T4 stages was respectively 87 %, 80 % and 46 %. In 7 of the 8 cases where the primary tumor invaded the brain parenchym, tumor recurrence was observed within 7 months after the end of radiotherapy. In one case no relapse is observed, but the follow-up is only 3 months. The tumor recurrence was local for 6 patients and distant for 1 patient. Only one of the 6 local relapses was observed in-field (= inside the radiation field), for the other 5 cases 4 relapsed intracranially and one at the margin of the radiation field in the sphenoid sinus. For T4 patients without invasion of the brain tissue, the 3-year and 5-year locoregional tumor control were respectively 75 % and 60 %. The locoregional tumor control for all T-stages without the T4's with intracranial invasion was 82 % and 68 % at respectively 3 and 5 years.

Radiation induced severe dry eye syndrome, characterized by chronic conjunctivitis and keratitis, and accompanied by a significant decrease of the visus (visus < 20 % compared to the visus before radiotherapy) was observed in seven cases, all of them treated with conventional radiation techniques (= no IMRT). In one of these patients enucleation of the eye was necessary to control the symptoms. Optic neuropathy was observed in two patients, for one of them bilateral. No neuropathy was observed in the group treated with IMRT.

4 Discussion

The rarity of ethmoid sinus cancer results in a lack of prospectively collected data for this tumor site. Treatment results for ethmoid sinus cancer are mostly reported together with tumors originating in the maxillary sinus and nasal cavity. Grau et al. [9] reported on the outcome of 315 sinonasal cancer cases, of which only 14 were categorized as ethmoid tumors (= 4%). Spiro et al. [10][11] published results for 211 patients with paranasal and nasal cavity cancer, for which 10 % of the primary tumors were located in the ethmoid sinuses. Nevertheless ethmoid sinus tumors differ from other sinonasal tumors in terms of diagnostic features, surgical and radiotherapy techniques, prognostic factors and treatment complications, as reported by several authors [12][5][13]. The data presented in this study are very uniform with respect to tumor location, histology and treatment regimen.

Figure 1
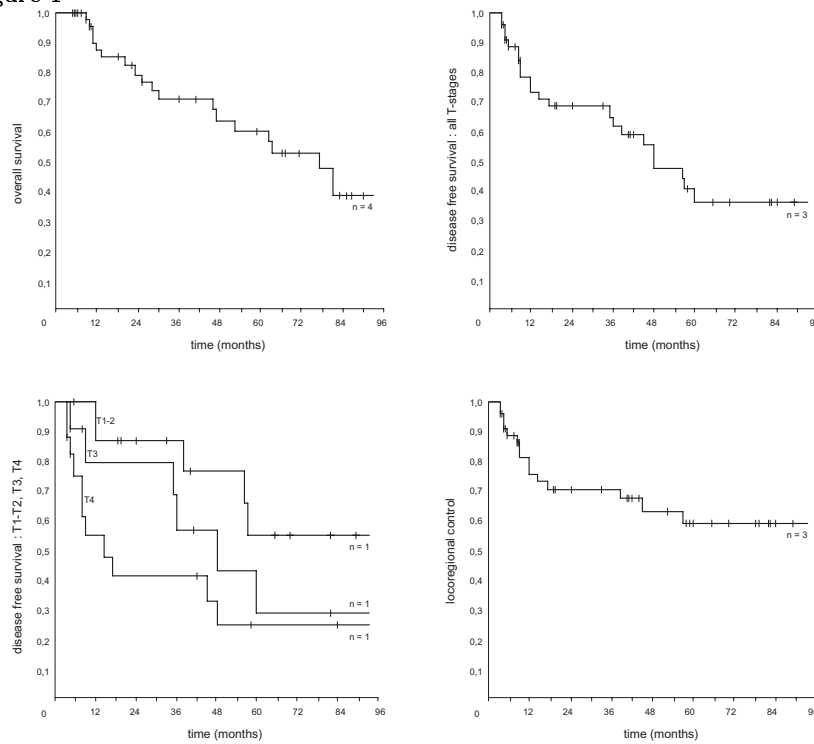
Legend : Kaplan-Meier plots for overall survival (upper left), disease free survival (upper right), disease free survival for T-subgroups (lower left) and locoregional control (lower right).

Various etiologic factors have been linked to malignant tumors of the sinonasal tract, most of them occupational exposures, including nickel, chromium, isopropyl oils, volatile hydrocarbons, and organic fibers that are found in wood, shoe and textile industry [14]. Hardwood (angiosperm) dust is proven to be carcinogenic to humans and possesses genotoxic properties [15][16]. The carcinogens consist of insoluble high-molecular components, such as cellulose and lignin, and insoluble low-molecular components, such as terpenes. Adenocarcinoma of the ethmoid sinuses is clearly associated with exposure to hardwood dust, as illustrated by the high incidence among people working in the wood furniture industry [17][18]. In the present study 81 % of the patients reported professional exposure to wood dust. More attention should be paid to prevent exposure to wood dust, and to make physicians aware of the higher risk of sinonasal cancer in this professional category. Repeated MRI imaging for high risk groups may detect lesion in early disease stages (T1-T2).

Essential prognostic factors for paranasal sinus cancer are the primary tumor extent and lymph-node involvement [2]. This is illustrated by the very poor prognosis of T4 tumors with cranial invasion. For the presented study, the 3-year and 5-year overall survival for all T-stages without the T4's with intracranial invasion are respectively 83 % and 71 %, compared to 71 % and 60 % for all patients. The incidence of lymph node involvement at the time of diagnosis for ethmoid sinus cancer is very low. In this study for none of the 47 patients clinically positive lymph nodes were observed. In the series reported by Tiwari et al., none of the 50 patients presented with clinical lymph node metastasis at the time of diagnosis, with 50 % of the patients staged as T4. Moreau et al. [18], Jiang et al. [19] and Waldron et al. [20] reported incidences of lymph node invasion at the time of diagnosis of respectively 0 % (0/25), 3 % (1/34) and 7 % (2/29).

Treatment recommendations are based on retrospective studies, the majority reporting small numbers of patients and/or being very inhomogeneous with respect to sinonasal subsite, histology and treatment schedule. A combined treatment of surgery and radiation therapy is generally recommended [21][22][19]. Table 1 summarizes the treatment results for ethmoid sinus cancer reported in the literature (series with $\geq$ 25 patients). The difference in survival rates may be explained by the small number of patients, the difference in patient selection, histology, T-subgroups and treatment regimens. Treatment outcome is likely to be influenced by the skills of the surgeon and the experience of the center.

The high incidence of local recurrence, despite invasive surgical techniques and high radiation doses (example in Figure 2), focuses research towards new treatment regimens in order to improve local control. Knegt et al. [24] reported on the outcome of 62 patients, treated with a regimen of surgical debulking and topical fluorouracil between 1976 and 1997 ($\geq$ 20 year). The overall survival was 79 %. However, as the authors observed themselves, the validity of this treatment regimen is based on retrospective survival data and was not tested in a controlled clinical trial. The rarity of ethmoid sinus cancer makes it difficult

to evaluate such new advances in cancer treatment. At our department, since 1998 all ethmoid sinus cancer patients are treated with CT- and MRI-based IMRT. The hypothesis to implement IMRT is to improve local control while preserving binocular vision [28].

At this moment follow-up is too short, but the short term toxicity profile is encouraging (no corneal or lacrimal gland injury clinically observed). New advances in the treatment of ethmoid sinus cancer may result in improved local control rates. Therefore, efforts should be made to investigate optimal treatment regimens in prospective multicenter trials.

Figure 2
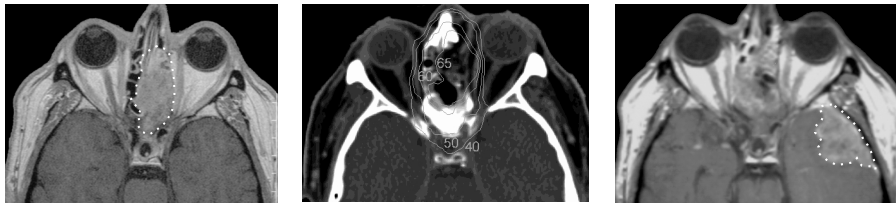
Legend : Illustration of a local relapse after craniofacial surgery : status before treatment (left panel) with the gross tumor volume in white dots, postoperative status (middle panel) with the isodoses in Gy of the radiotherapy plan, 4 months after treatment (right panel) with the outfield relapse in white dots.

Acknowledgements

Table 1 : Literature review on treatment results of ethmoid sinus cancer.

	cases	adenoca	T1/T2/T3/T4*	R/	R/	5-year-OS
	#	%	%	modality	period	%
Cantu et al.[23] *Head Neck '99*	91	55	0 / 40 / 30 / 30	S	1987-1994	47
Claus et al. *this study*	47	100	4 / 36 / 24 / 36	S,R	1985-2001	60
Jiang et al.[19] *Radiother Oncol '98*	34	26	0 / 18 / 38 / 44**	S,R,C	1969-1993	55
Knegt et al.[24] *Arch Otolaryngol Head Neck Surg '01*	62	100	5 / 16 / 39 / 40	S,C	1976-1997	79
Moreau et al.[18] *Neurochirurgie '97*	25	100	4 / 24 / 36 / 36	S,R	1985-1993	48
Salvan et al.[25] *J Laryngol Otol '98*	41	76	ns / ns / ns / ns	S,R,C	1986-1994	36
Stoll et al.[26] *Rev Laryngol Otol Rhinol (Bord) '01*	76	100	3 / 18 / 58 / 21***	S,R	1975-2000	80
Tiwari et al.[27] *Eur J Surg Oncol '99*	50	58	2 / 16 / 32 / 50	S,R	1975-1994	63
Waldron et al.[20] *Int J Radiat Oncol Biol Phys '98*	29	31	10 / 17 / 7 / 66	R	1976-1994	39

abbreviations : S : surgery R : radiotherapy C : chemotherapy OS : overall survival ns : not specified
* UICC TNM classification (1997)**Kadish staging converted to UICC staging***Roux classification [26]

References

1. Schantz S, Harrison L, Forastiere A. Tumors of the nasal cavity and paranasal sinuses, nasopharynx, oral cavity and oropharynx. In: Cancer: Principles and Practice of Oncology. 5th ed. Lippincott Raven 1997. p. 741-801.

2. Gospodarowicz M, Henson D, Hutter R, et al. (eds): Prognostic factors in cancer, 2nd ed. New York, Wiley-Liss, 2001.

3. Sobin LH, Wittekind C, (eds): UICC TNM classification of malignant tumors, 5th ed. New York, Wiley-Liss, 1997.

4. McCutcheon I, BlackLock J, Weber R, et al. Anterior transcranial (craniofacial) resection of tumors of the paranasal sinuses : surgical technique and results. Neurosurgery 1996;38:471-80.

5. Ellingwood K, Million R. Cancer of the nasal cavity and ethmoid/sphenoid sinuses. Cancer 1979;43:1517-26.

6. Parsons J, Bova F, Fitzgerald C, et al. Severe dry-eye syndrome following external beam irradiation. Int J Radiat Oncol Biol Phys 1994;30:775-80.

7. Parsons J, Bova F, Fitzgerald, et al. Radiation optic neuropathy after megavoltage external-beam irradiation: analysis of time-dose factors. Int J Radiat Oncol Biol Phys 1994;30:755-63.

8. Jiang G, Tucker S, Guttenberger R, et al. Radiation-induced injury to the visual pathway. Radiother Oncol 1994;30:17-25.

9. Grau C, Jakobsen MH, Harbo G, et al. Sino-nasal cancer in Denmark 1982-1991–a nationwide survey. Acta Oncol 2001;40:19-23.

10. Spiro J, Soo K, Spiro R. Squamous carcinoma of the nasal cavity and paranasal sinuses. Am J Surg 1989;158:328-32.

11. Spiro J, Soo K, Spiro R. Nonsquamous cell malignant neoplasms of the nasal cavities and paranasal sinuses. Head Neck 1995;17:114-8.

12. Dulguerov P, Jacobsen MS, Allal AS, et al. Nasal and paranasal sinus carcinoma: Are we making progress? Cancer 2001;92:3012-29.

13. Parsons J, Mendenhall W, Mancuso A, et al. Malignant tumors of the nasal cavity and ethmoid and sphenoid sinuses. Int J Radiat Oncol Biol Phys 1988;14:11-22.

14. Perez CA, Brady LW. Principles and Practice of Radiation Oncology, 3rd ed. Philadelphia, Lippincott-Raven, 1998.

15. Health Council of the Netherlands: Hardwood and softwood dust; evaluation of the carcinogenicity and genotoxicity. The Hague: Health Council of the Netherlands,2000; publication no. 2000/08OSH.

16. International Agency for Research on Cancer (IARC). Wood dust and formaldehyde. Lyon IARC, 1995:32-215 (IARC Monographs on the evaluation of carcinogenic risks to humans; vol.62).

17. Hadfield EH, Macbeth RG. Adenocarcinoma of ethmoids in furniture workers. Ann Otol Rhinol Laryngol 1971;80:699-703.

18. Moreau JJ, Bessede JP, Heurtebise F, et al. Adenocarcinoma of the ethmoid sinus in woodworkers. Retrospective study of 25 cases. Neurochirurgie 1997;43:111-7.

19. Jiang G, Morrison W, Garden A, et al. Ethmoid sinus carcinomas : natural history and treatment results. Radiother Oncol 1998;49:21-7.

20. Waldron JN, O'Sullivan B, Warde P, et al. Ethmoid sinus cancer: twenty-nine cases managed with primary radiation therapy. Int J Radiat Oncol Biol Phys 1998;41:361-9.

21. Budihna M, Smid L. Carcinoma of the paranasal sinuses: results of treatment and some prognostic factors. Strahlenther Onkol 1992;168:322-7.

22. Physician Data Query (PDQ) of the National Cancer Institute : Treatment options for health professionals. Paranasal Sinus and Nasal Cavity Cancer. CancerNet http://cancernet.nci.nih.gov.

23. Cantu G. Solero CL, Mariani L, et al. Anterior craniofacial resection for malignant ethmoid tumors : a series of 91 patients. Head Neck 1999;21:185-91.

24. Knegt P, Ah-See K, vd Velden LA, et al. Adenocarcinoma of the ethmoidal sinus complex. Arch Otolaryngol Head Neck Surg 2001;127:141-6.

25. Salvan D, Julieron M, Marandas P, et al. Combined transfacial and neurosurgical approach to malignant tumours of the ethmoid sinus. J Laryngol Otol 1998;112:446-50.

26. Stoll D, Bebear JP, Truilhe Y, et al. Les adenocarcinomes de l'ethmoide : etude retrospective de 76 patients. Rev Laryngol Otol Rhinol (Bord) 2001;122:21-9.

27. Tiwari R, Hardillo JA, Tobi H, et al. Carcinoma of the ethmoid: results of treatment with conventional surgery and post-operative radiotherapy. Eur J Surg Oncol 1999;25:401-5.

28. Claus F, De Gersem W, De Wagter C, et al. An implementation strategy for IMRT of ethmoid sinus cancer with bilateral sparing of the optic pathways. Int J Radiat Oncol Biol Phys 2001;51:318-31.

Filip Claus

5 Discussion

IMRT for head and neck cancer is routinely clinically implemented in only a few centers around the world [1][2][3][4][5][6][7]. Much research is ongoing to increase the implementation status of this new radiation technique. The developmental process of IMRT can roughly be divided into 4 categories : (1) the development of an IMRT planning platform, (2) the clinical implementation of IMRT for a particular tumor site, (3) the treatment delivery, quality control (QA) and dosimetry of IMRT, and (4) the design of clinical trials to investigate the potential of IMRT.

(1) Software development for IMRT planning, in particular computer optimization software, is very complex and requires a team of highly specialized researchers. Today, very few commercially available IMRT planning systems are capable to compete with university-developed or -adapted planning systems. Certainly for head and neck cancer most of the clinical IMRT experience is reported with in-house developed software platforms.

(2) The implementation of IMRT for head and neck cancer requires a close collaboration between radiation oncologists and physicists. The potential of IMRT to achieve a higher degree of target conformity and/or normal tissue sparing results in a need for respectively more precise delineation guidelines for the CTV and more accurate tolerance parameters for various OARs. For instance, the introduction of IMRT for elective lymph node irradiation of the neck in order to preserve parotid gland function, has led to the need for more precise delineation guidelines for lymph node target volumes [8] and for more accurate dose-volume and -function relationships of the parotid gland [9]. Likewise for paranasal sinus cancer, interobserver differences in target volume delineation have a significant impact on the dose to the target volume and organs at risk, in particular for highly conformal treatment techniques [10]

(3) The transfer to and the delivery on a linac of IMRT plans and the subsequent QA and dosimetry is an intense topic of research. The lack of communication between several commercial treatment planning systems and different types of accelerators is still an obstacle for radiotherapy departments to clinically implement IMRT. The complex 3D dose gradients of IMRT treatment plans, in particular for head and neck cases, necessitates more preclinical

testing and verification compared to other radiation techniques [11][12].

(4) At last, the setup of well designed clinical trials is the ultimate way to investigate the clinical value of IMRT. At this moment, no randomized clinical trial for IMRT of head and neck cancer is reported. The labour-intensive delineation process for these type of treatment plans, the limited experience of IMRT for this treatment site and the lack of plan automation are possible explanations.

The proximity of the eyes, cranial nerves and brain tissue complicate radical surgery and high dose radiation therapy for ethmoid sinus cancer. By selectively reducing the dose to surrounding OARs, IMRT has the potential to improve the therapeutic ratio for this type of cancer. The rarity of ethmoid sinus cancer and the continuous advances and new insights in related medical specialisms, such as imaging and surgery, make it difficult to evaluate the full clinical potential of this new treatment technique. At this moment, follow-up is too short to report on the impact of IMRT on local tumor control and its potential to reduce the incidence of radiation induced neuropathy. The main clinical achievement of the presented work is the reduction in radiation induced short term toxicity, in particular the avoidance of symptoms related to dry eye. Dry eye syndrome is a severe side-effect due to radiation injury of the lacrimal glands, characterized by signs and symptoms with early onset after radiation treatment. As reported in paper 4.9, none of the 17 patients treated with IMRT for ethmoid sinus cancer developed dry eye syndrome, while 7 of the 30 patients in the non-IMRT group developed severe dry eye syndrome. In the IMRT protocol for ethmoid sinus cancer presented in the thesis, the systematic use of a larger CTV, the higher PTV dose homogeneity and the higher prescribed dose to the PTV (70 Gy), are all arguments to predict a higher local control with IMRT. This new radiation technique also offers the opportunity to treat cases with very extended inoperable disease, normally treated with conventional techniques to a low palliative dose, to a high dose with an acceptable risk of adverse effects. However, patients presenting with intracranial tumor spread still have a very poor prognosis, and further advancement in treatment should address these cases. With regard to optic neuropathy, arguments for

a very low NTCP with the presented IMRT approach include the safe dose constraint of 60 Gy, which constrains the maximal dose and is applied to the 2 mm expanded structures, the use of a biological optimization model, which results in an inhomogeneous irradiation of the nerves and a low mean dose, and the maximum daily fraction size of 1.7 Gy (35 fractions of 2.0 Gy prescribed to the PTV corresponds to 35 fractions of 1.7 Gy for a maximum dose constraint of 60 Gy).

An in-depth discussion of the various aspects involved in the quality control of IMRT falls outside the scope of this thesis. Nevertheless we want to stress on the importance of this step in the IMRT implementation process, and much research is ongoing in this domain [11][12][13][14][15][16]. Besides the need for an accurate dose-calculation algorithm, much attention should be paid in comparing the IMRT planning system calculations with dose measurements, and the verification of IMRT treatment equipment should be performed on a regular basis. Examples include the verification of the isocenter localization and table positioning, the calibration of the leaf positions and the quality assurance for the delivery of small numbers of monitor units. In particular for sinonasal irradiations, the presence of air cavities within the PTV is a challenge for dosimetrical verification.

Apart from the delineation of the CTV and the OARs, the class solution directed strategy enables to automate the treatment planning process. This results in a predictable treatment planning timing and quality, which makes the planning process less dependent on the individual skills of the planner and hence minimizes the learning curve for new planners. Inherently, an automated approach is suboptimal, since it can always be used as an input for further case-specific optimization. However, to maintain patient flow, the goal of the planning process should be to customize the treatment plan closely to the clinical protocol constraints rather than focusing on an endpoint of optimization. In an automated approach, treatment plans are very uniform and modifications to the existing protocol can easily be investigated.

The impact of internal organ motion/deformation and patient setup error on the planned treatment dose still remains a challenging topic of research [17][18]. The variation in dose delivery, per fraction and cumulative, for each OAR makes it difficult to analyze accurate dose-toxicity relationships. Data obtained by acquiring multiple CT/MRI datasets in treatment position and on-line portal imaging can be used to calculate variations between planned and delivered doses, and should in a next step be taken into account during plan optimization. This may hence increase the robustness of the IMRT plans. Despite the recommendation given in ICRU Report 62 [19] to define a PRV (Planning Organ at Risk Volume), in analogy with the PTV concept, the use of expansion margins for organs at risk are rarely reported. The lack of data on the internal motion of organs at risk, e.g. the motion amplitudes of optic nerves or eyeballs, and the clinical experience in generating treatment plans without expansion margins, may make clinicians/planners unfamiliar with the PRV concept and consider the risk of complications in omitting margins acceptable.

Likewise, little is known about the effect of inhomogeneous irradiation of small critical structures such as the optic nerves and the optic chiasm. Dose-toxicity data are based on homogeneous irradiation of these volumes with conventional techniques [20][21][22]. The use of image coregistration (CT-MRI) in order to delineate the optic nerves and the chiasm more precisely, and the availability of more accurate dose computation algorithms, will enable us in the future to analyze more reliable NTCP values for these nervous structures.

Current research at GUH for ethmoid sinus cancer addresses the outlining of clinical follow-up protocols for this subsite, in order to obtain more insight in the relapse pattern of this disease and to register the long term toxicity profile of IMRT. In a next step a shortening of the overall radiation treatment time, by giving 6 fractions/week or increasing the daily fraction size, will be investigated. For patients presenting with intracranial tumor spread, new treatment regimens will be investigated to increase the local tumor control. Future collaboration with the Departments of Epidemiology, Occupational Health and

Industrial Medicine should include efforts to map industrial regions with a high activity of woodworking, in order to start specific prevention programs and screening of high risk individuals.

References

1. Verellen D, Linthout N, van den Berge D, et al. Initial experience with intensity-modulated conformal radiation therapy for treatment of the head and neck region. Int J Radiat Oncol Biol Phys 1997;39:99-114.

2. Kuppersmith RB, Greco SC, Teh BS, et al. Intensity-modulated radiotherapy: first results with this new technology on neoplasms of the head and neck. Ear Nose Throat J 1999;78:238, 241-6, 248 passim.

3. De Neve W, De Gersem W, Derycke S, et al. Clinical delivery of intensity modulated conformal radiotherapy for relapsed or second-primary head and neck cancer using a multileaf collimator with dynamic control. Radiother Oncol 1999;50:301-14.

4. Fraass BA, Kessler ML, McShan DL, et al. Optimization and clinical use of multisegment intensity-modulated radiation therapy for high dose conformal therapy. Semin Radiat Oncol 1999;9:60-77.

5. Chao KS, Low DA, Perez CA, et al. Intensity-modulated radiation therapy in head and neck cancers: The Mallinckrodt experience. Int J Cancer 2000;90:92-103.

6. Sultanem K, Shu HK, Xia P, et al. Three-dimensional intensity-modulated radiotherapy in the treatment of nasopharyngeal carcinoma: the University of California-San Francisco experience. Int J Radiat Oncol Biol Phys 2000;48:711-22.

7. Hunt MA, Zelefsky MJ, Wolden S, et al. Treatment planning and delivery of intensity-modulated radiation therapy for primary nasopharynx cancer. Int J Radiat Oncol Biol Phys 2001;49:623-32.

8. Gregoire V, Coche E, Cosnard G, et al. Selection and delineation of lymph node target volumes in head and neck conformal radiotherapy. Proposal for standardizing terminology and procedure based on the surgical experience. Radiother Oncol 2000;56:135-50.

9. Eisbruch A, Ten Haken RK, Kim HM, et al. Dose, volume, and function relationships in parotid salivary glands following conformal and intensity-modulated irradiation of head and neck cancer. Int J Radiat Oncol Biol Phys 1999;45:577-87.

10. Rasch C, Eisbruch A, Remeijer P, et al. Irradiation of paranasal sinus tumors, a delineation and dose comparison study. Int J Radiat Oncol Biol Phys 2002;52:120-7.

11. Intensity Modulated Radiation Therapy Collaborative Working Group. Intensity-modulated radiotherapy: current status and issues of interest. Int J Radiat Oncol Biol Phys 2001;51:880-914.

12. Arnfield MR, Wu Q, Tong S, et al. Dosimetric validation for multileaf collimator-based intensity-modulated radiotherapy: a review. Med Dosim 2001;26:179-88.

13. Martens C, De Wagter C, De Neve W. The value of the LA48 linear ion chamber array for characterization of intensity-modulated beams. Phys Med Biol 2001;46:1131-48.

14. Martens C, De Wagter C, De Neve W. The value of the PinPoint ion chamber for characterization of small field segments used in intensity-modulated radiotherapy. Phys Med Biol 2000;45:2519-30.

15. De Deene Y, De Wagter C, Van Duyse B, et al. Three-dimensional dosimetry using polymer gel and magnetic resonance imaging applied to the verification of conformal radiation therapy in head-and-neck cancer. Radiother Oncol 1998;48:283-91.

16. De Wagter C, Martens C, De Deene Y, et al. Dosimetric verification of intensity modulation executed by a conventional accelerator equipped with a multileaf collimator. Cancer Radiother 1999;3S1:171-82.

17. Yan D, Lockman D. Organ/patient geometric variation in external beam radiotherapy and its effects. Med Phys 2001;28:593-602.

18. Manning M, Wu Q, Cardinale R, et al. The effect of setup uncertainty on normal tissue sparing with IMRT for head-and-neck cancer. Int J Radiat Oncol Biol Phys 2001;51:1400-9.

19. International Commission on Radiation Units and Measurements. Prescribing, recording and reporting photon beam therapy (supplement to ICRU Report 50), ICRU Report 62, 1999, Bethesda, MD, USA.

20. Burman C, Kutcher G, Emami B, et al. Fitting of normal tissue tolerance data to an analytic function. Int J Radiat Oncol Biol Phys 1991;21:123-35.

21. Parsons J, Bova F, Fitzgerald, et al. Radiation optic neuropathy after megavoltage external-beam irradiation: analysis of time-dose factors. Int J Radiat Oncol Biol Phys 1994;30:755-63.

22. Jiang G, Tucker S, Guttenberger R, et al. Radiation-induced injury to the visual pathway. Radiother Oncol 1994;30:17-25.

Notes

. . . .
. . . .
. . . .
. . . .
. . . .
. . . .
. . . .
. . . .
. . . .
. . . .
. . . .
. . . .
. . . .
. . . .
. . . .
. . . .
. . . .
. . . .
. . . .
. . . .
. . . .
. . . .
. . . .
. . . .
. . . .
. . . .
. . . .
. . . .
. . . .
. . . .
. . . .

6   Abbreviations

ABST	:	Anatomy Based Segmentation Tool
BEV	:	Beam's Eye View
ca	:	cancer
CT	:	Computed Tomography
CTV	:	Clinical Target Volume
DVH	:	Dose Volume Histogram
EPID	:	Electronic Portal Imaging Device
GUH	:	Ghent University Hospital
Gy	:	Gray
GTV	:	Gross Tumor Volume
ICD	:	International Classification of Disease
IMRT	:	Intensity Modulated Radiation Therapy
linac	:	linear accelerator
MLC	:	Multi Leaf Collimator
MRI	:	Magnetic Resonance Imaging
NTCP	:	Normal Tissue Complication Probability
OAR	:	Organ At Risk
PRV	:	Planning organ at Risk Volume
PTV	:	Planning Target Volume
SOWAT	:	Segment Outline and Weight Adapting Tool
SWOT	:	Segment Weight Optimization Tool
TCP	:	Tumor Control Probability
TPS	:	Treatment Planning System
QA	:	Quality Control
2D	:	2-Dimensional
3D-CRT	:	3-Dimensional Conformal Radiation Therapy

7 Acknowledgements

There are two kinds of people, those who do the work and those who take the credit. Try to be in the first group; there is less competition there.

Indira Gandhi (1917-1984)

8 Curriculum vitae

Personalia

The author of this thesis was born on August 23, 1973 in Ostend, Belgium. He went to the primary school in Ostend (1979-1985) and finished his high school in Bruges (1985-1991). He started his medical studies in 1991 at the University of Ghent and obtained summa cum laude his degree of medical doctor (MD) in 1998. Since August the 1st 1998, he is a radiation oncologist in training at the Division of Radiotherapy of the Ghent University Hospital. Since October the 1st 1998, he is a research assistant of the Fund for Scientific Research (FWO).

Papers

Articles in journals listed in the Science Citation Index database (a1)

1. **F. Claus**, W. De Gersem, C. De Wagter, R. Van Severen, I. Vanhoutte, W. Duthoy, V. Remouchamps, B. Van Duyse, L. Vakaet, M. Lemmerling, H. Vermeersch and W. De Neve. An implementation strategy for IMRT of ethmoid sinus cancer with bilateral sparing of the optic pathways. Int J Radiat Oncol Biol Phys 2001;51:318-31.

2. W. De Gersem, **F. Claus**, C. De Wagter and W. De Neve. An anatomy based segmentation tool for intensity modulated radiotherapy of head and neck cancer. Int J Radiat Oncol Biol Phys 2001;51:849-59.

3. W. De Neve, W. De Gersem, G. De Meerleer, **F. Claus** and C. De Wagter. Reduction of target dose inhomogeneity in IMRT treatment planning using biologic objective functions - In response. Int J Radiat Oncol Biol Phys 2001;49:1518-20.

4. G. Budgell, C. Martens and **F. Claus**. Improved delivery efficiency for step and shoot intensity modulated radiotherapy using a fast-tuning magnetron. Phys Med Biol 2001;46:253-61.

5. **F. Claus**, W. De Gersem, I. Vanhoutte, W. Duthoy, V. Remouchamps, C. De Wagter and W. De Neve. Evaluation of a leaf position optimization tool for IMRT of head and neck cancer. Radiother Oncol 2001;61:281-6.

6. W. De Gersem, **F. Claus**, C. De Wagter and W. De Neve. Leaf position optimization for step and shoot IMRT. Int J Radiat Oncol Biol Phys 2001;51:1371-88.

7. **F. Claus**, W. Duthoy, T. Boterberg, W. De Gersem, J. Huys, H. Vermeersch and W. De Neve. Intensity modulated radiation therapy for oropharyngeal and oral cavity tumors : clinical use and experience. Oral Oncol 2002;in press.

Articles in scientific journals with an international referee system (a2)

1. W. De Neve, **F. Claus**, P. Van Houtte, S. Derycke and C. De Wagter. Intensity modulated radiotherapy with dynamic multileaf collimators. Technology and clinical experience. Cancer Radiother 1999;3:378-92.

2. **F. Claus**, L. Vakaet, W. De Gersem, M. Lemmerling, I. Vanhoutte, S. Vermael, R. Van Severen, B. Van Duyse, H. Vermeersch, M. Moerman and W. De Neve. Postoperative radiotherapy for paranasal sinus tumours : a challenge for intensity modulated radiotherapy. Acta Oto-Rhino-Laryngol Belg 1999;53:263-9.

3. **F. Claus**, Y. De Deene, V. Remouchamps, C. De Wagter, K. Van Vaerenbergh, J. Schauvliege, B. Van Duyse, B. Speleers, W. Duthoy and W. De Neve. An isocenter position verification device for electronic portal imaging : physical and dosimetrical characteristics. Cancer Radiother. Cancer Radiother 2001;5:759-65.

4. W. De Neve, **F. Claus**, W. Duthoy, G. De Meerleer and C. De Wagter. Intensity modulation techniques for improvement of normal tissue tolerance. Front Radiat Ther Oncol Basel Karger 2001;37:163-73.